

2021-08-01

# Development of a Laser Solder Process for use with Material Extrusion Additive Manufacturing and Rapid Electronics Prototyping in Embedded Sensing Applications

Emerson Roland Armendariz  
*University of Texas at El Paso*

Follow this and additional works at: [https://scholarworks.utep.edu/open\\_etd](https://scholarworks.utep.edu/open_etd)



Part of the [Mechanical Engineering Commons](#)

---

## Recommended Citation

Armendariz, Emerson Roland, "Development of a Laser Solder Process for use with Material Extrusion Additive Manufacturing and Rapid Electronics Prototyping in Embedded Sensing Applications" (2021). *Open Access Theses & Dissertations*. 3216.  
[https://scholarworks.utep.edu/open\\_etd/3216](https://scholarworks.utep.edu/open_etd/3216)

This is brought to you for free and open access by ScholarWorks@UTEP. It has been accepted for inclusion in Open Access Theses & Dissertations by an authorized administrator of ScholarWorks@UTEP. For more information, please contact [lweber@utep.edu](mailto:lweber@utep.edu).

DEVELOPMENT OF A LASER SOLDERING PROCESS FOR USE WITH  
MATERIAL EXTRUSTION ADDITIVE MANUFACTURING AND  
RAPID ELECTRONICS PROTOTYPING IN EMBEDDED  
SENSING APPLICATIONS

EMERSON ROLAND ARMENDARIZ

Master's Program in Mechanical Engineering

APPROVED:

---

David Espalin, Ph.D., Chair

---

Ryan Wicker, Ph.D.

---

Amit Lopes, Ph.D.

---

Stephen L. Crites, Jr., Ph.D.  
Dean of the Graduate School

Copyright ©

by

Emerson Roland Armendariz.

2021

## **Dedication**

*This thesis is dedicated to my mother, father, and sister, who have immensely supported me in my academic pursuits and have always inspired me to follow my dreams. For without their love and sacrifice, this truly would not have been possible.*

*Dwight Lynn Armendariz  
January 13, 1959 – August 25, 2019  
I love you and I miss you dad.*

DEVELOPMENT OF A LASER SOLDERING PROCESS FOR USE WITH  
MATERIAL EXTRUSION ADDITIVE MANUFACTURING AND  
RAPID ELECTRONICS PROTOTYPING IN EMBEDDED  
SENSING APPLICATIONS

by

EMERSON ROLAND ARMENDARIZ, B.Sc. in Mechanical Engineering

THESIS

Presented to the Faculty of the Graduate School of

The University of Texas at El Paso

in Partial Fulfillment

of the Requirements

for the Degree of

MASTER OF SCIENCE

Department of Mechanical Engineering

THE UNIVERSITY OF TEXAS AT EL PASO

August 2021

## **Acknowledgements**

I would like to express my gratitude to Dr. Ryan Wicker, Founder and Director of the W.M. Keck Center for 3D Innovation, for providing me the opportunity to conduct exciting research within his state-of-the-art additive manufacturing center, and his support in the completion of my thesis work as a member of my graduate advisory committee. It is truly an honor. I would personally like to thank my advisor and mentor, Dr. David Espalin, the Director of Research of the W.M. Keck Center, for taking a chance on me and allowing me the opportunity to follow my dreams of becoming the best engineer and scientist I can possibly be, and for guiding me to knowledge and skills that have enabled me tremendous growth as an individual. I will always be grateful for his unwavering patience and support during a difficult time in my life. I would also like to thank Dr. Amit Lopes of the Industrial Manufacturing and Systems Engineering Departments at UTEP for his support as a member of my research committee.

I would like to give a very special thanks to my research manager of the W.M. Keck Center, Mr. Jose Coronel, for leading by example and showing me what it truly means to work hard and aspire for excellence in the quality of my work, while also supporting me in friendship and faith. I will always be grateful to him for his prayers after the loss of my father. I would also like to express an extremely special thanks to my genuine and intelligent colleagues, who have become lifelong friends I will always appreciate, and who have always provided encouragement and assistance wherever possible; Mr. Leonardo Gutierrez for his considerable help in the design, development, and implementation of this laser application system, to where its current state would not have been possible. Mr. Jose Motta and Mr. Christopher Minjares for patiently training and educating me in this area of research as mentors and friends. Mr. Angel Vega for his infinite support and assistance in all my endeavors, and who also trained and educated me in the systems I used to enable my research experimentation. Another very special thanks to Mr. Nikki Martinez for assisting me during the development of our tooling systems, as our discussions truly motivated me to improve the compatibility of our tools within the Multi3D process plan. Dr. Kazi Billah for

his kindness in frequently offering a helping hand with my experimentation and/or documentation, and who made me feel valued as an engineer and colleague on our research team. Mr. David Sepulveda for his invaluable assistance in circuit fabrication and their testing, along with his assistance in data analysis. I would also like to thank the staff and students at the W.M. Keck Center, whose passion, work ethic, and professionalism motivated me daily. They include center manager Mrs. Mireya Perez, center representative Mrs. Alexandra Plasencio-Cooper, Safety engineer and friend Luis Ochoa, and post-doctoral researcher manager Edel Arrieta. I would also like to extend my thanks to the professors who I had the privilege of working with, Dr. Omar Cedillos Barraza, Dr. Methaq Abed, and Dr. Jack Chessa. I also offer a sincere thanks to Kiralise Silva, for her assistance in obtaining work within the Mechanical Engineering Department, and which ultimately allowed me to decide to pursue my current path. I also give thanks to project collaborators Mr. Michael Sears of XIA LLC, Mr. Tom Place of AURA, Mr. Kyle Cluff of Los Alamos National Laboratories, and Mr. Surjdan Petrovic of GN Resound. Special thanks to Lyan Gutierrez, Jaime Martinez, and Isai Mendez for their support during my graduate and undergraduate studies.

Lastly, I would like to thank my truly outstanding family; my incredible parents who made me the person I am today, and who never left my side, and my sister whom is truly a blessing in my life. My mother, Guadalupe Baeza, who has sacrificed so much for me to succeed. Her love and compassion have enabled me to get where I am in life, and I firmly believe that this work would not have been possible without her boundless love and support. I would like to thank my father, Dwight Armendariz, heaven rest his soul, who had always inspired me to achieve greatness, who elevated me to believe in myself and my purpose in life, and who was always there for me. My sister, Andrea Armendariz, the smartest and wisest individual I know, for her endless love and support in all my endeavors, and for her inspiring nature which helps me in becoming the best version of myself in this life. Also, I would like to give thanks to my Uncle Norman, for it is he who had a huge part in my decision to become an engineer; his impressive willingness to change the world of science and technology is inspiring, and it is his superior intelligence that enables him to do so repeatedly. I would also like to thank my best friends, Christian Monzon, Mathew

Gonzalez, Lloyd Parker, and Elijah Valle, who have become my brothers and family, for being a part of my journey and for always supporting me to grow and succeed. I'd also like to offer an extended thanks to Cameron Castillo for her love and support throughout my graduate studies.



## **Abstract**

Industrial and rapid prototyping (RP) trends toward miniaturization of electronic devices containing temperature sensitive electronics and surrounding materials are calling for highly controllable, selective laser soldering technologies. Laser soldering is a non-contact technique that eliminates the risk of marring or damaging sensitive components by precisely focusing a laser beam on a solder filler alloy, leading to a fast and non-destructive electrical joint. Using the benefits of accurate and controlled heat delivery via inexpensive low power laser diodes (LPDL's) in conjunction with ever-increasing additive manufacturing capability in producing complex internal features and geometries, development and testing of a laser application system capable of soldering electrical interconnections embedded within thermally sensitive thermoplastics is investigated, with intent of producing electrically multifunctional end-use parts with embedding sensing capabilities, and with little human intervention. This system is intended to reinforce UTEP's Multi<sup>3D</sup> hybrid additive manufacturing (HM) system which pauses prints produced via fused deposition modeling (FDM) to ultrasonically embed wire within any plane of a 3D printed thermoplastic substrate, followed by insertion of electronic components housed within predesigned cavities before print continuation to create functional and embedded circuits for rapid prototyping and embedded sensing applications. Methods for creating and placing the conductive pathways required for embedded circuitry have been explored, while non-contact methods for embedding and terminating of these circuits has yet to be investigated. Investigation of discrete, passive surface mount technology (SMT), as well as methods in which such components are terminated, is presented in this research in order to develop a laser soldering system and methodology for the Multi<sup>3D</sup> hybrid manufacturing system. A process plan for embedding and terminating a circuit during a build interrupt is reviewed, along with methods for machining designated electronic component cavities and preparation of all constituent materials for paste deposition before laser soldering testing. Tooling for laser system integration and positioning was designed, along with laser controller programming for adequate temperature control.

## Table of Contents

Dedication .....	iii
Acknowledgements .....	v
Abstract .....	viii
Table of Contents .....	ix
List of Tables .....	xi
List of Figures .....	xi
Chapter 1 Introduction .....	1
1.1 Additive Manufacturing .....	1
1.2 W.M. Keck Center for 3D Innovation .....	3
1.3 The Multi <sup>3D</sup> System and Hybridized Manufacturing (HM) .....	5
1.4 Laser Soldering .....	7
1.5 Research Motivation .....	9
1.6 Thesis Objectives .....	11
Chapter 2 Literature Review .....	12
2.1 Outline .....	12
2.2 Material Extrusion and Fused Deposition Modeling (FDM) in Additive Manufacturing .....	12
2.3 Hybrid Manufacturing (HM) .....	20
2.4 Surface Mount Technology (SMT) in PCB Manufacturing .....	23
2.5 Metallurgy of Soldering and Solderability in SMT .....	31
2.6 Soldering Methods in SMT .....	39
2.7 Laser Types and Characteristics in Reflow .....	48
2.8 Evaluation of Temperature History .....	52
Chapter 3 Exploratory Work .....	57
3.1 Machining of Cavities for SMD Placement .....	57
3.2 Laser Soldering Tests with ABS, Passive SMT Components, and 450 nm Laser .....	61
3.2 Laser Soldering Tests with Polycarbonate (PC), Passive, and Active SMT Components .....	66
3.4 Process Plan Improvements .....	69

Chapter 4 Tool Design .....	71
4.1 Overview .....	71
4.2 Semiconductor Laser and Power Supply .....	73
4.3 Gantry Mount.....	74
4.4 Controller and Software .....	76
Chapter 5 Methodology .....	80
5.1 Overview .....	81
5.2 Materials .....	81
5.3 Experimental Setup .....	82
5.4 Temperature Observations using Thermocouple, IR Thermography, and HD Camera .....	84
5.5 Wire-to-Wire Joining: Parameterization and Repeatability.....	87
5.6 Wire-to-Component Joining: Parameterization and Repeatability .....	91
Chapter 6 Results and Discussion.....	98
6.1 Temperature Observations using Thermocouple, IR Thermography, and HD Camera .....	98
6.2 Wire-to-Wire Joining: Parameterization and Repeatability.....	106
6.3 Wire-to-Component Joining: Parameterization and Repeatability .....	121
Chapter 7 Conclusions .....	137
References.....	141
Vita.....	143

## List of Tables

<b>Table 1:</b> Fundamental principles, technology examples, and materials processed for each of the seven process categories per ISO/ASTM 52900 (Tofail et al, 2018) .....	14
<b>Table 2:</b> Select properties of commercially available FDM materials.....	20
<b>Table 3:</b> Classification of fundamental hybrid and sub-hybrid manufacturing processes with descriptions, research areas, and examples .....	23
<b>Table 4:</b> Melting point of select compositions of solder for the electronics industry.....	34
<b>Table 5:</b> Flux categories and characteristics (courtesy of Hwang, 1991) .....	35
<b>Table 6:</b> Reflow methods – Key features, benefits, and limitations (Hwang, 1991; Vivari and Kasman, 2007). .....	47
<b>Table 7:</b> Array of laser power and time duration combinations used for laser soldering with Sn 63/Pb 37 solder paste alloy's manufacturer temperature profile .....	91
<b>Table 8:</b> Laser power and time duration combinations used for laser soldering of wire-to-component joining, respective of phases during reflow. ....	97
<b>Table 9:</b> Laser power and time duration combinations used for initial laser soldering of wire-to-wire joining, respective of phases during reflow. ....	102

## List of Figures

<b>Figure 1:</b> Generic AM process flow. ....	3
<b>Figure 2:</b> Multi <sup>3D</sup> System CAD concept (courtesy of Ambriz, 2015). ....	7
<b>Figure 3:</b> Schematic Illustration of FDM process with liquefier head melt states. ....	16
<b>Figure 4:</b> Features of deposited material inherent to FDM. ....	17
<b>Figure 5:</b> Mechanism of bonding between adjacent and interlayer FDM beads (left), void formation inherent to FDM part fabrication (right). ....	18
<b>Figure 6:</b> Anatomy of a printed circuit board ....	25
<b>Figure 7:</b> SMT passive (top row) and active (bottom) components alongside their through-hole equivalents ....	27
<b>Figure 8:</b> Construction details of a surface mount resistor and capacitor. ....	28
<b>Figure 9:</b> Three initial assembly formats used in surface mount technology ....	30
<b>Figure 10:</b> Once confined to board surfaces (top), passive components can now be embedded within substrate of PCB's (bottom). ....	31
<b>Figure 11:</b> Phase diagram plotting temperature vs. composition (wt. %) for the binary eutectic system of elements lead ( $\alpha$ ) and tin ( $\beta$ ). ....	32
<b>Figure 12:</b> (a) Example IMC layers of Cu <sub>3</sub> Sn and Cu <sub>6</sub> Sn <sub>5</sub> formed between bulk solder and a Cu solder pad (courtesy of Jiang et al., 2019) (b) solder joint failure between a 1608 resistor and a Cu surface associated with thick IMC formation (courtesy of Element Materials Technology, 2021). ....	36
<b>Figure 13:</b> Criteria for contact angles in wetting of solder joints (top), desired joint formations for SMC terminations and THC leads (bottom). ....	37
<b>Figure 14:</b> Schematic illustration of the wave soldering process. ....	41
<b>Figure 15:</b> Example temperature (°C) vs. time (s) reflow profile for a solder alloy composition. ....	42
<b>Figure 16:</b> Schematic for a (a) in-line infrared, (b) convection, and (c) vapor phase reflow soldering systems. ....	44
<b>Figure 17:</b> Principle of an infrared (IR) thermal camera receiving radiation. ....	56
<b>Figure 18:</b> (a) Top view of 2 mm thick ABS test coupon with ultrasonically embedded wire, (b) ultrasonic horn embedding on 3D printed substrate. ....	58
<b>Figure 19:</b> (a) CNC spindle's toolpath on example coupon within Autodesk's Fusion 360 (b) front view of CNC routing station and test platform. ....	59
<b>Figure 20:</b> Milled cavities for electronic components on ABS 1.18 mm thick test coupon with ultrasonically embedded wire, with closely spaced cavity slots near wire. ....	60
<b>Figure 21:</b> Lulzbot Taz-6 gantry with mounted diode and infrared lasers. ....	61
<b>Figure 22:</b> Machining of cavities with an $\varnothing = 0.5$ mm end mill (top), placement of components within cavities for solder testing (bottom). ....	62
<b>Figure 23:</b> (a) Flux/solder paste placement at desired joint locations, (b) pre-applied flux and solder paste along cavity edges. ....	63
<b>Figure 24:</b> (a) Failed solder joint at left and right sides of 50 $\Omega$ resistor, (b) passing capacitor (100nF) with functional solder joints on both sides, (c) resistor failure with acceptable solder joint on left side but failed solder joint at right side. ....	65
<b>Figure 25:</b> (a) CAD of top plane of circuit, (b) CAD of bottom plane of circuit. ....	67
<b>Figure 26:</b> (a) Resulting top plane portion of circuit (b) resulting bottom plane portion of circuit. ....	68

<b>Figure 27: (a)</b> CAD rendering of laser soldering tool alongside other tools on CNC gantry, <b>(b)</b> finished laser soldering tool alongside IR thermography camera used for process evaluation. ....	72
<b>Figure 28:</b> 808 nm 2W - 4W low power IR semiconductor laser system used for this research (courtesy of CivilLaser Suppliers) .....	73
<b>Figure 29: (a)</b> CAD image of laser soldering tool in exploded view <b>(b)</b> CAD image of laser soldering tool assembly.....	75
<b>Figure 30:</b> 8-slot cRIO-9047 CompactRIO Controller with C-Series Modules inserted within its chassis. ....	77
<b>Figure 31:</b> Partial views of <b>(a)</b> front panel and <b>(b)</b> block diagram for the laser control VI. ....	78
<b>Figure 32: (a)</b> Front panel and <b>(b)</b> block diagram for the targeting camera VI.....	80
<b>Figure 33:</b> General setup at CNC routing station for laser soldering experimentation. ....	82
<b>Figure 34: (a)</b> Temperature vs. time reflow profile for Pb 63/Sn 37 solder paste alloy <b>(b)</b> partial view of Laser Control VI's front panel depicting current output controls. ....	83
<b>Figure 35:</b> Current to power curve fitted to manufacturer power settings.....	83
<b>Figure 36: (a)</b> Conceptual side view of a solder junction point prepped for laser soldering, <b>(b)</b> image of solder junction point with flux (barely visible) and solder paste.....	85
<b>Figure 37: (a)</b> Initial wire-to-wire test coupons (PC) used for IR pseudo temperature evaluation, <b>(b)</b> deposited solder paste volume on crossing wire with correction fluid coating on wire, <b>(c)</b> IR image as seen on IR analysis software with designated ROI's on correction fluid coating.....	87
<b>Figure 38: (a)</b> Partial view of wire-to-wire test coupon (PC) used for wire joining tests, <b>(b)</b> corner of a test coupon with severed wire within additional cavities along with flux and solder paste placed at intersecting wire locations. ....	88
<b>Figure 39:</b> Reference image of the amount of solder paste deposited onto solder joint locations using a precision scraping tool, attempting to remain within the copper wire's diameter. ....	90
<b>Figure 40:</b> Solder joint location being targeted as seen on the Targeting Camera VI screen, with an inner red circle the bounding target reticle and the dashed outer circle the approximated affected area. ....	91
<b>Figure 41: (a)</b> Toolpath generation in Fusion 360 CAM <b>(b)</b> machining through wire within cavities, <b>(c)</b> component, flux, solderpaste, and whiteout placement <b>(d)</b> targeting of solder paste. ....	93
<b>Figure 42:( a)</b> Press-fit placement into cavity, cleaned with Isopropyl Alcohol <b>(b)</b> Dabbing of flux at intersections (termination & wire edges) <b>(c)</b> Dabbing of solder paste at intersections above flux.....	94
<b>Figure 43:</b> Conceptual drawing of setup used for wire-to-component joining with close up view of resistor being targeted at its right side termination.....	94
<b>Figure 44: (a)</b> Embedded resistor being targeted within the Targeting Camera VI video feed <b>(b)</b> image of component, wire, and ROI's as seen in IR software, with heat seen at laser turn on. ....	95
<b>Figure 45: a)</b> Before & after images of first coupon at 2 W for 10 s, 3.3 W for 30 s, 3.7 W for 30 s <b>b)</b> Before & after images of second coupon at 3.3 W for 15 s, 3.3 W for 45 s, 3.7 W for 45 s. ....	99
<b>Figure 46:</b> Sequence of images depicting actions observed during reflow of solder paste for solder junction test coupon 2 as seen in video recodring.....	100
<b>Figure 47:</b> Plot comparing IR thermography and thermocouple temperature history. ....	101
<b>Figure 48:</b> Before and after images for 4 rows of 20 solder joints tested (parameter testing). .	107
<b>Figure 49:</b> Images of solder joints post-scraping and cleaning processes, with each image enclosed in red to represent failed solder joints attempts and in green to denote successful solder joint attempts.....	108

<b>Figure 50:</b> Metrology of solder Joint 13 within Fusion 360 for calculation of fillet thickness (n).	111
<b>Figure 51:</b> Time-temperature profile, total energy delivered, fillet thickness number, and reported resistance values between for <b>a)</b> Joint 13 <b>b)</b> Joint 14 and <b>c)</b> Joint 15.	113
<b>Figure 52:</b> Time-temperature profile, total energy delivered, fillet thickness number, and reported resistance values for <b>a)</b> Joint 16 <b>b)</b> Joint 17 and <b>c)</b> Joint 19.	114
<b>Figure 53:</b> <b>a)</b> Original time-temperature profile provided by the manufacturer alongside hallmarked Joints 13 of Row 3 <b>(b)</b> and 17 of Row 4 <b>(c)</b> for comparison.	116
<b>Figure 54:</b> Time-temperature profile, total energy delivered, fillet thickness number, and reported resistance values for Joint 12.	117
<b>Figure 55:</b> Images of the 10 solder joints produced during repeatability testing, with parameter settings for Joint 13 in Row 5 and settings for Joint 19 in Row 6.	118
<b>Figure 56:</b> <b>a)</b> Total energy delivered to each passing solder joint and <b>(b)</b> values calculated for fillet thickness (n) of all passing solder joints.	119
<b>Figure 57:</b> Single sheet containing coupons prepped for variability testing, with each row labeled R1 to R18 (resistor number 1, resistor number 2, etc.) to denote order of execution.	122
<b>Figure 58:</b> Series of images for resistor 1 during testing of Power-2 and Time-2 at 2 W for 10 s in preheat duration 1 <b>(a)</b> , 3.3 W for 30 s in ramp duration 2 <b>(b)</b> , and 3.7 W for 30 s in ramp duration 3 <b>(c)</b> at its left side termination; Power-1 and Time-1 for right.	123
<b>Figure 59:</b> Image of failed solder joints for resistor 2 post laser soldering and before cleaning; at 6 s for duration 1, 18 s for duration 2, 18 s for duration 3.	124
<b>Figure 60:</b> <b>a)</b> Image of failed solder joints for Resistor 3 at P1-P1 post laser soldering and before cleaning, <b>b)</b> image of failed solder joints for Resistor 4 at P2-P2 post laser soldering and before cleaning, <b>c)</b> Image of failed solder joints for Resistor 9 at P2-T1 with tombstoning	125
<b>Figure 61:</b> Images of resistors subjected to adjusted time settings, along with power settings, time duration, total energy delivered, and reported resistance values.	127
<b>Figure 62:</b> 18 resistors tested on sheet 2 at 0.3 W, 2 W, 3.3 W for 18 s, 18 s, 12 s.	129
<b>Figure 63:</b> Time-temperature profiles for select resistors on sheet 2.	131
<b>Figure 64:</b> <b>a)</b> commonly occurring result seen during wire-to-component experimentation, <b>b)</b> concept of a flux dispensing/dabbing tool, <b>c)</b> concept of a precision solder paste dispensing tool, and <b>d)</b> suggested placement/orientation for future experimentation.	134
<b>Figure 65:</b> Pseudo temperatures values reported at the polycarbonate surface surrounding the solder joint area for 2R11R, with a scale of temporal values for the general ROI that is the full image.	136

# **Chapter 1**

## **Introduction**

### **1.1 Additive Manufacturing**

Additive Manufacturing (AM), most commonly known as 3D printing (3DP) or rapid prototyping, is a four-decade young fabrication process that has grown in relevance due to its convenient and easy to use computerized interfaces for creating solid homogenous 3D parts from thermoplastics, metal powders, resins, or composite materials, in a layer-upon-layer fashion using direct hardware and computer-aided design (CAD) software (ASTM F2792). This process of joining layered materials on to one another lies contrary to conventional subtractive manufacturing methodologies seen in industry where material is wastefully and mechanically removed from a base of that same material with the use of fixtures, cutting tools, coolants, or other auxiliary resources. Despite its rather young lifespan and integration into commercial markets in the late 1980's, advancements within AM technologies have evolved to create seven core additive manufacturing processes, all of which join materials to make objects from 3D model data. In 2010, the American Society for Testing and Materials (ASTM) committee created the set of standards that classify the seven core processes into categories, each of which deposit materials in a different manner. The AM processes vary with material, hardware, and methodology used, but all offer the freedom of design to produce highly customized parts with increased complexities at reduced costs and lead times, ultimately providing massive potential in almost every market including automotive, medical/dental, aerospace, and robotics (Attaran, 2017). These technologies have become more sophisticated with the onset of new IT capabilities and as such have raised familiarity and acceptance among manufacturers in seeing the technology as transformative to the future of manufacturing. Parts fabricated via AM methods vary in application and have gone so far as to be used as surrogate parts for training and education more recently, integral parts of business processes like that of aerospace giant Boeing or the British automotive manufacturer McLaren . In 2017, aerospace giant Boeing received FAA approval to use 3D-printed titanium parts in its 787



thanks to reduced material waste associated with on demand additive manufacturing (Aerospace America, 2018). Within the same year, McLaren signed a four-year partnership deal with Stratasys, an American manufacturer of 3D printers and 3D production systems, making the company the official supplier of additively manufactured parts to the McLaren Honda Formula One team. The team is said to bring a Stratasys 3D modeling machine to track testing's and races to make parts and tools on site, producing parts including hydraulic line brackets, cooling ducts, and rear wing flaps composed of polymers (Holmes, 2018).

The seven process categories in AM apply a similar formula that typically begins when a part designed within a CAD file is converted to a stereolithography (STL) file, and then 'sliced' on slicing software in order to provide manufacturing equipment instructions in fabrication of a single part model. Made possible through utilization of other existing technologies, mainly the computer aided functions of design and manufacturing (CAM) software and advanced automated hardware such as computer numerical control machines (CNCs), AM technologies are evolving rapidly from producing single material objects to those with functionally defined geometric shapes of varying materials and microstructures (Hernandez, 2012). In turn, the STL has become the industry interchange file format standard for transferring information between design programs and additive manufacturing equipment for decades, and whose primary function is to define a part's surface mesh (52915:2016, 2016). A slicing software or variant is the program which then effectively translates the STL file containing the 3D rendering into instructions for the additive manufacturing machine to create every individual layer until its complete fabrication. A typical process flow plan made possible by these technologies is shown in Figure 1. This approach to rapid prototyping exemplifies the advantages of AM, which can provide major advances in manufacturing efficiency and sustainability, mass customization, and increased part complexity and functionality. Fundamental AM processes include material extrusion, most commonly known as fused deposition modeling (FDM) or fused filament fabrication (FFF), primarily used to produce thermoplastic parts via softening of a filament to produce semi-molten plastic before

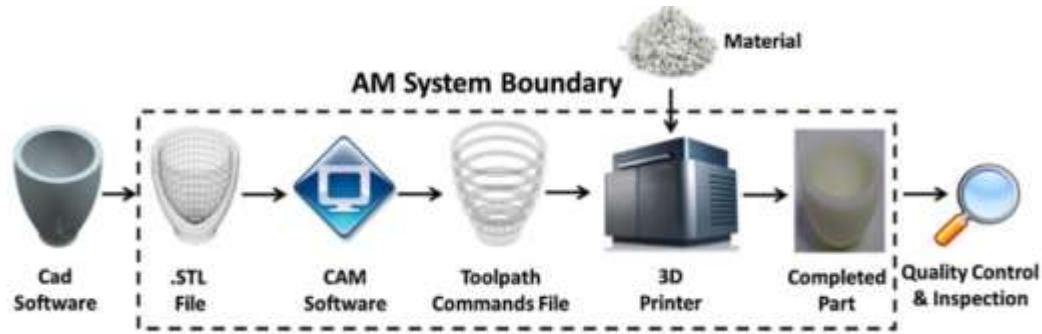


**Figure 1:** Generic AM process flow.

cooling to a solid part (David Espalin, 2012); Photo-polymerization also known as stereolithography, uses liquid photopolymers (resins) to be selectively cured by UV light radiation in a vat (Hernandez, 2012); Directed energy deposition (DED), or laser-engineered net shaping (LENS), which uses focused thermal energy to fuse metal alloys as they are deposited on to previous layers; Powder bed fusion, forming a broad category of melting or sintering a bed of metal or plastic powders one layer at a time, make up the category of electron beam melting (EBM), selective laser melting (SLM), and direct metal laser sintering (DMLS) (Vock & Bhurghardt Kloden, 2017); the material and binder jetting processes of using ceramic and metal materials which are joined using bonding agents in a dissimilar manner (Gibson, Rosen, & Stucker, 2010), and lastly, the less traditional sheet lamination method which uses form-then-bond or bond-then-form methods of assembling individual layers using a form of adhesion (e.g., ultrasonic energy, adhesive). Further comparisons of the different processes become clear when considering material properties, part size and accuracy, manufacturing costs, and most importantly, the intended application, as additive manufacturing is not always the right choice. It has distinct advantages and disadvantages, and it is up to the user to decide if AM is the best process for their projects.

## **1.2 W.M. Keck Center for 3D Innovation**

The work for this research was conducted at the W.M. Keck Center for 3D Innovation, a unique multidisciplinary research facility focused on the use and development of AM technologies with primary focus in AM technology development, engineered and structured materials, and

advanced AM applications. Located at the University of Texas at El Paso (UTEP), the center was established through grants and funding from the W.M. Keck Foundation in 2000, and then additional expansion through funding and support from the Texas Emerging Technology Fund (ETF), The University of Texas System, and multiple industry partners that have made possible the center's dedication to research and innovation in additive manufacturing (Innovation, 2021). Each year the lab draws local and international interest from multi-disciplinary professionals ranging from scientists and engineers to government officials, and even K-12 students and educators involved in higher education. Today, the center has progressed into one of the leading laboratories for additive manufacturing, exhibiting over 75 different AM machines of six of the seven AM process categories, all heavily used for both commercial and research use with capabilities of at least 10 distinct layer processing methods and multiple custom AM-based patented or patent-pending engineering systems (Innovation, 2021). Ever developing research subjects include fabrication of end-use devices involving 3D structural electronics, metallic structures utilizing various alloys, cardiovascular flow research, and even tissue engineering (Innovation, 2021). The center employs over 50 faculty, staff, and students of different fields to collaborate in any of the various multi-disciplinary projects.

In 2015, UTEP became the first satellite center of America Makes as a result of the growing relationship between the Keck Center and the National Center for Defense Manufacturing and Machining (NCDMM). America Makes is the nation's leading and collaborative partner in AM and 3DP technology research, aiming to increase our nation's global manufacturing competitiveness in the AM sector. Structured as a public-private partnership with member organization from industry, academia, government, non-government agencies, and workforce or economic development resources, the America Makes satellite center model (AM-SC) engages with local companies and educational institutions to supply education and training in additive manufacturing technologies with focus on bringing additive technologies from the research lab to commercialization. Through multi-disciplinary national and international collaborations such as these, the Keck center continues to grow. In addition to its 13,000 square feet of on-campus

research space, the Keck Center recently expanded its operations to a 17,000 square foot off-campus facility, providing additional space for research, economic development, and training (Innovation, 2021). With continued investment in research infrastructure, combined facilities for AM, metrology and reverse engineering, materials characterization and testing, as well as synthetic and analytical chemistry, the center continues to develop strong national and international collaborations with other universities, government agencies, and industrial partners, which has strengthened and expanded rapport for UTEP and the southwest Texas borderland region.

### **1.3 The MULTI<sup>3D</sup> System and Hybridized Manufacturing (HM)**

Many 3D printers in the AM space are transitioning to a hybrid manufacturing (HM) approach to solve complex manufacturing problems. Large volume production speed in additive manufacturing does not allow economical usage of this technology, and so its inclusion into conventional manufacturing product chains is still being researched. While not formally defined with ASTM terminology, hybrid manufacturing can be considered to be a combination of additive manufacturing (3D printing) and subtractive manufacturing (CNC milling) technologies in a single machine. Through ASTM standards, the combination of these processes would fall under a multi-step process, in which parts are fabricated in two or more operations to provide both a basic geometric shape and the fundamental properties of the intended material, as opposed to a single-step process where both shape and properties are achieved simultaneously (Z. Zhu, 2013). HM technologies are often built using a base CNC mill to which the additive and subtractive technology is added. This usage of both additive and subtractive methodologies is not a new concept, as post-processing 3D printed parts typically involves a form of subtractive or manual material removal. With the high accuracy of CNC machining, a smoother surface finish can be obtained. For instance, directed energy deposition additive technology is used for solutions developed by HM techniques. DED works by melting the material by a laser or electron beam as it is deposited through a nozzle onto the build platform. The deposited material can then be CNC milled to achieve a better surface finish as well as tighter tolerances. Critics of the hybrid approach disapprove that hybrid systems

combine two expensive processes into one machine, wherein only one technique can be used at a time. Common objections to these approaches would believe it to be more efficient to have two separate systems that can be run in parallel. This logic is not definitive and depends on the volume and variability of production. While it makes perfect sense to use separate machines for high volume production, the lower volume, high variability jobs seen by most 3D printers are best tackled with a hybrid approach.

The versatility of the W.M. Keck Center's hybrid additive manufacturing capabilities demonstrates the benefits of hybrid manufacturing to create end-use products containing electronic circuits housed within while benefitting from AM geometric freedom of design. The center offers non-standard and unique AM services through the use of its many hybrid AM systems, including its Multi<sup>3D</sup> hybrid manufacturing system with material extrusion, machining, wire embedding, and robotic placement, or the multi-functional Big Area Additive Manufacturing (BAAM) System with material extrusion and wire embedding (Innovation, 2021). The implementation of the tool designed and tested in this paper is intended for use on the Multi<sup>3D</sup> system in order to add to its functional capability. The system is made of two Stratasys 400mc industrial grade 3D printers, a Techno CNC router, and a Yaskawa MH50 anthropomorphic robotic arm (Figure 2). The systems work in tandem to produce parts by pausing prints to ultrasonically embed wire within any plane of a 3D printed substrate, followed by the insertion of electronic components housed within intentionally designed cavities before print continuation to create a multifunctional part. The robotic arm grasps the FDM printer's build platforms for transfer to and from the CNC platform, where the tooling add-ons are adapted and used to complete hybrid operations. Together with micromachining, the system has successfully integrated the use of wire or conductive foil embedding along with various robotic pick and place capabilities (Shemelya et al., 2015). Methods for completion of the circuits required for these electronic processes have been explored, i.e., conductive inks and wire placement before manual soldering to components, with wire embedding becoming a favorable solution due to its higher conductivity (Coronel et al., 2017). In turn, methods for termination of these circuits have yet to be explored, as most of these circuits were

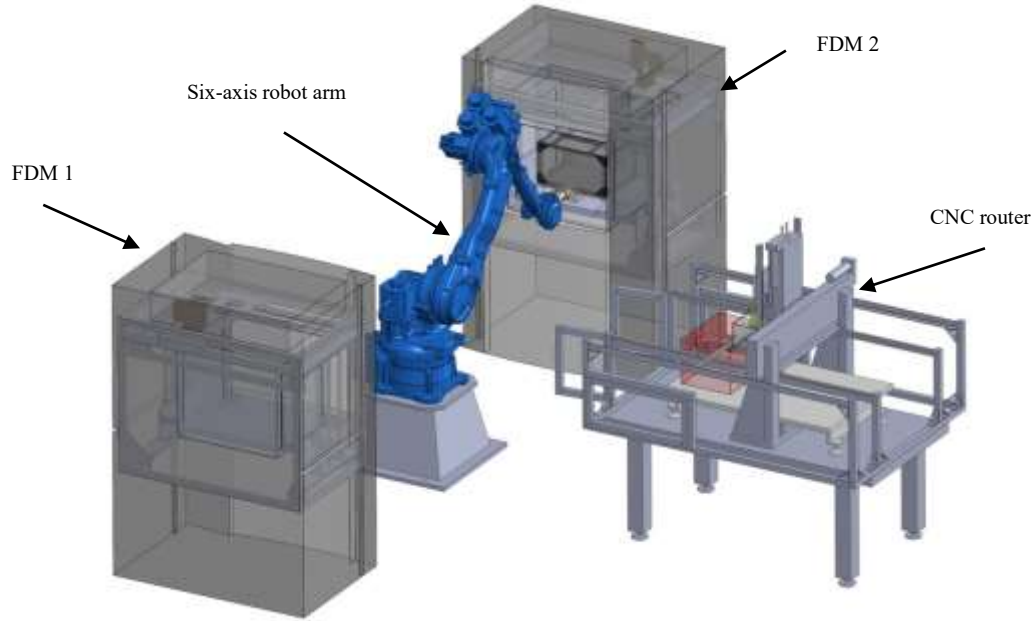


**Figure 2:** Multi<sup>3D</sup> System CAD concept (courtesy of Ambriz, 2015).

completed via traditional and manual hand soldering techniques. In addition, the different types of electronic components currently tested and used with this system are limited, as traditional circuitry has evolved to incorporate extremely high-density integrated circuits which can contain conductors 1-2 microns in size, making automation of a soldering process capable of terminating such connections challenging. Investigation of the different sized electronic components, as well as the methods in which such components are terminated, is presented in this research in order to develop a laser soldering add-on process for the Multi<sup>3D</sup> system. With implementation of a soldering tool, the Multi<sup>3D</sup>'s evolved capabilities would eliminate the need for designated volumes to house conventional PCB's within a designed part, free up space to serve other functions, and in the primary focus of this investigation, allow for the placement of 3D printed electronic subassemblies.

#### 1.4 Laser Soldering

A conventional approach of terminating circuitry in the PCB industry is soldering, in which two or more items are joined by melting and inserting a filler metal (solder) into the joint, and where the filler metal has a lower melting point than the adjoining metal. Typical soldering

methods for printed circuit boards (PCB's) involve SMD (surface mounted devices) reflow soldering, which indicates mounting of the component on the surface of the circuit board in contrast to Through-Hole Soldering which mounts components within holes, and with most reflow equipment involving use of furnaces or ovens. The area of soldering for this project is most relatable to surface mount reflow soldering as components are placed on a 3D printed substrate in a similar manner, and utilizes solder paste to complete terminations. Although, with the glass transition temperatures associated with FDM materials being substantially lower than traditional operating temperatures required for reflow of surface mount assemblies (SMA's) within ovens, an alternative soldering method is investigated. Traditional tip soldering can be accomplished by hand via tip soldering iron, but modern high-density electronic subassemblies can have thermally sensitive components, and in the context of the hybrid additive manufacturing technology developed in this research, complex three-dimensional circuitry that cannot be soldered using these conventional techniques. Laser Soldering is garnering attention as a new method, which is a technique where a precisely focused laser beam provides controlled heating of a solder point which can form fast and non-destructive electrical joints. A controlled laser beam can transfer heat energy to a specific soldering location with flux and solder paste, which can then absorb heat irradiation energy until reaching its melting temperature to complete a solder joint. In contrast to other conventional soldering techniques, laser soldering provides several advantages useful to this project: contactless, locally limited application of energy, temporally and spatially controlled energy input, low thermal stress and maintenance, as well as flexibility and easy adaptation. Types of lasers used in soldering can include carbon dioxide lasers, Nd:YAG lasers, and diode lasers. For simplicity and immediate experimentation, a diode laser was selected for investigation. Laser soldering systems have already been explored, with most including a connecting element for a soldering head, solder wire dispensers, focusing optics, and various pneumatic and electrical actuators, depending on a particular system's design and application. A fully automated system such as this can be considered as the end goal for this project, although largely in its initial phases, a simplistic and manual approach for targeting solder joints is first investigated.

## 1.5 Research Motivation

Traditional AM techniques have largely produced single-function structures in facilitation of rapid prototyping for fit and function design purposes while lowering research and development costs in the creation of proofs-of-concept for testing. When used correctly, AM integration has helped to cut impressive amounts of time and money required for conventional design, prototyping, and manufacturing timeframes, ultimately changing the way companies design and manufacture products. Although widespread in application, rarely have AM produced parts had capability in performing functionalized tasks other than supporting loads or acting as housings for other components. Recently, developments into research of printing functional structures with custom and embedded sensing capability, including formulation of conductive and non-conductive filaments via fused deposition modeling (Marasso, 2018), or printing of channels in otherwise non-conductive materials via vat photo-polymerization to infuse conductive inks to incorporate various sensors and actuators (Sung-Yueh Wu, 2015). These methods of combining dielectrics and non-conductive materials with conductive parts have evolved to alter and complement pre-existing AM approaches into new application fields like that of hybrid additive manufacturing into what is now referred to as 3D printed electronics, where the automated assembly combinations of 3-D printing with non-AM produced parts like wiring and electronics using mechatronic equipment have been adopted to produce 3-D packaging with complex geometries enclosing sophisticated electronics (MacDonald Eric, 2014). These attempts to develop a fabrication process which can endorse both form and functionality simultaneously are driven by the goal of promoting 3-D printing as the preferred manufacturing method for industries involving the use of complex structures. Particularly, in that of the printed circuit board (PCB) industry where electronic components are mechanically supported and electrically connected using conductive tracks, pads, or other features etched from one or more sheet layers of copper laminated onto sheet layers of non-conductive substrates like epoxy resins or glass fibers. Traditional PCB design and fabrication methods can take weeks to produce a functional 2-D PCB prototype, as they require design of a particular printed board on a CAD software before sending the PCB design information to a third-party



manufacturer for production of a limited number of circuits via conventional subtractive manufacturing techniques. Since there are multiple layers in each PCB, the manufacturing process alone can be quite extensive in aligning, pressing, and bonding each layer properly for a secure fit before conducting the etching and solder mask application process. With the influential concept of printing multi-functionality, the multi-step methodology described aims to fabricate 3D printed volumetric circuits which can occupy areas that traditional electronics subassemblies may not. With advancements in integrated circuitry combined with the non-planar freedoms of additive manufacturing, 3D printed electronics can theoretically be designed to fill any space, form, or shape. Functional elements such as sensors and switches are now being integrated into 3D printed products, paving the way for exciting new applications and opportunities (Medina Francisco, 2009).

As methods for functional electronics integration are researched, disadvantages within each approach become transparent. The straightforward integration of multi-material printing contains a limited availability of suitable material combinations, anisotropic conduction properties, and relatively high resistivity's (Dijkshoorn Alexander, 2018). The infusion of conductive inks into printed channels presents the challenge of homogenous filling requiring consistent pressure-driven flows through multiple channel networks, and with respect to electrical interconnections, both can demonstrate variations in contact resistances when subject to mechanical loading or temperature changes (Dijkshoorn Alexander, 2018). Although a hybrid approach can be cumbersome in that it may not allow full freeform placement of conductors (limited to single plane component embedding) and can require extensive mechatronic equipment for wire routing and other tooling, it can incorporate any conductor of choice for a respective application as copper wiring allows for the largest possible current densities and thus minimum losses by resistive heating. Additionally, advances in the 3-D printing process categories of SLA (stereolithography) and FDM, along with their respective hardware and tooling abilities, have begun to enhance various multi-step methodologies with potential for substantial growth to entertain commercialization of such unique fabrication methods in producing three-dimensional electronics. The 'pause and go' hybrid AM

method developed at the W.M. Keck Center utilizes FDM industrial grade printing technology in tandem with micromachining, and has evolved to incorporate various tooling abilities including wire placement and pick and place abilities. With the addition of a laser soldering apparatus capable of soldering connections as small as 0.6 x 0.6 mm in size, an electrical circuit can be embedded and soldered on the surface of or within any FDM produced part. Furthermore, the innate ability of white-colored objects to reflect all visible wavelengths of light that hit them, namely, thermoplastics like polycarbonate or ABS white in color, can receive high intensity heat radiation while experiencing minimal damage from a red near-infrared (NIR) 808 nm semiconductor diode laser beam, facilitating an efficient transfer of heat energy to solder paste volumes alone for effective solder joint creation.

## **1.6 Thesis Objectives**

There are four thesis objectives and are listed as follows:

- Investigate discrete, passive surface mount technology (SMT) in PCB manufacture while defining characteristics, challenges, and behaviors of the constituent materials typically used to enable the greatest metallurgical bonding and solderability.
- Investigate soldering processes to determine the most applicable approach within the context of this application.
- Develop and test a temperature-controlled heat application system including its tooling, programming, and integration within a Techno CNC system for soldering of SMT components on thermoplastic substrates.
- Design and test methods for component embedding and soldering in order to establish adequate and repeatable guidelines for the Multi3D system.

## **Chapter 2**

### **Literature Review**

#### **2.1 Outline**

To begin to provide context for this work, Section 2.2 will aim to deliver a generalized background on additive manufacturing (AM) with emphasis on the material extrusion AM process, also commonly known as fused filament fabrication (FFF), and its role in producing the thermoplastic substrate on to which discrete, passive electronic components are to be actively embedded within for this research. A technology-based classification method of existing manufacturing processes is then applied in Section 2.3 to categorize hybrid manufacturing (HM) techniques based off existing combinations carried out within a single platform, in order to classify the hybrid manufacturing technique used in this work. Traditional PCB fabrication and assembly methods, electronic components, and challenges associated with modern PCB manufacture is reviewed in Section 2.4. This is followed by a basic review of the soldering mechanism with respect to metallurgy and solderability, with emphasis on traditional solders, fluxes, and solder joint design utilized in the PCB industry (Section 2.5). Section 2.6 aims to review and classify existing soldering methods and tooling with emphasis on the reflow process, in order to reinforce selection of laser soldering as the most viable method for integration within the Multi<sup>3D</sup> system. Section 2.7 will review available lasers for soldering along with their defining characteristics. Lastly, Section 2.8 will investigate potential evaluation methods of temperature history for the soldering used in this work, with emphasis on the nondestructive evaluation method of infrared (IR) thermography.

#### **2.2 Material Extrusion and Fused Deposition Modeling (FDM) in Additive Manufacturing**

As previously discussed in Chapter 1, Additive Manufacturing (AM) is a new generation of manufacturing technologies with capabilities of producing three-dimensional objects through layer-by-layer addition of materials with little to no need for tooling respective of traditional

material removal or material formative processes. Since conception, AM has evolved from its initial stages of solely rapid prototype production (RP) with limited hardware and material selections to what is now a variety of different categorized processes, many of which allow for unprecedented freedom in manufacturing complex structures; in what is now a wide range of materials including metals, ceramics, polymers, or in some combination, to form composite, hybrid, or functionally graded materials (FGMs) for fully functional parts (Tofail, 2018). These recent advancements have ultimately paved way for shifts to Direct Digital Manufacturing (DDM), where a high-focus to produce end-use parts directly from digital data is now a revolutionary aspect of advanced additive manufacturing.

Despite the wide range of hardware, methods, and materials used, most AM technologies utilize three main components which aim to encompass the direct digital manufacturing process flow: 1) three-dimensional modeling software (Computer Aided Design or CAD) to create and process a digital model of an object, 2) machine equipment and tools to physically drive and lay material, and 3) a digital control system to instruct equipment to build parts layer-by-layer in some manner. Other fundamental components in between include conversion of the CAD file to stereolithography format (STL), generating tooling commands from the STL file on a slicing software variant, and transfer to an AM fabricator via universal serial bus (USB). Once completion of a part is reached, the part is removed from the AM fabricator and may require post-processing, depending on the AM process. The manner in which materials are deposited upon each successive layer however, let alone bonded, vary largely in principle and process, associated into what is now seven categories (52915:2016, 2016). Table 1 provides the basic additive principles used, as well as example technologies and materials which are typically processed in each of the seven categories. Further categorization of these technologies is typically based on the range of materials processed as well as the extent of product quality, accuracy, and build speed which can be achieved using the many different types of AM fabricators. In consideration of the many commercially available AM fabricators and their origins, a detailed history of additive manufacturing is chronicled which now spans the 30-year period of its existence, beginning with its earliest com-

**Table 1:** Fundamental principles, technology examples, and materials processed for each of the seven process categories per ISO/ASTM 52900 (Tofail et al, 2018)

ASTM Category	Additive Principle	Example Technology	Process Materials
<b>Material Extrusion</b>	Material is selectively dispensed through a nozzle or orifice	<ul style="list-style-type: none"> <li>Fused Deposition Modeling (FDM)</li> <li>Fused Filament Fabrication (FFF)</li> <li>Fused Layer Modelling (FLM)</li> </ul>	<ul style="list-style-type: none"> <li>Polymers</li> <li>Composites</li> <li>Glass</li> </ul>
<b>Powder Bed Fusion</b>	Thermal energy fuses regions of a powder bed	<ul style="list-style-type: none"> <li>Direct Metal Laser Sintering (DMLS)</li> <li>Selective Laser Sintering/Melting (SLS/SLM)</li> <li>Electron Beam Melting (EBM)</li> </ul>	<ul style="list-style-type: none"> <li>Metals</li> <li>Ceramics</li> <li>Polymers</li> <li>Composites</li> <li>Hybrids</li> </ul>
<b>Vat Photopolymerization</b>	Liquid photopolymer in a vat is selectively cured by light-activated polymerization	<ul style="list-style-type: none"> <li>Stereo Lithography (SLA)</li> <li>Digital Light Processing (DLP)</li> </ul>	<ul style="list-style-type: none"> <li>Polymers</li> <li>Polymer/Ceramic Composites</li> </ul>
<b>Binder Jetting</b>	Liquid bonding agent is selectively deposited to join powder materials	<ul style="list-style-type: none"> <li>3D inkjet technology</li> </ul>	<ul style="list-style-type: none"> <li>Polymers</li> <li>Ceramics</li> <li>Composites</li> <li>Metals</li> <li>Hybrids</li> </ul>
<b>Directed Energy Deposition</b>	Focused thermal energy is used to fuse materials by melting as they are deposited	<ul style="list-style-type: none"> <li>Laser Engineered Net Shaping (LENS)</li> <li>Laser Deposition (LD)</li> <li>Electron beam</li> <li>Plasma arc melting</li> </ul>	<ul style="list-style-type: none"> <li>Metals</li> <li>Metal/Ceramic Composites</li> <li>Hybrids</li> </ul>
<b>Sheet Lamination</b>	Sheets of material are bonded to form an object	<ul style="list-style-type: none"> <li>Laminated Object Manufacturing (LOM)</li> <li>Ultrasound Consolidation/Ultrasound Additive Manufacturing (UC/UAM)</li> </ul>	<ul style="list-style-type: none"> <li>Polymers</li> <li>Metals</li> <li>Ceramics</li> <li>Hybrids</li> </ul>
<b>Material Jetting</b>	Droplets of build material are selectively deposited	<ul style="list-style-type: none"> <li>3D inkjet technology</li> <li>Direct ink writing</li> </ul>	<ul style="list-style-type: none"> <li>Polymers</li> <li>Composites</li> <li>Hybrid</li> <li>Biological Materials</li> </ul>

-rcialization of stereolithography in 1987 to the present, including tables of systems, materials, software tools, and emerging technologies (Wohlers, 2020). Despite having existed for over 30 years, AM has only recently risen in popularity amongst technology experts and the public due to

a few key factors, namely, the expiration of founding patents on AM fabricators, high-level governmental focus on AM as an advanced manufacturing process, and the proliferation of low-cost AM printers based largely on material extrusion (Bourell, 2017). The exponential increase of AM technology is mostly attributed to its versatility and low cost for rapid prototyping and manufacturing applications, as well as superior customizability to fabricate complex monolithic structures with micrometer resolutions, all of which have allowed AM to grow into a multibillion-dollar industry (T.J. Horn, 2012).

Of the first AM processes to see extensive development and attention, material extrusion has become a popular AM technology due to the number of available fabricators and low costs of respective hardware. Widespread and inexpensive compatible materials like ABS, Nylon, Polycarbonate, and other production-grade plastics are readily available for purchase and use in manufacturing, industrial, and consumer environments, along with AM fabricators for as low as \$100 USD - \$120,000 USD depending on the quality of performance and accuracy desired by a company or consumer. The material extrusion methodology involves continuously pushing a filament of thermoplastic or composite material through a heated nozzle while selectively depositing that heated material layer by layer to build a 3D object once subsequent layers cool and harden. The nature of this process ultimately allows for convenient deposition of materials with relatively low processing temperatures, and as such, brings the ground breaking ability to manufacture in ambient conditions with no need for vacuum or inert gas environments. Furthermore, polymers' lower melt characteristics and curing temperatures, excellent ability to flow when molten or softened, and chemical stability allow for processing in multiple feed forms such as liquids, powders, pellets, or filaments, make material extrusion a very attractive solution for rapid prototyping and product development (Vyavahare, 2019).

Fused deposition modeling (FDM), sometimes referred to as fused filament fabrication (FFF, trade name variant), is currently the forerunner of the material extrusion process category. FDM is one of the earliest types of AM processes, originally developed and marketed by Stratasys Company in the United States during the early 1990s. The FDM process was invented and patented

by Scott Crump in 1988, where he then founded Stratasys Company in 1989 in Minnesota, followed by sale of its first FDM machine in 1992, the 3D Modeler (T. Wohlers, 2020). As a result of its safe and efficient operation paired with the ability to process engineering-grade thermoplastics, it has become one of the most widely used AM processes in industry for functional prototypes and low volume production. At its most fundamental state, an FDM printer is essentially a computer controlled (CNC) gantry machine equipped with one or several heated extruder nozzle heads, which move along an XY-plane to superimpose multiple layers of melted thermoplastic polymer filament into a predefined area of a fixtureless, heated build stage, and upon completion of that layer, the stage or gantry will adjust itself in the Z-direction by exactly one layer thickness to extrude a subsequent layer above the previous layer's cross-section until completion of the predesigned part. Figure 3 depicts a typical melt-extrusion print head assembly containing a heated liquefier as it is moved over a platform via stepper motor-controlled gantry. Drive wheels draw feedstock filament from a spool of model material to where it is heated into a semiliquid state within a liquefying extrusion head and extruded out as ultrathin beads through a nozzle-orifice of varying diameter. Feedstock filament composed of support material, a low-density structure

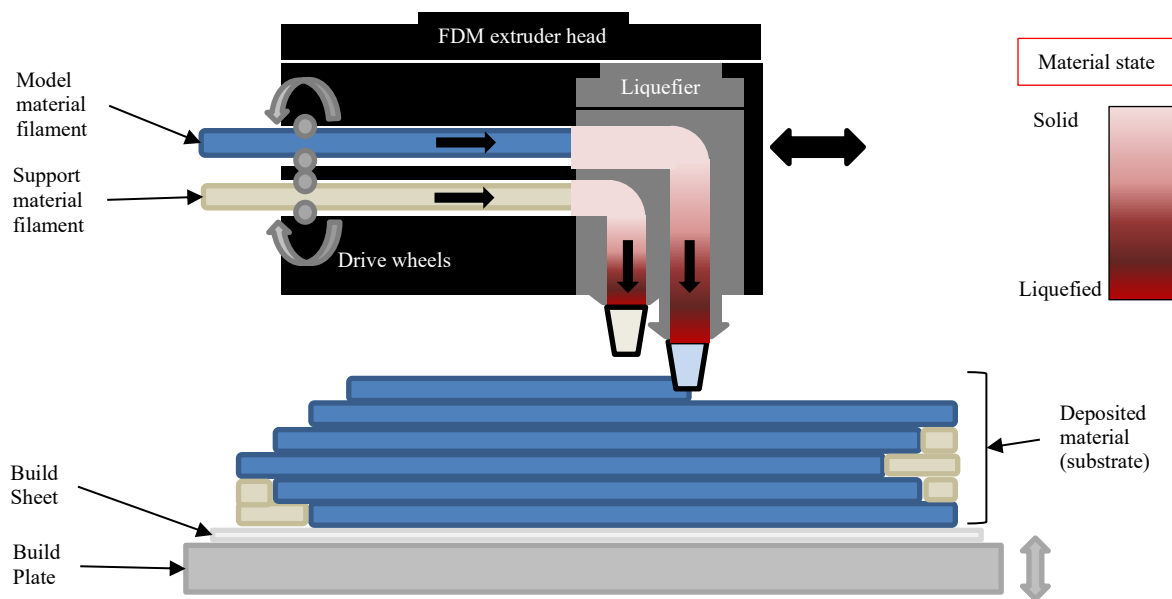


**Figure 3:** Schematic Illustration of FDM process with liquefier head melt states.

typically of the same material as the model material or other sacrificial material, is used for supporting any overhanging sections of a model and is drawn from a separate spool and extruded through a separate adjacent nozzle when needed.

The quality and performance of FDM produced parts depends highly upon the processing parameters, materials used, and their temperature histories during builds. Among the most important processing parameters are contour and raster width along with raster orientation, layer thickness, and air gap sizing left between beads as a result of an extrusion head's traversed toolpaths (Figure 4). The dimensioning of these features are a direct result from other important build parameters such as selection of nozzle tip size ( $\varnothing = 0.010, 0.014, 0.020, 0.020, \text{ or } 0.026 \text{ in.}$ ), tool pathing or infill percentage selections during digital file preparation, and temperature processing conditions, all of which dependent on the Stratasys fabricator being used and its respective capability. In general, low-cost fabricators will offer smaller build volumes with fewer options for changing process parameters to create parts with a varying degree of quality and accuracy, while some high-end machines can offer extremely high precision and accuracy ( $\pm 0.005\text{-in}$ ).

Able to process both amorphous and some semi-crystalline polymers, the deposition of semi-molten thermoplastics creates thermal bonds between beads from a newly deposited layer unto a subsequent layer, as well as adjacent beads within each layer. Amorphous polymers are

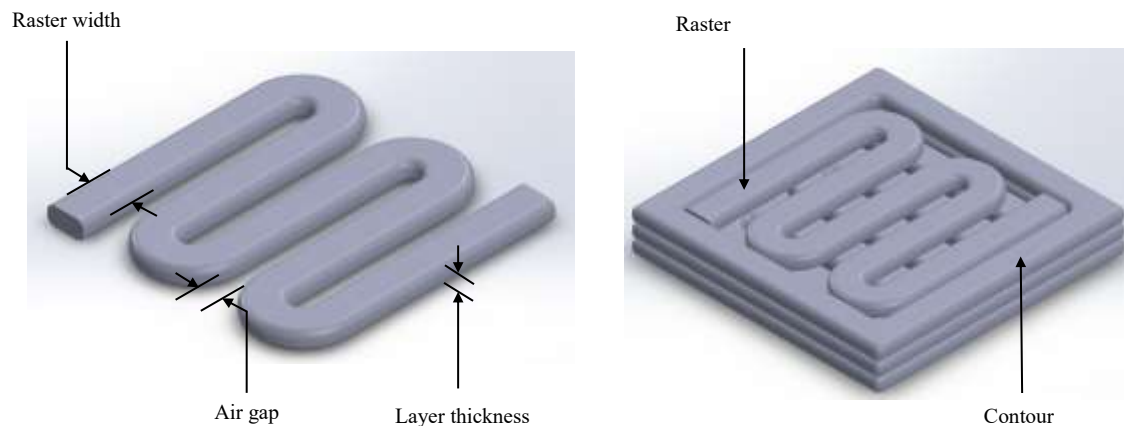


**Figure 4:** Features of deposited material inherent to FDM.



preferred due to their absence of a melting temperature, randomly ordered molecular structure, and a viscous tendency to retain their extruded shape as opposed to the lattice-like order of crystalline polymers, which can induce shrinkage during crystallization and hinder shape retention after extrusion (Gibson et al, 2010). It is for this reason that the thermal history of selected polymers need be understood during their transition from solid to liquid states, including the temperature at which they no longer resemble a glasslike structure (commonly referred to as the glass transition temperature,  $T_g$ ), to their extended heating for elasticity loss to experience desirable flow characteristics during extrusion (Espalin, 2013). The mechanism of fusion between layers depends upon the time taken for solidification, as fibers can only interact with each other while one of them is in a molten condition. As such, the thermal bonds that are created do not have mechanical properties similar to a conventionally manufactured part (Vyavahare and Teraiya, 2020), and in turn, directly impact both density and bonding. Figure 5 portrays thermal bonding between beads from initial stages of surface contact, through to their neck growth and molecular diffusion at interface. It can also be seen from this figure the voids which are naturally left between beads.

As FDM gains popularity and recognition as a production method apart from the design and functional prototype application, key obstacles inhibit its transition to Direct Digital Manufacturing (DDM) and industry wide adoption. The clear disadvantages of weak bonds

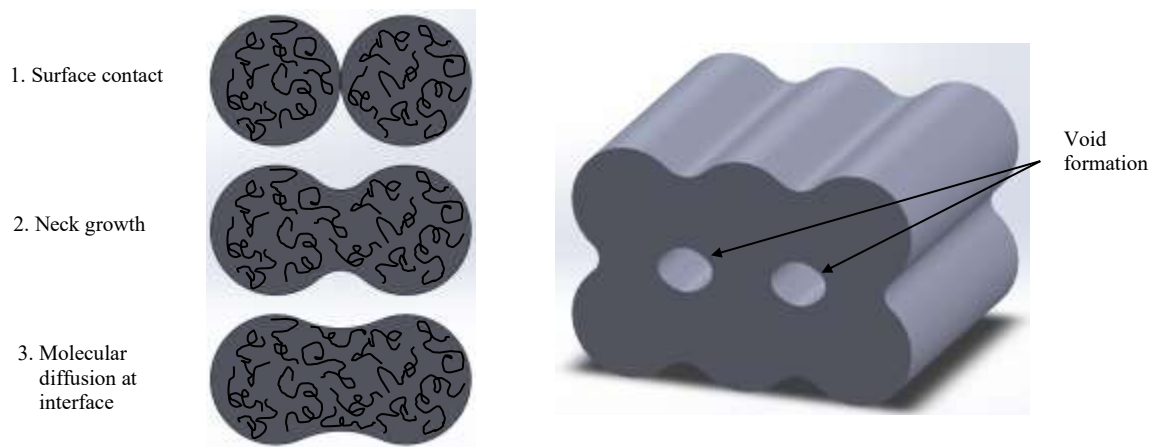


**Figure 5:** Mechanism of bonding between adjacent and interlayer FDM beads (left), void formation inherent to FDM part fabrication (right).

between adjacent beads, interlayer bonding porosity, and weak Z strength anisotropy combine to create difficulty in forecasting the mechanical properties of FDM parts. Other limitations include the limitation to low temperature materials, shrinkage due to thermal gradients within a part during fabrication (warping), low accuracy and resolutions, and poor surface finish. It is for these reasons that the FDM process continues to receive considerable attention in academia and industrial research in the areas of part quality and process improvement, with a large focus on improving interlayer and adjacent bonding between beads via optimization of processing parameters, determination of optimum pressure and temperature conditions, and even implementation of pre-deposition heating systems to promote bonding of polymer fibers and layers (Partain, 2007). Another vast improvement in mitigating void formation, material shrinkage, and the development of internal stresses was originally implemented by Stratasys by intuitively designing their FDM machines to contain temperature controlled build envelopes, which are now a highly sought after design feature for most material extrusion fabricators.

Despite what seems like a multitude of disadvantages in using FDM as a production process, the maturity of this AM technology allows for consistency in speed, accuracy, affordability, ease of use, and an ability to scale parts, which can outweigh its deficiencies depending on the application. In comparison to other AM technologies with capability in processing polymers (SLA and laser sintering), FDM has the advantage of processing a variety of engineering-grade thermoplastics with robust mechanical, thermal, and chemical resistance properties. These include acrylonitrile-butadiene-styrene (ABS), polycarbonate (PC), PC-ABS blends, ABS-M30, and polyetherimide (ULTEM 9085). Table 2.2 lists materials which are commercially available for Stratasys FDM systems including select properties for each. As with other AM technologies, FDM continues to grow in maturity due to research & development of new materials and procedures, better hardware/equipment, and deeper understandings of the physics involved which lead to stable and robust processes. Further expiration of major patents has also allowed the aerospace, electronics, and defense sectors to implement these technologies into new manufacturing strategies without infringing on intellectual property, breeding newfound

resurgence of applications for FDM and other AM technologies within their respective industries (Van Lancker, 2015). Within the context of this application, industrial FDM machines will be used to produce the substrate into which surface mount electronic components will be embedded within for rapid prototyping of circuitry and other electrically and thermally conductive materials. Material selection for the substrate to hold these components is of particular importance to this work, as the coefficient of thermal expansion (CTE) of the substrate chosen should align with that of constituent materials seen in PCB manufacture to reduce thermal expansion in areas for soldering. The substrate chosen should also exhibit a high glass transition temperature and low thermal conductivity in order to survive the reflow soldering method selected in Section 2.6. These concepts are further discussed in the remainder of this chapter.

**Table 2:** Select properties of commercially available FDM materials

FDM Material	Tensile Strength MPa	Tensile Modulus MPa	Glass Transition Temperature °C	Coefficient of Thermal Expansion mm/mm °C	Thermal Conductivity at 23°C W/(m*K)
ABS	22	1,627	104	$10.08 \times 10^{-5}$	0.1
ABS-M30	36	2,413	108	$8.46 \times 10^{-5}$	----
PC	68	2,280	140	$3.80 \times 10^{-5}$	0.19 – 0.22
PC-ABS	41	1,917	125	$7.40 \times 10^{-5}$	3.11
ULTEM-9085	71.64	2,220	186	----	0.22

## 2.3 Hybrid Manufacturing (HM)

Although many are led to believe that additive manufacturing initiated the digital manufacturing revolution, these technologies did not. Rather, AM did much to fuel its development. Digitally driven manufacturing consists of producing physical goods by commanding digital resources. Computer numerical control manufacturing (CNC), a form of subtractive manufacturing (material removal), was the first digital manufacturing technique (Krar

et al., 2001). With its early stages of development spanning from the 1950's through to the 1980's, its then realized potentials set up for its growth and adoption well into the 1990's and beyond; enabling the groundbreaking benefits of distributed manufacturing and customized manufacturing, both of which allowing for a cost effective means of consistently producing durable parts with smooth surface finishes in low volume.

As previously mentioned in Ch. 2.2, it was during this time that the digitally driven additive manufacturing technologies emerged to join CNC as another digital manufacturing technology. It compliments CNC in that there are now multiple means of digital manufacturing. Starting with mostly softer materials (polymers, resins), AM has now shifted into fabricating metal parts due to the coalescence of interest from academia and industry, ultimately paving a way forward as a technology to fabricate metal parts of similar mechanical properties to that of CNC fabricated parts. This concerted expansion to metal processing added capability along with complications, and these complications are really what enabled the birth of hybrid manufacturing (HM). The dilemma of additive manufacturing, well known to the AM community as the 'staircase effect', has been a topic of discussion since the conception of planar-layer manufacturing. Inherent in nature to most AM categories, the staircase effect results from the offset between a parts' printed layers when it's bounding curves vary, and become more evident on slanted or curved surfaces (Yasa et al, 2016). This phenomena not only affects the fitment and tolerance of mating parts within assemblies due to poor surface finish, but greatly influences build times. In general, the thicker the layer produced in a single pass, the faster the cycle time at the cost of further deviation from the intended surface. As such, build times are often extended for better surface finish. With newfound interest in the potentials of metal AM along with realization of its complications, attempts to improve surface finish while limiting cycle-times ushered in implementation of secondary subtractive processes to machine away unwanted staircase artifacts. These included machining operations (turning, milling, CNC machining), abrasive machining, chemical machining, laser surface machining, etc. (Kumbhar and Mulay, 2016), and thus combined for initial traces of HM.

Whether digitally or traditionally (manually) driven, hybrid manufacturing is vaguely considered to be a combination of two or more manufacturing processes. The soft label of hybrid manufacturing was determined from attempts to classify current manufacturing processes into technologies, clarification of different techniques and terms used by researchers, followed by definition, identification, and classification into categories for HM labeling (Zhu, 2013). Nassehi *et al.* (2011) proposed a technology-based classification method of existing manufacturing processes consisting of the five categories listed below, along with examples for each:

1. Joining technology: processes by which two or more parts are joined to form a new part (e.g., welding, assembly).
2. Dividing technology: processes in which parts are divided (e.g., sawing, disassembly).
3. Subtractive technology: processes in which material is removed from a single part to reveal a new part.
4. Transformative technology: processes in which a single part is used to create another part without changes in mass (e.g., forming, heat treatment, cryogenic cooling).
5. Additive technology: processes in which material is added to an existing part to build a new part, typically with increases in mass (e.g., RP, AM, injection molding).

Zhu et al (2013) goes on to assign many of these technologies into hybrid categories based off existing combinations which can be carried out simultaneously or in a serial manner within a single platform. Distinction is made between hybrid and sub-hybrid processes, labeling sub-hybrid processes as those which contain constituent processes within a single manufacturing technology, i.e., hybrid processes which predominantly utilize techniques from one of the single technologies listed above (excluding joining and dividing technologies). Table 2.3 lists the major HM process categories existing in various research areas, along with brief descriptions in part production, general focuses, and example processes for each. As the nature of this thesis work revolves mainly around usage of additive technology (FDM) to fabricate multi-functional parts with embedded

electronics, it's pairing with minor subtractive processing, namely, the machining of material to reveal cavities for placement of small electronic components, a definitive classification of this process remains somewhat indistinct. Essentially a combination of additive and subtractive manufacturing, one could argue that this particular hybrid process aligns more with a hybrid AM methodology; using several mounted tooling heads to deposit various materials for the fabrication of additively manufactured circuitries.

**Table 3:** Classification of fundamental hybrid and sub-hybrid manufacturing processes with descriptions, research areas, and examples

HM Technology	Description	Research Areas	Example(s)
<b>Subtractive</b>	Use of thermal, chemical, electrical, & mechanical combinations to remove materials	Reduce tool wear & production time; improve tolerances & surface finish	CNC machining with laser cutting
<b>Additive</b>	Deposit materials using mounted additive heads	Fabricate multi-functional parts, reduce production time, improve accuracy & bonding	Multi-material deposition using multiple heads
<b>Transformative</b>	Use of various forming techniques to alter, cool, or harden materials	Reduce springback effects, improve formability & mechanical properties	Material forming with heat treatment
<b>Additive &amp; Subtractive</b>	Combinations of additive & subtracting techniques	Increase manufacturing flexibility & near-net part production, reduce staircase effects	Laser cladding with arc welding
<b>Additive &amp; Transformative</b>	Combinations of additive & transformative techniques	Produce multi-material parts, improve feasibility, develop new techniques (in initial stages)	Sheet metal forming with injection molding
<b>Subtractive &amp; Transformative</b>	Combinations of subtractive & transformative	Machining of hard-to-machine materials, prolonged tool life, increased material removal rate	Thermally enhanced machining with heated cutters

## 2.4 Surface Mount Technology (SMT) in PCB Manufacturing

With ever increasing usage of computer technology and electronics in virtually every aspect of modern life, it can become easy to dismiss or disregard the foundation on which they are built: printed circuit boards, most commonly known as PCBs. Their fundamental premise is to laminate conductive pathways on insulated substrates to control and carry electrical current between mechanically supported electronic components via solder. Additive in nature, PCB manufacturing is highly complicated, capital-intensive, and requires large equipment investments

to complete over 50 sequential fabrication steps (LaDou, 2005). As there exist stages in PCB manufacture that utilize subtractive methods (chemical etching) to reveal designated conductive pathways, it can be considered an additive & subtractive approach, although, not a hybrid technology as the process involves multiple workspaces, machines, and manufacturers. The fabrication process may differ slightly in terms of technique and execution depending on the manufacturer, number of intended layers, automated machines used, and component mounting methods, however, typically encompass the major steps listed below:

1. Design and output of PCB layout using PCB design software.
2. Bonding of conductive material to a flexible or rigid polymer, glass, or ceramic substrate (FR-4 glass epoxy most common), typically on both sides.
3. Drilling or punching of holes for layer-to-layer interconnections (VIA's); subsequently "plated through" or coated with conductive material.
4. Image transfer of circuit patterns to substrate from film, glass, or directly from PCB design software image files.
5. Chemical etching or electroplating to remove or build desired traces, respectively.
6. Application of solder resist to areas for bridge prevention to adjacent component leads or pathways during soldering.
7. Testing for proper functionality.
8. Positioning and mounting of various electronic components on respective holes or pads for soldering.

PCB production can be categorized in several general ways. Layer count is fundamental as it represents the overall level of technology. Higher layer accounts (up to 40 layers) are associated with more sophisticated capability, and require repetition of the steps listed above for every double-sided layer before bonding to previous layers. Another major classification lies between flexible or rigid substrate materials and their intended application. Higher-caliber PCBs for commercial or industrial applications usually employ a woven fiberglass substrate material impregnated with epoxy resins (also known as prepregs), which are excellent insulators against

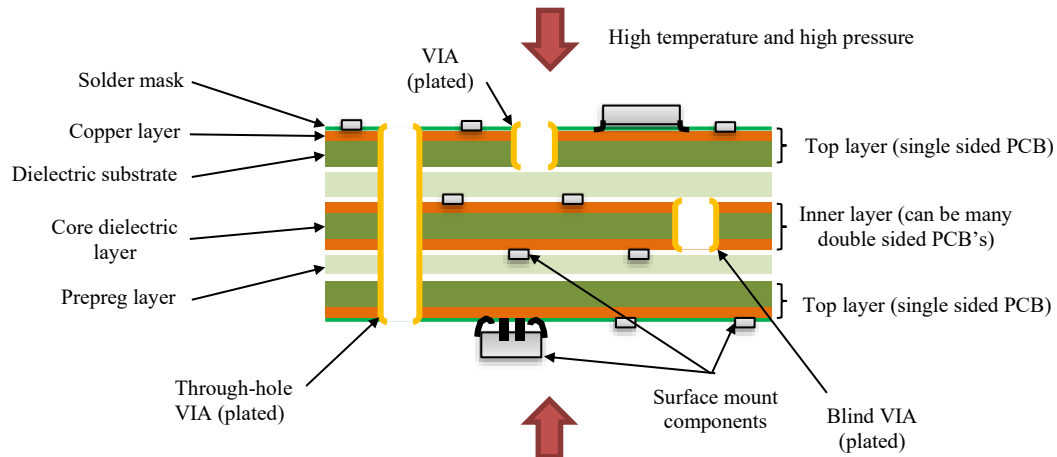


**Figure 6:** Anatomy of a printed circuit board

aggressive environments while contributing to the mechanical strength of a PCB. PCBs for high-power radio-frequency applications favor polymer materials with low dielectric constants to avoid capacitance between layers in a board, in addition to low dissipation factors for minimal dielectric heating. Other methods for categorization include minimum VIA size and trace widths, which affect overall board size (layer count reduction) and routing or interconnect density (LaDou, 2005). Figure 6 shows an example of a multilayer PCB currently seen in industry. Throughout the years, a myriad of changes and adjustments have been implemented to improve to the current assembly concepts. Material developments, computer aided (digital) manufacturing, and advanced packaging techniques are seen as major contributors to its evolution into the multi-layered, flexible, and miniaturized designs seen today. Petherbridge et al. (2004) provides a condensed timeline overviewing the extensive origins and evolution of the different variations and precursors to the design and manufacture of the PCB.

The development of PCB's heavily revolved around the electronic components used and the manner in which they were mounted to these substrate materials. Electronic components can be classified into two main categories, passive and active components. Passive electronic components are those that cannot generate power or gain in their operations, including resistors, capacitors, and inductors. Primary functions include managing busses/bias, acting as by-passes and filters, tuning, converting, sensing, and protecting active circuitry (Gerke, 2005). Active



electronic components are those that generate power or gain in their operations including transistors, diodes, and integrated circuits. Their primary functions are to control the flow of electricity (Das, 2019). Gerke (2005) revealed that almost three-quarters of the total electronic components seen on any typical PCB are solely passive components, providing the composition of 4% connectors, 33% resistors, 40 % capacitors, 5 % integrated circuits, and 18 % miscellaneous parts.

The evolution of passive components from large rounded geometries with long, axially-wired leads to substantially smaller, rectangular components dramatically altered the PCB manufacturing industry. Electronics assembly originally used through-hole-technology (THT) to insert wired-leads of rounded components into two separate drilled holes in the PCB, where leads would protrude out to the other side for soldering. Although THT allowed for strong mechanical bonds to substrates, this technology was expensive, time consuming, limited use to only one side of the PCB, and occupied valuable real estate needed for additional circuit routing (presence of numerous holes). Not until invention and development of semiconductor devices (active electronic components) in the 1960's did surface mount technology (SMT) begin to emerge. The first semiconductor device was a dual in-line package (DIP) with two rows of pins, developed when the restricted number of leads available on transistor-style packages became limited. These devices were mounted in holes already used by resistors and capacitors (Texas Instruments Collection, 1987). DIP's inspired design of hybrid components, which featured surface mount components (SMC's) soldered inside a through-hole or surface mounted ceramic or plastic packaged body (Prasad, 1989). These hybrids also allowed for mounting SMCs on the outer surface of an SMD package as well. Most of the passive components used today were originally made for the hybrid industry, in addition to current placement and soldering techniques.

Demand of higher-density package sizes for active components with larger pin counts further drove development of SMT throughout the 1970's; leaded ceramic or plastic chip carriers (LCCCs or PLCCs) in the U.S. for military applications and industrial markets (respectively), and small outline integrated circuits (SOICs or SOs) in Europe for consumer electronics (Prasad,

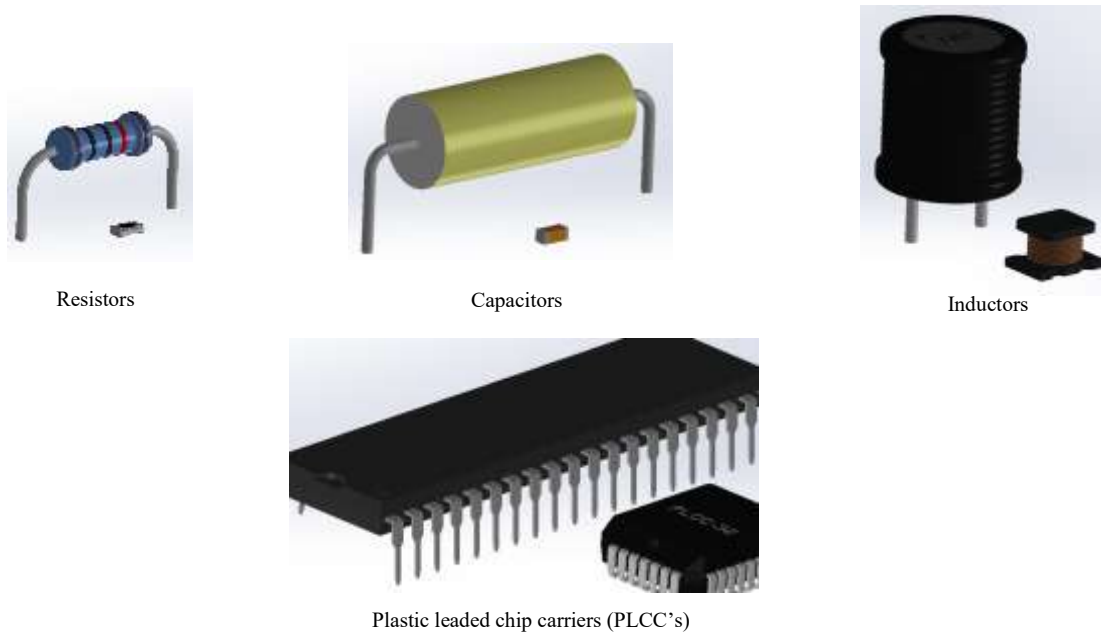


**Figure 7:** SMT passive (top row) and active (bottom) components alongside their through-hole equivalents

1989); into what is now numerous variations of integrated circuits and other SMD's. The trend for continuous miniaturization also led to shortening and bending of SMD leads underneath packages for shorter heights, and eventually, completely removed to resemble modern SMT. Passive electronic components were also continuously miniaturized to fit within constantly shrinking package sizes. Figure 7 depicts examples of passive and active SMT components alongside their through-hole equivalents. Ultimately, the overall merit of SMT is superior performance-cost ratio for PCB manufacture; resulting in increased circuit density, decreased component and board size, shorter interconnectivity, and therefore improved electrical performance and adaptability to automation (Hwang, 1991). Additionally, component mass is typically 10 times less than that of leaded devices, which drove extensive use and mass adoption in automotive and aerospace electronics, rendering them relatively inexpensive.

Since the majority of electronic components seen on PCB's are predominantly passive, this research focuses on implementation of solely passive SMC's, particularly, discrete resistors and capacitors and their mounting methods. The electrical function of SMC's is not unique to SMT;

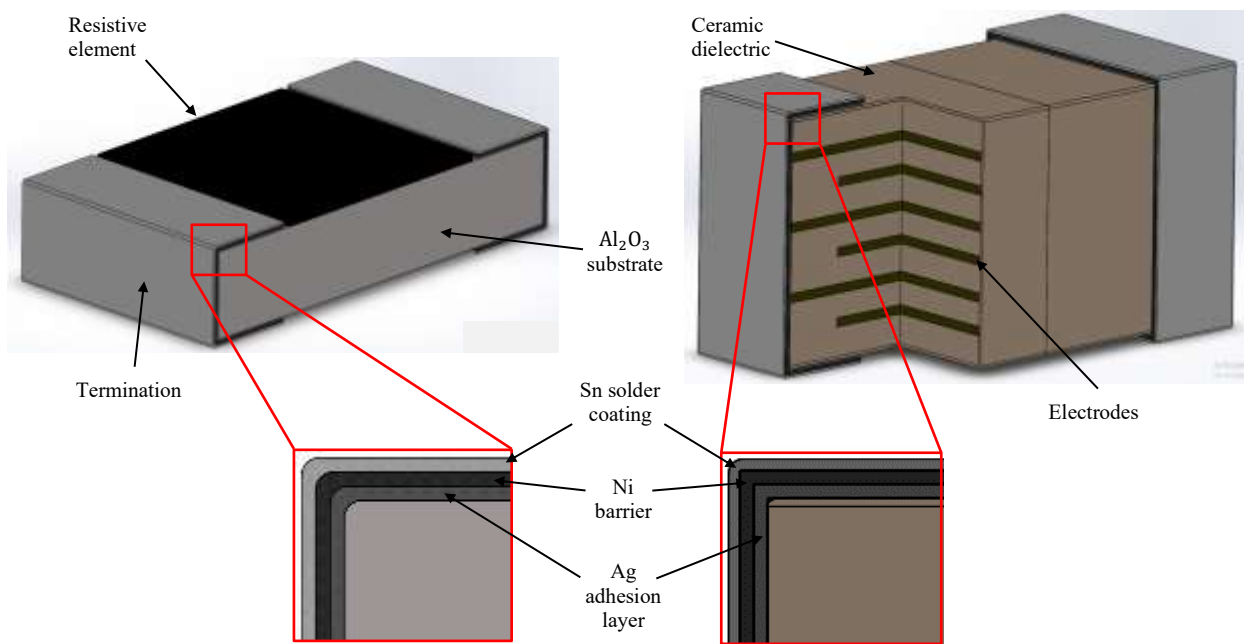


**Figure 8:** Construction details of a surface mount resistor and capacitor

SMD's, active or passive, are functionally no different from their THT counterparts, and as such, out of the scope of this document. Multilayer ceramic capacitors (MLCC's) and thick/thin film resistors form the fundamental passive group. Design and construction details for a SMC resistor and capacitor are shown in Figure 8. Resistors are constructed by screening resistive film (ruthenium oxide based paste or similar material) on a flat, high purity alumina-ceramic substrate surface. Resistance values are obtained by varying the composition of resistive paste before screening and laser trimming the newly formed film. This resistive layer will typically receive a protective glass coating (passivation), and also act to dissipate heat. In place of leads, these components have dipped or electroplated solderable terminations (tin-lead) on each side, mounted with an adhesion layer of silver paste along with a nickel barrier underplating (Prasad, 1989). The nickel barrier is necessary to preserve the solderability of terminations by preventing dissolution of the silver electrode during soldering. Capacitors are similar in construction to that of resistors, with single-layer capacitors forming the bulk of MLCC's due to improved volumetric efficiency. Within a capacitor, electrodes are lined between a ceramic dielectric, with alternate electrodes

connected at each end termination. The terminations will also utilize silver adhesion layers, nickel barriers to prevent leaching, and solder coating layers. SMT resistors are available in various sizes and tolerances (1, 5, 10, and 20%), and come in 1/16, 1/6, and ¼ watt rating in 1Ω to 100 MΩ resistances, while capacitors come in numerous ratings and sizes. Resistance and capacitance values are related to their designated case sizes, and can be referred to in Electronic Industries Association (EIA) and International Electro-technical Commission specifications (IEC).

Despite clear advantages and redirection of the PCB industry towards SMT, its implementation required new design rules, materials, processes, and equipment. Use of smaller components meant much smaller solder joints to withstand the stress associated with PCB manufacture and reliability: mechanical handling, vibration, soldering processes, and temperature fluctuations during its service life. This meant selection and procurement of substrates with matching CTE to prevent generation of stress in solder joints, or development of substrates with compliant top layers, or adding leads to surface mount packages to absorb stress. As SMD's could no longer be mounted within holes, solder pads (locations onto which SMD's were mounted) had to be developed and sized accordingly for adequate metallurgical bonding. This led to extensive research, development, and redesign of solder formulations and soldering strategies, which required new equipment. The difficulty in handling small SMD's also proved difficult with regards to automation, consequently requiring pick-and-place equipment which could place components on circuit boards. Prasad (1991) overviews initial surface mount assembly (SMA) formats used during transition to SMT throughout the 1990's, which included THM, as through-hole components were still used although infrequently. Figure 9 shows the three principal SMA categories which attach surface mount components both active and passive. Type 1 assemblies contain only surface mount components, and can be either single sided or double sided. Their assembly consists of screening, or 'squeegeeing' solder paste onto solder pads, placement of components, then baking of the entire PCB in a convection or infrared oven for soldering. If double-sided, the board would be turned over to repeat process, and previously soldered joints would be reflowed again. Type 3 assemblies contain only discrete surface mount components (now

referred to as chip components) glued to the bottom side with through-hole components inserted on the top surface. The PCB would then be wave soldered in its entirety. Type 2 assemblies, a combination of Type 1 and Type 3 assemblies, were the most difficult to produce due to their numerous process steps. They would almost always require two soldering operations: reflow soldering for surface mount components and wave soldering for through-hole components for a single side.

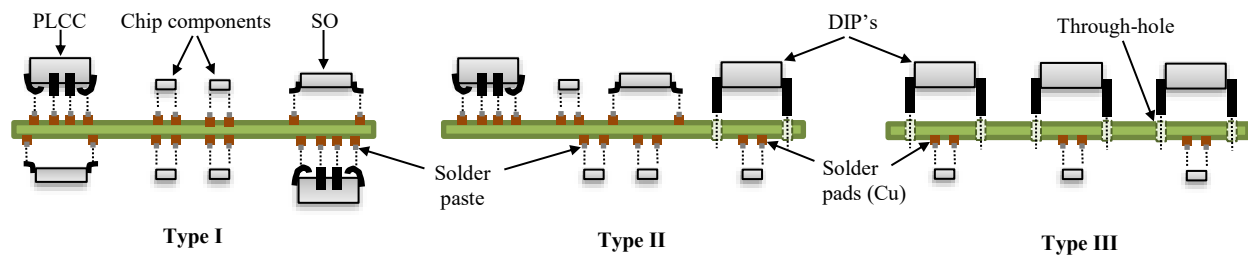


**Figure 9:** Three initial assembly formats used in surface mount technology

As the integrated circuit continued achieving faster speeds by continuously shrinking technology, solutions for passive components also needed to shrink. The number of passive components required by newer technologies at the time required up to 2,200 passive components or more (Prismark Partners, 2000). This led to embedding passive components into the substrate material by fabricating resistors and capacitors during board fabrication by additively placing materials used for manufacturing discrete capacitors and resistors, using similar chemical and electroplating techniques. Resistors and capacitors could be individually embedded as 'singulated' components for particular output values, while capacitors were eventually also embedded as entire 'planar' layers between power and ground planes to achieve higher capacitance values (Gerke, 2005). Figure 10 shows an example of embedded, singulated passives along with an embedded, planar capacitance layer. The switch from discrete SMC's to embedded passives ultimately reduced the amount of space initially required by discrete passives, and the shorter leads and lower inductance of embedded passives improved electrical performance. Additionally, embedded passives did not require solder joints, resulting in greater reliability (Gerke, 2005).

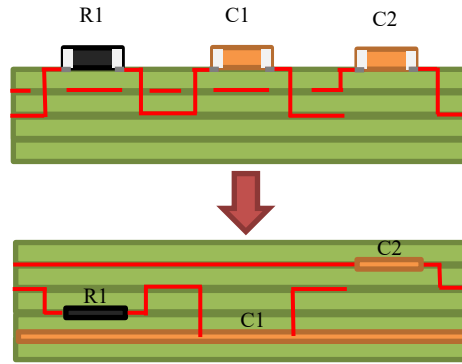


**Figure 10:** Once confined to board surfaces (top), passive components can now be embedded within substrate of PCB's (bottom)

Requiring expensive machinery, usage of hazardous chemicals (etching), and over 50 process steps, the complexity in fabricating PCB's is apparent. Taking and learning from the challenges associated with PCB manufacture, this research aims to investigate embedding discrete passive components at various depths for soldering to enable rapid prototyping of circuitries within a novel hybrid format for substrate fabrication using fused deposition modelling.

## 2.5 Metallurgy of Soldering and Solderability in SMT

The conventional approach of terminating circuitry in the PCB industry is soldering, in which two or more closely fitting items are joined together by inserting and heating a filler metal (solder) to form a solder joint via capillary action. Items for joining are typically coated or composed of two similar metals, or certain dissimilar metals or alloys. The mechanism for joining is governed by formation of intermetallic compounds (IMC) between constituent materials. As such, a basic knowledge of metallurgical properties and phase diagrams is necessary for understanding the principals involved.

Solder is normally a non-ferrous ( $< 1\%$  Fe) alloy. Alloys are materials formed from a combination of two or more elements by means of dissolving and mixing them in a liquid state, followed by freezing into a solid state through a proper solidification process (Hwang, 1991). Solder is typically composed of fusible metal alloys exhibiting a liquidus temperature below  $400^{\circ}\text{C}$ . These include various compositions of tin (Sn), lead (Pb), silver (Ag), bismuth (Bi), indium

(in), antimony (Sb), and cadmium (Cd) (Prasad, 1989). Phase diagrams are useful tools for predicting metallurgical behavior between metals and compounds. They indicate solubility of one metal into another over a range of temperatures, and thus, melting points of various alloy compositions. Most commonly used in the electronics industry are binary and ternary systems, which are phase diagrams containing two elements or compounds (tin-lead) versus three elements or compounds (tin-lead-silver). Figure 11 shows an example phase diagram plotting temperature vs. composition (wt. %) for the binary eutectic system of elements lead ( $\alpha$ ) and tin ( $\beta$ ). At left-most point 'Pb', composition is as follows: Pb - 100%, Sn - 0%. Conversely, Pb - 0%, Sn - 100% at right-most point 'Sn'. The solid lines of the phase diagram represent equilibrium between the liquid and solid phases of the system, with the region above the highest boundary (liquidus line) representing a complete liquid state of the alloy (L) and the region below the centermost boundary (solidus line) representing a complete solid state ( $\alpha + \beta$ ). The leftmost region  $\alpha$  represents the solid solution of tin in lead, while rightmost region  $\beta$  represents the solid solution of lead in tin. The combined liquid and solid solution regions  $\alpha + L$  or  $\beta + L$  can be seen in between, where the composition will resemble a 'pasty' form. From Figure 11, we can denote the maximum solubility

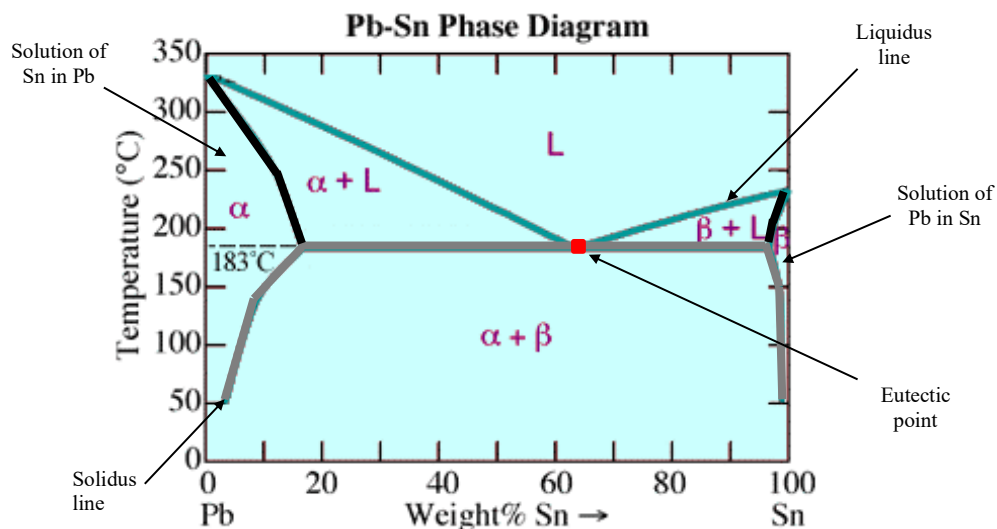


**Figure 11:** Phase diagram plotting temperature vs. composition (wt. %) for the binary eutectic system of elements lead ( $\alpha$ ) and tin ( $\beta$ ).

of tin in lead, or lead in tin, occurs at the eutectic temperature 183°C, the lowest temperature at which melting is observed for this particular composition of 63% Sn with 37% Pb. At temperatures above this eutectic point, the composition will be liquid, whereas any other composition will be pasty (Hwang, 1991). Note that this temperature is lower than that of only tin (327°C) or only lead (231°C).

Traditionally, tin-lead alloys are favored in various proportions due to their lower melting temperatures and are ideal for applications for delicate temperature requirements involving thermally-sensitive electronic components and substrates. They provide good electrical properties, mechanical strength, and resistance to corrosion. However, concerns for negative environmental and human health impacts caused the European Union's Restriction of Hazardous Substances (RoHS) directive to eliminate materials deemed hazardous from products manufactured with solder containing lead, forcing global electronics industries to adopt new lead-free solders (Zhou, 2010). The primary concern in moving away from leaded solder is compromising the integrity of the solder joint. As all connecting constituents expand and contract at different rates during heating and cooling, the joint must be able to remain linked and move without fracturing during the many thermal cycles it will typically experience (Howard, 2006). The tin-silver-copper ternary system consisting of 96.5% Sn, 3% Ag, and 0.5% Cu (SAC305) has shown somewhat promising results as a substitute, albeit with hurdles in solderability, reliability, and other stringent requirements; lead-free solder requires higher processing temperatures which can stress PCB's during manufacture, formed joints are typically brittle in nature, and the formation of tin whiskers in high tin compositions can cause short circuits, to name a few (Jiang et al, 2019). Other varying compositions of silver like SAC387 and SAC405 are also used, as they exhibit true eutectic melting points of 217°C like that of SAC305.

For surface mounting, solder paste is mostly used due to its deformable viscoelastic form, readiness for automation, and easily manageable characteristic (Hwang, 1991). The deformable form allows for easy application in any size and shape, and its tacky characteristics provides capability in holding components in a mounting position without need for adhesives. By definition,



solder paste is a homogenous and kinetically stable mixture of solder powder and flux, which is capable of forming metallurgical bonds at a given set of temperature conditions and can be readily adaptable to automated production in making reliable and consistent solder joints (Hwang, 1991). From a technological standpoint, paste formulation is interdisciplinary; incorporating metallurgy and particle technology, chemistry, physics, rheology, and formulation technology (Hwang, 1991). The metal alloy powder remains the only permanent item after soldering, forming the metallurgical bond. Flux (also known as the vehicle), which can be organic chemicals from carboxylic, amine, and salt groups, ‘activates’ (mobilizes) to join constituent materials in a clean and metallic state but can provide many functions depending on its classification; as a binder, protective layer, wetting catalyst and deoxidizer within the same system. The final performance of a solder paste can be congregated by its applicability, solderability, residue characteristics, and solder joint integrity, with various methods of evaluation. Vendor data and industry specifications, including IPC-SP-819, can be used to establish solder paste specification for vendor qualification (Prasad, 1989). Table 4 lists melting points of select compositions of solder paste used for the electronics industry, including temperature ranges and usage properties. Table 5 lists several types of flux that have been used in industry, for reference.

**Table 4:** Melting point of select compositions of solder for the electronics industry

Composition (wt. %)	Range, Difference (°C)	Properties and Uses
75 Pb/25 In 50 Pb/50 In 25 Pb/75 In	250S-264L, 14 180S-209L, 29 156S-165L, 9	More ductile than Sn/Pb alloys; die attachment, closures, and general circuit assembly
80 Au/ 20 Sn	134S-181L, 47	Highest quality for gold surfaces; die attachment and closures
63 Sn /37 Pb 60 Sn/40 Pb 50 Sn/50 Pb 10 Sn/90 Pb 5 Sn/95 Pb	183E, 0 183S-188L, 5 183S-216L, 33 268S-302L, 34 308S-312L, 4	Widely used for surface mounting and general circuit assembly; low cost and good bonding properties
96.5 Sn/3 Ag/Cu 0.5 95.5 Sn/3.8 Ag/Cu 0.7 95.5 Sn/4 Ag/Cu 0.5	217S-218L, 1	Good resistance, solder joint reliability; developed as replacement for lead based solders in general circuit assembly

**Table 5:** Flux categories and characteristics (courtesy of Hwang, 1991)

Flux Type	Properties and Uses
Type R	Rosin without presence of activator; mildest flux
Type RMA	Rosin activated; contains both rosin and activator; no halides
Type RA	Rosin activated; higher flux strength than RMA; contains halides
Type OA	Organic acid; high fluxing strength and corrosiveness; aqueous cleaning
Type SA	Synthetic activator; equivalent fluxing activity to OA; chlorofluorocarbon and alcohol cleaning

As previously mentioned, the role of surface mount solder joints are critical. They must provide both mechanical and electrical connections and remain reliable as they endure the many conditions involved with continuous PCB use, but also easy to produce repetitively. This is ultimately dependent on the solder and its solderability with all constituent materials. Component leads, terminations, and solder pads must have clean and solderable surfaces in order for good metallurgical bonds to be formed for joining. An accepted definition of “solderability” is the ability to solder easily. If constituent materials do not solder easily, rework costs increase and the reliability of the product is compromised (Prasad, 1989). The fundamental requirement for effective soldering is to provide the right amounts of heat, flux application to prevent oxide formation at elevated temperatures, as well as the right amount of alloy solder paste or wire. Methods for heat application are reviewed in Chapter 2.6. When solder is heated to its melting point, it acts not by melting the base metal but by dissolving a small amount of it to form a layer of intermetallic compound, and upon cooling, holds the parts together by the same attractive forces between adjacent atoms as in the case of any solid metal. The soldering process involves three closely related factors: wetting, alloying and spreading, and joint filling via capillary action.

Wetting is the ability of a liquid to spread over a solid surface. It is essentially a chemical reaction which takes place when one or more elements of the solder react with the base metal being soldered to form an intermetallic compound. Intermetallic compounds are stoichiometric combinations of two or more metal atoms where the atomic fractions of the metals are generally fixed (Hare, 2001). With the case of copper pads soldered with tin-lead paste, an intermetallic layer

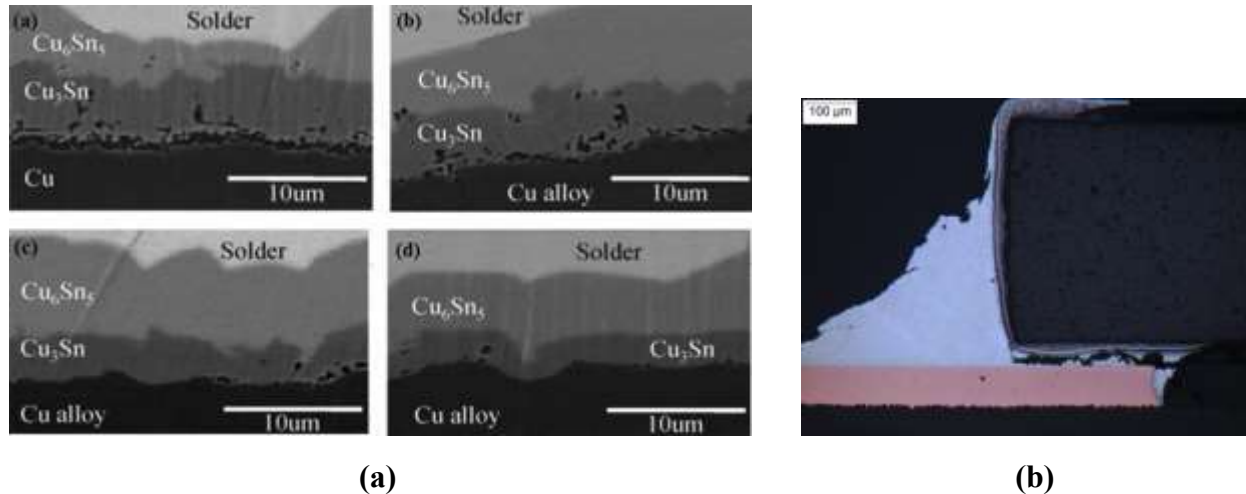


**Figure 12: (a)** Example IMC layers of  $\text{Cu}_3\text{Sn}$  and  $\text{Cu}_6\text{Sn}_5$  formed between bulk solder and a Cu solder pad (courtesy of Jiang et al., 2019) **(b)** solder joint failure between a 1608 resistor and a Cu surface associated with thick IMC formation (courtesy of Element Materials Technology, 2021).

of  $\text{Cu}_6\text{Sn}_5$  will form nearest the bulk of the solder, while an intermetallic layer of  $\text{Cu}_3\text{Sn}$  will form nearest the copper, and is required to occur rapidly to ensure good joint formation (Prasad, 1989). Intermetallic formation is inevitable and once formed, will continue to grow throughout the lifetime of the solder joint during use until eventual crack formation, propagation, and failure. This is why excessive IMC formation has been typically considered an undesired characteristic, as their presence significantly alter both the composition and weaken mechanical performance of the solder joint. As such, scanning electron microscopy is typically performed on cross-sectioned solder joints for microstructural evaluation to ensure thin interfacial layer formation. Figure 12a shows example IMC layers of  $\text{Cu}_3\text{Sn}$  and  $\text{Cu}_6\text{Sn}_5$  formed between bulk solder and a Cu solder pad. Figure 12b shows a solder joint failure between a 1608 resistor termination and a Cu surface associated with thick IMC formation. Thicker IMC layers can be associated with excessive time and temperature involved during soldering, and extremely thin IMC layers are associated with effective time and temperature parameters. Typically, the combination of  $\text{Cu}_6\text{Sn}_5$  and  $\text{Cu}_3\text{Sn}$  layers seem to result in very strong bonds between solder and copper, and is likely to form when in close proximity.

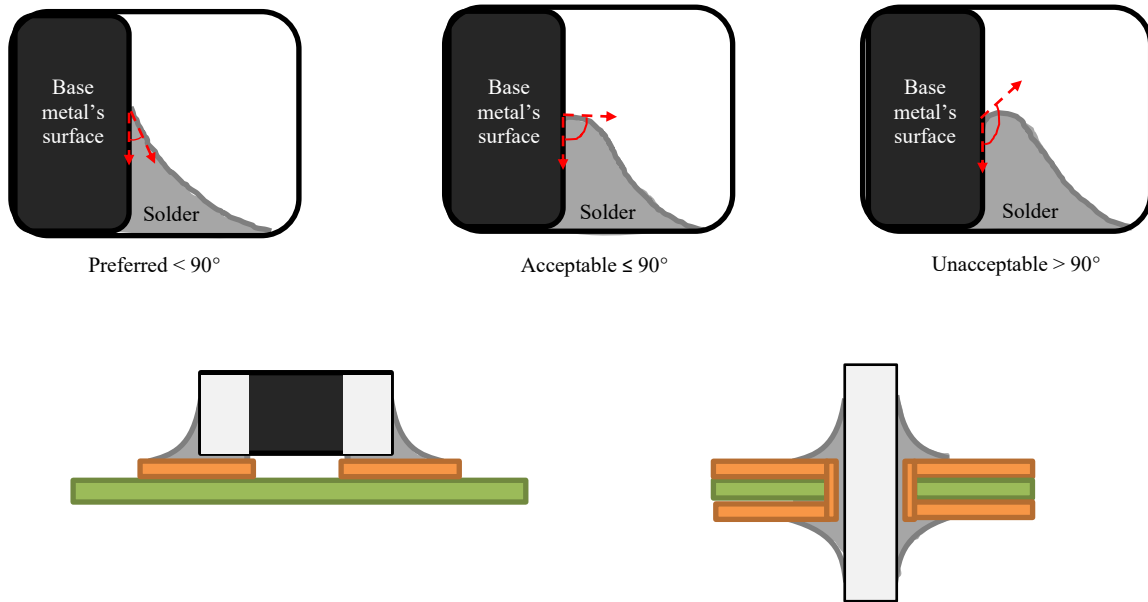


**Figure 13:** Criteria for contact angles in wetting of solder joints (top), desired joint formations for SMC terminations and THC leads (bottom).

Good wetting can be characterized by the angle of contact created on the surface of the base metal after soldering; complete wetting will exhibit a close to  $0^\circ$  angle at a solder joint's edge, while poor wetting (non-wetting) will exhibit a large angle above  $90^\circ$ . The preferred condition will have solder joining less than  $90^\circ$ , although an angle of exactly  $90^\circ$  is still acceptable. Any joint with an angle above said conditions is considered unacceptable as a non-wetted joint. Figure 13 shows the criteria for assessing wetting characteristics in solder joint formation, with a termination or base metal depicted along with a solder joint formed at its vertical surface. An example for proper solder joints for both through-hole and surface mount components is also shown. Concavity along a fillet is desired, along with a smooth and uniform surface. Solder that spreads out and wets the base metal will produce a sound joint between the two surfaces and can be removed only by scraping or filing, implying adequate formation of an intermetallic compound. Good wetting is a desirable property in a solder for making the solder flow smoothly, quickly, and continuously to joint openings, however, is not an absolutely essential requirement for the formation of a bond. As solid metal surfaces are typically not wetted by molten solders (contact angles between  $25^\circ$  and

70°), if molten lead is allowed to solidify in contact with a clean oxide-free steel surface, this can still result in a strongly bonded soldered joint (Shrijit, 2010).

Although, covering a metallic surface in molten solder does not always guarantee proper wetting. If a layer of oxides remain between molten solder and surface, it will not adhere to the base metal and can be easily knocked off during mechanical stress, which will lead to failure during service. Flux is paramount in removing or cleaning surfaces of oxides once activated (heated) during soldering, and the higher the temperature, the lower the surface tension of the solder, allowing better wetting action. The ability of a solder to alloy with the base metal is related to its ability to wet the surface, and also related to the cleanliness of the base metal. Alloying also aids spreading; if the liquid solder dissolves in the solid it can diffuse beneath the oxide layer and detach, thus guiding proper flow of molten solder over the entire surface. The characteristic and degree of spread depend upon the nature of the base metal, the temperature, the presence or absence of flux, the roughness of the metal surface and its degree of oxidation. The maximum spread of tin-lead solders occurs with alloys close to eutectic temperature, with such alloys exhibiting the best flow characteristics in practical soldering.

The manner in which a solder will fill a space between two mating surfaces influences its joint filling capacity and the degree to which the surface imperfections are filled. The fluidity of the molten solder must be such that it can flow into the narrow spaces by capillary action (surface tension). The main factors influencing the effectiveness of joint filling include the wetting angle between the solder and the base metal, clearance of gap between the two surfaces to be joined, heating rate and uniformity, temperature, nature of solder used and the use of flux (Shrijit, 2010). Since solder joints exhibit low strength compared to the metals they are required to join, it is important to design the spaces to be filled between mating faces in close proximity, with some form of mechanical interlocking preferred. This allows solder to easily fill and seal openings, while also improving joint strength. The two most common types of solder joints are the lap joint and the butt joint, with the lap joint preferred as more surface area is in contact for soldering. Complex soldered joints may be made by manual soldering via soldering iron, but for processes employing

automated fluxing, soldering and post-cleaning, chosen designs should remain simple while allowing accessibility to the joint. For optimal capillary action, clearance between mating surfaces must be adequately spaced so that flux may be drawn within. Clearances between 0.07 to 0.12 mm are preferred for most joints to achieve maximum strength, but in some specific cases like soldering of pre-coated metals, clearances can be as low as 0.025 mm (Shrijit, 2010).

The clearance for light metals (aluminum or magnesium) are considerably greater (0.125 – 0.625 mm) than that of copper alloys (0.05 – 0.40 mm). If issues in solubility between solder and alloyed surfaces exist, small clearances may lead to excessive contamination, increase of melting points, or premature solidification (Shrijit, 2010). Such conditions can be remedied to a large extent by faster rates of heating. Uneven heating leads to irregular filling of the gap leading to poor quality joints. Straight joints are difficult to heat evenly, which is why curvilinear joints are preferred, where possible. Composition of solders and the nature of flux used considerably influence the joint filling capacity and quality of the soldered joint.

As ensuring adequate solderability, joint formation, and electrical and mechanical properties from surface mount solder joints is of large concern to solder vendors and PCB manufacturers, various standards, specifications, and guidelines for surface mounting can be obtained from the following sources:

- IEC (International Electrotechnical Commission)
- EIA (Electronics Industries Association)
- IPC (Institute for Interconnection and Packaging Electronic Circuits)

IPC/EIA J-STD-002 provides the general requirements for solderability and soldering of PCB's with their components.

## **2.6 Soldering Methods in SMT**

As discussed in Ch. 2.5, supplying the right amounts of heat to solder for reflow and wetting is crucial in all soldering processes. There are three major requirements for selected solder alloys and the soldering method used; the reflow temperature of the solder alloy must be

compatible with the metallization (coat) used on the components, the substrate, and the reflow system, i.e., the solder alloy should melt around the same temperature as the component's lead coatings and substrate pads. The next requirement involves creating surface tension strong enough to provide a continuous surface between mating surfaces during reflow to reveal desired fillets around discernible mating surfaces upon cooling. Lastly, the strength formed by virtue of the metallic bond should be high enough to provide reliable joints depending on the application.

Typical soldering methods on PCB's involving SMT include wave and reflow soldering. These methods typically involve a three-step process that encompasses preheating of soldering points, applying heat to begin supplying the solder, followed by post-heating to shape and complete a solder joint, typically using special tools and machinery. The basic differences between wave and reflow soldering lie in the source of heat and the solder. In wave soldering for example, vats containing more than 500 pounds of heated, molten solder, mechanically produce a center stream or wave of liquid solder for soldering multiple PCB's in a single pass through its surface on a conveyor belt. The wave serves the dual purpose of supplying both heat and solder (Prasad, 1989). With reflow soldering, a predetermined amount of solder paste is applied and then an external heat source supplies heat for reflow and soldering. Use of industrial machinery for soldering is motivated by repeatedly producing the greatest yield of solder joints while maintaining adequate solder joint properties.

Wave soldering is the preferred method for mass soldering of through-hole mounted assemblies, but was also widely used for soldering discrete surface mounted components glued to the bottom of Type 2 and Type 3 assemblies. Design of plated through-hole leads allows for easy wicking and climbing of molten solder up through their channels via wetting force, and exits out through the top to wet the top portion of the lead followed by spread onto the nearby solder pad before cooling and solidification (Figure 14). Many technical issues have arisen in wave soldering. As the laminar flow of the solder wave has no problem of hitting all through-hole leads if kept at the same height, difficulties in the constant accommodation of targeting various sizes and

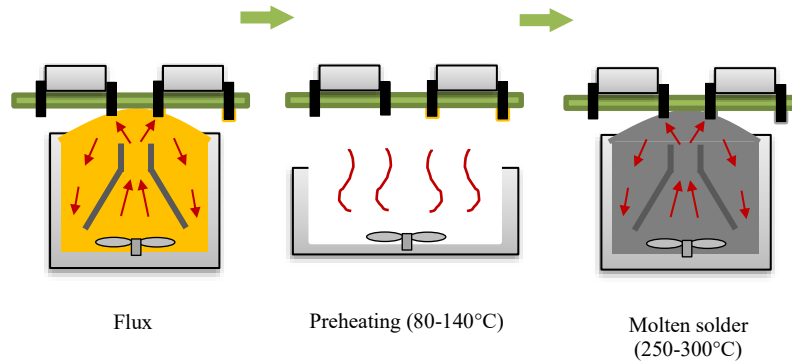


**Figure 14:** Schematic illustration of the wave soldering process.

configurations of SMT components and PCB's have proven expensive. This includes the difficult task of targeting small leads on rectangular SMC's without hitting and damaging center areas, especially the thermally sensitive plastics on PLCC's. Another issue lies in the uneven preheating of PCB's; the higher temperatures of molten solder in vats can be as high as 260°C, and upon passing through a wave, can experience severe residual stresses in other areas of the board, leading to warping. As this process is only applicable to Type 2 and Type 3 assemblies, a specific process flow is required for each side of the PCB, and typically limits applicability of most SMT configurations.

With multiple ways to apply heat, there exists many techniques for heat transfer to a solder paste for reflow soldering. Each technique requires its own particular equipment for heat delivery. The most commonly used reflow methods are the infrared furnace, vapor phase system, convection oven, conductive belt, and laser, with the order given also an approximate order of popularity and frequency of use (Hutchins, 1991). The primary purpose of the reflow process is to melt solder particles, wet surfaces to be joined, and then solidify the solder into a strong metallurgical bond (Hutchins, 1991). Specific temperature profiles are used to ensure proper melting of the solder paste without damaging electronic components in excess heat. This is usually at a peak temperature of 220-250°C, but ultimately depends on the melting point of the metal alloys that a particular solder is composed of.



With consideration of the metallurgical concepts for solder alloy melting discussed in Ch. 2.5, a recommended temperature vs. time profile will be tailored by a manufacturer for that specific alloy composition and will typically look like the profile shown in Figure 15. This profile depicts the phases which occur during a reflow process, with several local and global actions occurring throughout a specific temperature range, or zone. The first phase induces solvent evaporation via preheating of all materials; if preheating is too violent, implosions can occur and cause solder balls to scatter away from intended joining areas, reducing available solder volume to result in weak or open joints, or cause extraneous shorts if they fall between two other leads or conductive pathways. In the next phase, flux activates and melts to begin the chemical cleaning reaction with metal oxides to prepare a clean metal surface for the solder to adhere to. Near the end of this phase, solder spheres begin to melt in the hottest areas of the paste, replacing the flux to wet the nearest metal surfaces. As the next phase is reached, growing wetting action promotes wicking of the solder onto the hottest and cleanest metal surfaces, with the speed of this wetting action highly

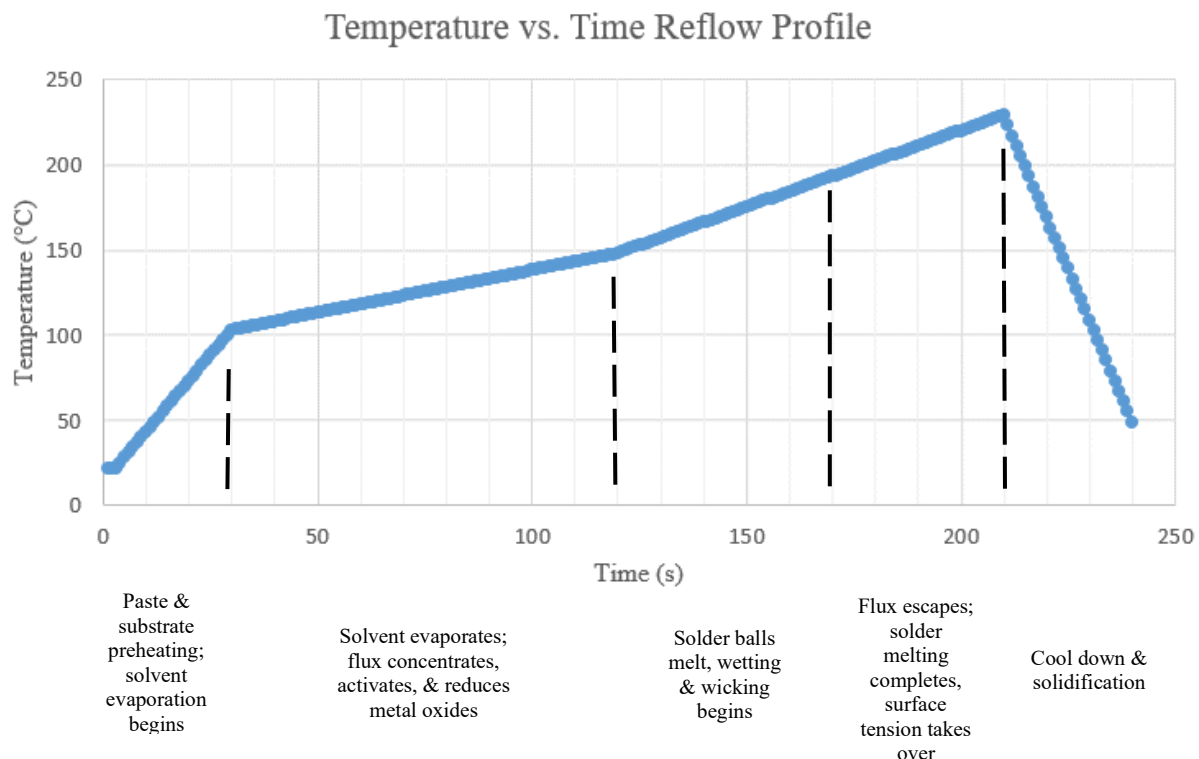


**Figure 15:** Example temperature (°C) vs. time (s) reflow profile for a solder alloy composition.

dependent upon the fluxing action, local temperature, and the metal alloys used for all constituent materials (Hutchins, 1991). Within the second to last phase, any remaining flux breaks out of the general solder volume while remaining reflowed solder volumes coalesce into the general volume through surface tension. The heat source used should reach 20 to 40°C above the selected alloy's melting (liquidus) temperature for at least 1 to 2 seconds to ensure adequate metallurgical bond formation, but no more than 30 to 50 seconds to minimize formation of undesired metallics or damage to the board (Hutchins, 1991). The temperature rise after the eutectic melting temperature will also give additional time for trapped flux or residual solvents to escape, and consequently, minimize void formation as the paste solidifies. These conditions will depend on the localized temperature of the assembly. The final cool down phase allows the fully melted solder paste to solidify, and should be no greater than 3°C/sec to prevent thermal shock damage to some components (Hutchins, 1991). If all conditions and temperatures are reached, then good solder wetting and fillet formation between surfaces can be achieved. Thus, matching of solder paste properties to a reflow environment must enable such actions. It is also important to minimize temperature non-uniformity at and near solder joining areas, but is ultimately dependent on the method of heat application and control of the time-temperature profile.

Infrared (IR) and convection soldering is the most widely used for reflow soldering (or in combination), as they allow for mass soldering of multiple PCB's by traversing them through IR furnaces or convection ovens on conveyor belts, typically through heating zones for different durations to emulate time-temperature profiles. IR soldering involves transfer of heat via absorption of radiant energy transported by electromagnetic waves. The infrared radiation used in this method lies between 0.72 to 1000  $\mu\text{m}$  on the wavelength spectrum, with most useful ranges lying in the short/near wave (0.7 to 3  $\mu\text{m}$ ) to far wave regions (3 to 8  $\mu\text{m}$ ) (Hutchins, 1991). Radiation wavelength is a function of the emitter source's temperature and the reflectance characteristics of objects targeted, i.e., their ability to absorb and reradiate heat energy (Hutchins, 1991). The "volumetric" heat transfer takes place indirectly as the molecular structure of objects absorb IR energy before increasing local temperatures, with organic materials (solder paste, flux,

substrate, etc.) absorbing most of the heat energy. As such, the PCB will get hot first, transfer heat to the solder pads, then the solder piles, then to the leads and/or terminations on components. The major difficulty with IR reflow is that it is not an “equilibrium” method of heating, which suggests that the object being heated will never reach the same temperature as the heat source. Quartz lamps, a common IR heat source, can achieve high temperatures of 1000°C and must surpass the safe reflow temperature of 220°C to enable heat transfer throughout all constituent materials before allowing solder paste to reflow without damaging SMD’s. Additionally, temperature differences throughout the length of a PCB induced by uneven heating (outer areas get hotter than center areas) of various PCB sizes and configurations makes control of time-temperature profiles difficult. PCB

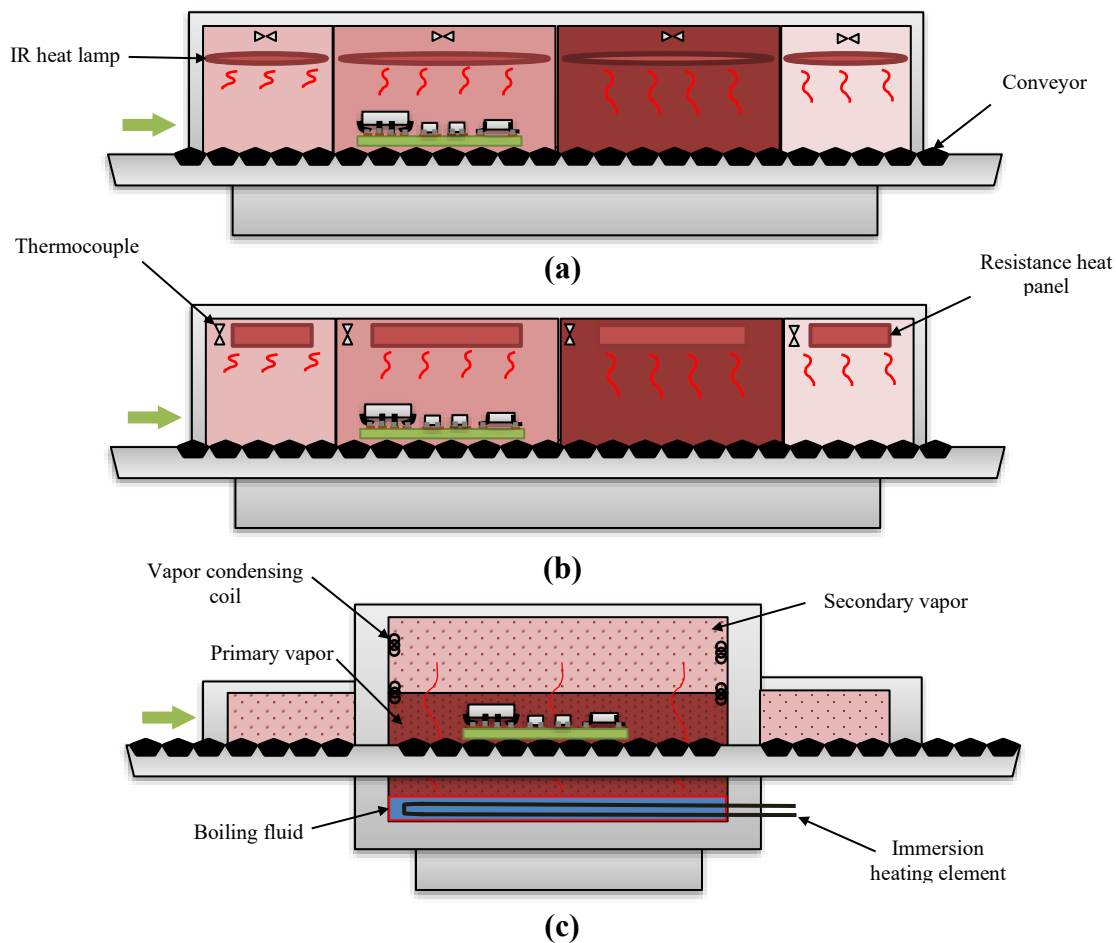


**Figure 16:** Schematic for a (a) in-line infrared, (b) convection, and (c) vapor phase reflow soldering systems.

manufacturers must depend on accurate pulse operation of heaters and belt speed adjustments such that heated PCBs exit a heating zone at the correct time-temperature (Hutchins, 1991).

Similarly, the resistance panel heaters used in convection ovens can reach temperatures of up to 400°C, and typically surpass reflow temperatures for compensation albeit slightly. Convection soldering relies on exposing SMA's to heat in an oven for convective heat transfer, with the temperature of the atmosphere and the speed of the belt making up the time-temperature profile. Vapor phase soldering (VPS) utilizes the same tactics, except instead of an oven or furnace, a deep container filled with boiling liquid will introduce latent heat to PCB's carried through its vapor at different heights for temperature control. The conveyor belt and heated environment pairing with varying techniques for heat transfer encompass the most commonly used combinations for reflow soldering (Figure 16). As these methods utilize multiple systems and tooling with focus in high volume mass production, high cost investment is apparent. Depending on the manufacturer, high equipment capital is acceptable only if a selected method guarantees high performance, operational efficiency, but most importantly, mass production capability to buffer a return of investment. It is for this reason that other lesser known reflow methods like laser soldering (LS), are overlooked.

Soldering via laser involves focusing and pulsing a beam on a desired solder volume until it absorbs enough heat irradiation to reflow. Depending on the design of the laser system used, the non-contact process is typically repeated for each individual solder joint and requires computer control and programming for its movement and focusing. Modern laser soldering systems will typically consist of a laser generator, fiber optic module, focusing optics, a computer vision module with camera, and an X-Y positioning stage (Ogochukwu, 2013). Despite quick reflow times of around 300 milliseconds for superior solder joints, laser soldering is largely associated with slow processing times for SMA's, low efficiencies, and the inability to mass solder (Prasad, 1989). Although, advancements in laser processing technologies in recent decades have evolved to produce more diverse techniques spanning various systems, materials, wavelengths, and time scales, and with higher speeds; enabling it most desirable for use in specialized soldering

applications including microelectronics and rework of solder joints failed during other reflow processes. The major advantage of soldering by laser lies in the ability to direct an energy beam accurately and precisely onto a target area for heating while subjecting surrounding parts to minimal heat, therefore reducing residual stress developed during traditional soldering methods (Beckett et al, 1999). This removes the need to pump heat into materials of high thermal mass (ceramics, metals, etc.), and is particularly useful when thermally sensitive components and thermoplastic materials are present in SMA's. By directing heat only to where required, temperature profiles become easier to measure and reproduce. Additionally, laser soldering allows for more control and versatility in soldering hard to reach areas or curved surfaces, and can be used to target SMD's with lead pitch sizes as small as 0.6 mm without damaging plastic packaging (Vivari and Kasman, 2007).

When considering heat sources as viable candidates for this application, namely, the soldering of discrete SMT components as little as 1.6 x 0.8 mm in size embedded within low melting range polymers, it is clear that conventional soldering methods are not feasible. Despite high customizability of the Multi<sup>3D</sup> system, integration of a controlled environment for heat soaking would be expensive and impractical. Use of these heat sources without an envelope would result in excessive heat loss, rendering them inefficient. Design and automation of tooling for heat application using focused hot air has non-contact potential, but could substantially damage constituent materials and increase the likelihood of compromising substrate design features if glass transition is reached. Implementation of a tip soldering tool requires mechanical contact, and the exceedingly high temperatures reached with a soldering iron could conduct into surrounding areas and also damage materials. Table 2.6 compares select reflow soldering methods with key features, benefits, and limitations within the context of this application, as the industrial focus to achieve high throughputs is not of concern in this area of rapid prototyping. As the substrate materials used in FDM cannot withstand the temperatures seen in industrialized soldering methods or equipment, the only potential options with respect to automation and integration within the Multi<sup>3D</sup> system in FDM cannot withstand the temperatures seen in industrialized soldering methods or equipment the

**Table 6:** Reflow methods – Key features, benefits, and limitations (Hwang, 1991; Vivari and Kasman, 2007).

Reflow Method/ Equipment	Area Heated	Benefits	Limitations
<b>Infrared (IR)</b>	Entire assembly if zone heating is used; area of IR exposure and surrounding areas via conduction if tool is used	<ul style="list-style-type: none"> <li>• Versatile temperature profiling and process parameter control</li> <li>• Non-contact heating</li> <li>• Wide ranging heating area (from 8 mm to theoretically unlimited area)</li> <li>• Easily automated</li> </ul>	<ul style="list-style-type: none"> <li>• Energy absorption is material dependent</li> <li>• Mass, geometry dependence</li> <li>• Impractical equipment setup</li> </ul>
<b>Convection Oven</b>	Entire assembly	<ul style="list-style-type: none"> <li>• Non-contact heating</li> <li>• Quick heating rate with decent temperature control</li> <li>• Uniform heating across assembly</li> <li>• Easily automated</li> </ul>	<ul style="list-style-type: none"> <li>• Damage to sensitive components &amp; plastics</li> <li>• Mass, geometry dependence</li> <li>• Impractical equipment setup</li> </ul>
<b>Vapor Phase</b>	Entire assembly	<ul style="list-style-type: none"> <li>• Uniform temperature</li> <li>• Equilibrium heating system</li> <li>• Easiest technique to use</li> <li>• Geometry independence</li> <li>• Easily automated</li> </ul>	<ul style="list-style-type: none"> <li>• High material &amp; equipment costs</li> <li>• High vapor loss</li> <li>• Damage to sensitive components &amp; plastics</li> <li>• Impractical equipment setup</li> </ul>
<b>Focused Hot Air</b>	Area defined by nozzle design, air dispersion, and conduction	<ul style="list-style-type: none"> <li>• Non-contact heating</li> <li>• More localized than convection oven</li> <li>• Low cost</li> </ul>	<ul style="list-style-type: none"> <li>• Damage to sensitive components &amp; plastics</li> <li>• Tight temperature control</li> <li>• Difficult to automate</li> </ul>
<b>Tip Soldering Iron</b>	Point of contact and surrounding areas via conduction	<ul style="list-style-type: none"> <li>• Low cost</li> <li>• Consistently produces reliable solder joints</li> <li>• Fast soldering process</li> </ul>	<ul style="list-style-type: none"> <li>• Contact heating</li> <li>• Damage to sensitive components &amp; plastics</li> <li>• Heat transfer dependent on surface area contact</li> <li>• Difficult to automate</li> </ul>
<b>Laser</b>	Area of focused beam diameter and surrounding area via conduction	<ul style="list-style-type: none"> <li>• Non-contact heating</li> <li>• Localized, high intensity heating</li> <li>• Versatile temperature profiling and process parameter control</li> <li>• Flexible heating area, as small as 0.6 mm</li> <li>• Precise, repeatable heating</li> <li>• Short reflow time</li> <li>• Superior solder joint with minimal IMC formation</li> <li>• Minimal damage to SMT</li> <li>• Capable reflow of most solder alloys</li> <li>• Easily automated</li> <li>• Line-of-sight targeting</li> </ul>	<ul style="list-style-type: none"> <li>• Energy absorption is material dependent</li> <li>• Typically a one-at-a-time component process</li> <li>• Inability to mass solder</li> <li>• Long processing times for SMA's</li> </ul>

only potential options with respect to automation and integration within the Multi<sup>3D</sup> system are tip soldering, focused hot air, or laser soldering, with the former options presenting high risk of substrate damage and difficulty in automation. A laser soldering tool for this specialized application would lend itself to address the crucial concerns of meeting reflow cycle time requirements, preserving contact-sensitive components and materials, and precise, repeatable targeting of solder joint areas for heating.

## **2.7 Laser Types and Characteristics in Reflow**

Generally, two types of lasers have been used in processing electronic assemblies: carbon dioxide gas (CO<sub>2</sub>) lasers and yttrium-aluminum-garnet/neodymium (YAG-Nd) lasers (Prasad, 1989). Although, advancements in semiconductor physics have brought about the availability of semiconductor (GaAlAs) laser diodes capable of providing continuous wave power of several watts from a single diode, and can be combined with additional diodes to achieve higher powers with greater electrical to optical energy conversion efficiencies (Yan and Takayama, 2020). Differences between each laser lie in the equipment and materials used for the active medium (mechanism used to amplify light), pumping source (mechanism for excitation), resonator (enclosure for the active medium which also acts to amplify), and the wavelength in which they operate. Wavelength is of particular importance when selecting a laser soldering system, as the absorption and reflectance characteristics of constituent materials change at different wavelengths. It will determine the extent to which a material will absorb photonic energy for heating versus reflecting it away; high energy absorbance of surrounding materials can cause burn and damage areas near a solder joint while high reflectivity of metals to be joined (and solder paste itself) will require a wider process window or higher power levels to achieve successful reflow (Ogochukwu, 2013). Other characteristics of importance in laser soldering implementation include size and cost of ownership, energy distribution, and intensity. The size and cost of a system depend on the type of laser used, its beam generation process, and equipment and maintenance required for application. Typically conical in length, energy distribution and intensity will also depend on the

laser used, and can be controlled by end optics to form sharp or distributed energy loadings throughout a selected beam size. Spot size can be adjusted by adjusting the distance of these optics from a laser source, in addition to Z-height positioning of the overall laser head from a work piece. Energy intensity distribution is generally higher and less intense with larger spot sizes, and increases the further away the laser head is from a targeted area. As a laser head is positioned closer to a work piece, its spot size will decrease along with its energy distribution to result in a sharper intensity of heat delivery.

CO<sub>2</sub> gas lasers operate by using electric current to excite nitrogen and CO<sub>2</sub> molecules within the active medium (gas), and upon introduction of helium to the mixture, release photon energy in the form of light (Scott, 2018). The pump source in this case is the electrical discharge of the gas, while the resonator is the tube of mirrors which hold the gas to amplify excitation (Scott, 2018). The CO<sub>2</sub> laser produces far-infrared light at a long wavelength of 10,600 nm with an efficiency of up to 20% (Vivari and Kasman, 2007). One of the earliest forms of laser processing, CO<sub>2</sub> lasers are most often used for metal cutting and welding, but can be used for laser soldering. This laser faced technological and economic adversity which prevented its widespread use for industrial soldering applications despite a higher power, 10-100W range. The far-infrared energy at 10.6  $\mu\text{m}$  is strongly reflected by metallic surfaces and solder paste (around 74%) while undergoing 90% absorption within the organic materials used for flux, printed circuit boards, and other substrates materials. As a result, the risk of burning the circuit board is high by primary or diffused scattered laser radiation (Beckett et al., 1995). Due to its electrical inefficiency and reliance on a maintained gas supply, the CO<sub>2</sub> laser can exhibit high operating costs (Beckett et al., 1997). Additionally, its rather large laser source and inability to deliver laser energy to workspaces via optical fiber is difficult to accommodate.

Nd:YAG laser is a solid state laser, which implies use of an insulating dielectric crystal, glass, or semiconductor material to alter laser energy as light from a lamp or another laser passes through it. The phenomena is based off the concept of population inversion, which occurs when a system's atomic energy is disturbed from external energy pumping, causing a population of atoms



to experience higher, excited states while the rest of the population remain in lower excitation states, leading to inversion and high photon energy emission (Ball, 2006). It uses an Yttrium aluminum garnet doped (introduction of impurities for optical and structural modulation) with neodymium as the active medium (Ogochukwu, 2013). Common pumping sources can include flash lamps, laser diodes, or X-rays (Yan and Takayama, 2020), and its resonator design utilizes two spherical mirrors at various distances from one other for beam propagation (Ezeonu, 2006). Nd:YAG lasers operate in the near-infrared wavelength at 1062 nm as opposed to the CO<sub>2</sub> laser, making it a more desirable candidate for soldering as this end of the spectrum is less reflective on metallic surfaces and less absorbent on organic materials (Vivari and Kasman, 2007). Its unique form of energy and wide-ranging power have enabled its application in manufacturing, electronic, consumer, and medical industries (Myers and McDaniel, 1991). Able to operate above 1000W, beam energies of 10-20 W are used for soldering and have been reported to reach efficiency near 50% (Ogochukwu, 2013). Despite better efficiency in energy conversion compared to CO<sub>2</sub> lasers, Nd:YAG lasers suffer from uneven energy distributions throughout their beam and can worsen the further away it is from a focal point. This reduces the overall amount of energy delivered and can damage materials if energy distribution remains uneven. Costs to operate and maintain are not over encumbering, but implementation of available systems can be costly, with most including all operational equipment within one device, thus requiring mounting of the entire system on a gantry for use. Design of a customized system using fiber optic cables to route beam energy from an off workspace location is possible, but less feasible with existence of other inexpensive, more practical laser systems.

Like the Nd:YAG laser, the diode laser uses a solid material as an active medium but instead utilizes a semiconductor. The diode laser operates via positive voltage application (forward biasing) through its p-n junctions, and achieves population inversion by injecting electrons to combine with electron holes along junction regions to release excess photons (Ogochukwu, 2013). The active medium in this case is the p-n junction of the diode, with the current passing through it acting as the pump source. The resonator consists of the polished, parallel plates of the p-n junction

which act to bounce photons back and forth to produce high intensity laser beams (Ogochukwu, 2013). The semiconductor laser is the most efficient in the solid-state category in terms of electrical to optical energy conversion because it can directly convert electrical energy into laser light and can be powered from a low-voltage DC source. The best semiconductor materials include gallium, gallium aluminum arsenide, and indium gallium arsenide (GaAs, GaAlAs, and InGaAs, respectively) (Steen and Mazumder, 2010). Similar to the Nd:YAG laser, the semiconductor laser operates within the near-infrared wavelengths of 790 to 980 nm, making it an even more desirable option for soldering due to its shorter wavelength. The 808 and 940 nm wavelength are the most commonly used with commercial laser soldering systems due to its high absorption in solder paste (Wolff et al., 2005). The semiconductor diode laser has been known to reach efficiencies of up to 63% and exhibit uniform energy density distribution throughout beam width regardless of size. Depending on the type of diode laser used, most can output power of up to 50W per charge carrier (semiconductor plates), which can be 'stacked' to achieve substantially higher powers if need be (Wolff et al., 2005). Diode lasers in the output power range of 30 to 80W are reported as sufficient for industrial soldering applications (Ogochukwu, 2013), but the desire to produce many solder joints as fast as possible for high yield motivates use of these high powers for instantaneous joint formation. Experimentally, Beckett et al. (1999) found that semiconductor laser power of 3 to 5W is sufficient to solder fine pitch leads by producing sound solder joints on a 208-lead package with leads 0.5 mm wide and with pulses of 600 ms per lead. Further testing on smaller lead sizes of 0.3 revealed similar results at a fraction of the time (200 ms), concluding that power requirements are ultimately dependent upon the mass and thermal conductivity of the joint and surrounding materials. Chaminade et al. (2005) performed an experimental soldering study with a 940 nm diode laser on the temporal evolution through an assembly for different laser powers and interaction times to reveal that high temperatures can be achieved with low power by increasing duration of application. Ultimately, the diode laser can be far superior depending on the application. When compared with CO<sub>2</sub> and Nd:YAG lasers, the technological advantages of the diode laser are clear (Ogochukwu, 2013; Yan and Takayama, 2020):

- Highest absorbance in metals (solder paste, joining surfaces) and lowest absorbance in organic materials (plastic substrates).
- Can be tuned over a broad wavelength, or ‘wave length-locked’ at single value by Al-doping the semiconductor (Guo et al., 2014).
- Quick pulse width modulation response and reliability.
- Maintenance free.
- Uniform energy density distribution
- Inexpensive, flexible, and powerful tool to solve heating problems.
- Can be used for soldering at lower powers due to greater absorption and reflectance characteristics of constituent materials.
- High electrical to optical conversion efficiency with low power requirements and operating costs.
- Ten thousand laser ‘on’ hours before failure.
- Compact size, easy to implement within a system as most have fiber optic cables to carry laser energy from a modulator to a mounted laser head within a workspace.
- Easily automated for analog control in continuous wave or modulation

Advanced diode laser applications can make further use of these advantages; Effective fiber optical focusing systems that can contain servo-operated X-Y positioning tables, computer-controlled positioning mirrors, or even wire feeding systems for dispensing solder paste, all of which can greatly contribute to accurate and consistent beam application and solder joint creation.

## **2.8 Evaluation of Temperature History**

The success of this research is highly dependent on reaching temperatures recommended by a solder paste manufacturer’s time-temperature reflow profile. As such, a means of ensuring the higher temperatures required to induce reflow are reached, which in the case of the Sn 63/Pb 37 solder paste used in this work, must be the eutectic melting point of 183°C at minimum, with a suggested spike of 10°C to 20°C past this temperature for optimal metallurgical bonding. It is also

imperative to model major phase temperatures as closely as possible for a minimum allotted duration, as certain conditions must be met within each phase of laser soldering. Attempts to verify temperature of constituent materials can be difficult in this application, as the selected component package and wire gauge are exceedingly small in size. As many techniques in traditional mass soldering methods contain controlled environments with thermocouples, the temperatures desired are always known and monitored, but require heat soaking an entire assembly. The soldering in this application via laser is conducted in an open environment, and as previously mentioned, would require a selective soldering technology like diode laser soldering to avoid damaging the polymeric substrate materials which could not survive the high temperature environments used for mass soldering. Pyrometers have been used as a means of contactless temperature measurement in combination with diode laser systems, and have become a well-established tool for process control during soldering of miniaturized components while serving as a reliable quality control, with most implemented within a closed-loop feedback system (Reinl and Hoppert, 2011). Unfortunately, the COVID-19 pandemic halted further progression of the tool design process presented in Chapter 4, and so other methods for temperature evaluation were considered. Thermocouples are the simplest and quickest approach to confirm temperature, and easily accommodated for use in a programming architecture to record and output temperature profiles. The difficulty in using thermocouples in this application lies in the size limitation of the hot junction bead at a thermocouple's end and its need to make contact with material surfaces for measurement. The bead, around 1.5 mm, is too large to accommodate for materials of equal or smaller size (termination width is 0.8 mm, 26 AWG wire is 0.4 mm in diameter), and find placement within substrate thicknesses of 2 – 4 mm (test coupon size) that allow for adequate, fixed surface contact. The need to determine temperature history of deposited solder paste droplets is most important, and with volumes as small as  $2.76 \times 10^{-1} \text{ mm}^3$ , simply inserting a thermocouple junction bead into its contents is impractical.

With no direct method to measure absolute temperature, all temperature measuring devices can only measure an effect of temperature, and report these 'pseudo' temperature values based upon measurement of changes seen in these effects (e.g., thermocouples measure temperature with

changes in voltage). IR thermography is a technique that measures the infrared radiation emitted by an object and converts the energy detected into a temperature value (Usamentiaga et al., 2014). An IR camera acts by measuring resistance changes with temperature; done so by utilizing a microbolometer focal plane array of IR detector elements (sensors/pixels) to absorb IR radiation from a heated object and measure resistance as they are being heated. The data from each of the several thousand elements is then digitized for calibration to a temperature, assigned a color or gray scale value, and then presented as an IR image (Yoon et al., 2021). Figure 17 depicts the principal of an Infrared thermal camera receiving radiation. An IR camera not only receives radiation emitted from an object of interest, but also the radiation emitted from other sources such as surrounding objects and the atmosphere. The IR camera receives all observed radiation as an effective temperature, performs mathematical calculations related to the calibration process, and then reports an apparent temperature (Tran et al., 2017). This technique is dependent on appropriately assigning emissivity ( $\epsilon$ ) values of an object's material(s) and accurately inputting atmospheric temperature and moisture levels. The amount of thermal radiation an object emits depends on the emissivity of an object's surface for any particular wavelength and temperature conditions.

Emissivity is defined as the ratio of energy radiated from a material's surface to that radiated from a perfect emitter, known as a blackbody, at the same temperature and wavelength and under the same viewing conditions. The emissivity of a surface will have a value between " $\epsilon = 0$ " (highly reflective) to " $\epsilon = 1$ " (highly absorbent blackbody). If an emissivity value higher than an actual temperature's emissivity is assigned to the sensor/camera, a lower apparent temperature will be output and vice versa. As such, accurate temperature measurements are difficult to make because of emissivity, particularly when there is rapid and variable temperature changes, as emissivity values will change with temperature. If a temperature or range of temperatures is expected for a particular object(s) during an inspection process, knowing the object's sure emissivity value at the known temperature will allow for  $\pm 2\%$  accuracy in pseudo (apparent) temperature reporting, and will deviate in accuracy further from a true value as the temperature deviates within that range (Szafron, 2016). The challenge in this application is confirming a true

temperature at key phases of a solder paste's temperature profile, and adjusting emissivity values within an IR software at each of these phases during analysis. Fortunately, most IR software is extremely powerful and paired with an IR camera of high resolution (the higher the resolution, the larger the number of detector elements) and frame rate (fast action scene capture), allows for streaming, measurement, and recording of infrared data for playback analysis. Additionally within an IR software, several regions of interest (ROI's) can be placed at desired locations which can each be assigned a different emissivity value, and will each output time vs. temperature profiles respectively.

Emissivity values can be assigned based off known emissivity values of a material from literature, or calculated within an IR software. To determine an appropriate emissivity or range of emissivity values, one of the following methods can be used (Transcat, Inc., 2018):

- Determine actual temperature of a material using a sensor such as an RTD or thermocouple, then adjusting the emissivity setting until the correct temperature value is reached.
- For relatively low temperatures (up to 260°C), placing a piece of electrical or masking tape on the object (large enough to cover field of view), measure tape temperature using an emissivity value of  $\epsilon = 0.95$ , and then measuring an adjacent area on the object to adjust the emissivity setting until the same temperature is reached.
- Coating a portion of the surface with a dull black paint, correction fluid, etc., with known emissivity value (these materials typically lie within  $\epsilon = 0.90 - 0.98$ ) and then measuring an adjacent area on the object surface to adjust and match a temperature value.

Other guidelines which help to avoid large deviations in accuracy lie in operating conditions, such as avoiding reflections by shielding an object from surrounding high temperature sources, mounting the camera/sensor perpendicular to a surface whenever emissivity is less than  $\epsilon = 0.9$ , and in all cases, not exceeding angles more than 30° from incidence. With the evident

benefits of non-destructive testing, real time capability in capturing fast moving operations, minimal equipment investments, and easily outputted temperature data of multiple bodies over a large area, IR thermography is an effective and convenient inspection tool. With an infrared (IR) thermography camera available in-house, investigation of its use for temperature evaluation was

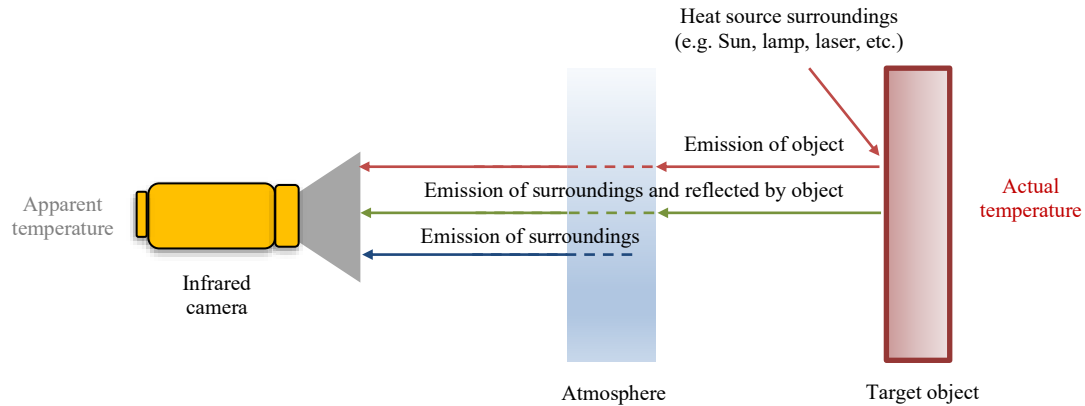


**Figure 17:** Principle of an infrared (IR) thermal camera receiving radiation.

considered for the experimentation presented in this work, with attempts to determine suitable emissivity's for the most accurate pseudo-temperatures reported within its IR analysis software.

## **Chapter 3**

### **Exploratory Work**

#### **3.1 Machining of Cavities for SMD Placement**

As previously discussed in Chapter 1, the Multi<sup>3D</sup> system is a novel manufacturing system which utilizes additive manufacturing in tandem with sub-hybrid and hybrid manufacturing processes to produce conceptual models, prototypes, and multifunctional end-use parts. The system was designed to focus on manufacturing functional 3D printed structures by integrating electronic functionality. It accomplishes this by interrupting builds at predetermined layers within either of the FDM printers, transferring them to a CNC router station via robotic arm for embedding of conductive materials and electronics placement, then returned to the printers for build completion. These multifunctional parts are largely dependent on the enhancement of the technologies mounted on the CNC gantry for electronics integration and their functional compatibility with one another, as the process oriented nature of this system creates interdependence between each. Currently, these technologies include wire embedding tooling for placement of conductive pathways, a machining spindle for cavity creation for electronic devices, pick-and-place equipment for placement of said electronics within respective cavities, and until recently, a soldering tool which can terminate devices to conductive pathways for electronic functionality.

This work leverages over a decade of electronics implementation into polymer substrate materials, which first focused largely on development of tooling and processes which could embed conductive materials (copper wire, mesh, or foils) into substrates for use with sensors, antennas, batteries, and microcontrollers. Previously developed wire embedding tools include a thermal embedding technique which utilized cartridge heaters to force wire into substrates, to what is now two variations of ultrasonic embedding techniques which use varying frequencies of ultrasonic energy to plastically embed wire into substrates. Also in previous works, electronic devices were typically placed within predesigned cavities included during CAD design, with excess wire left



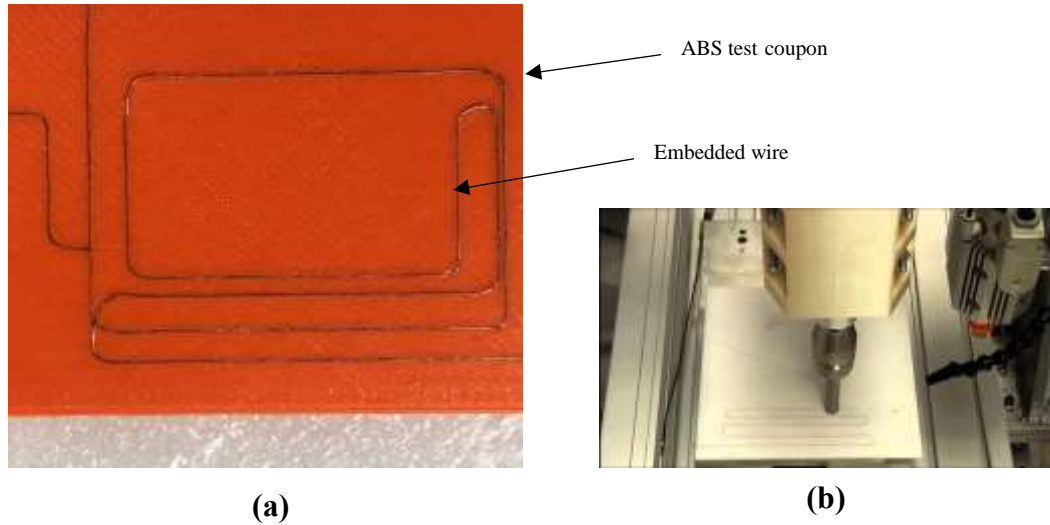
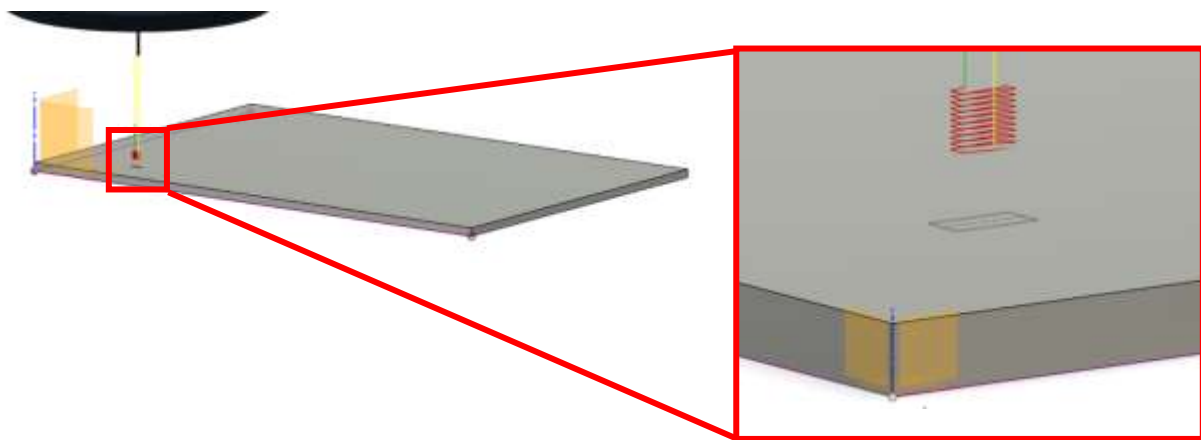


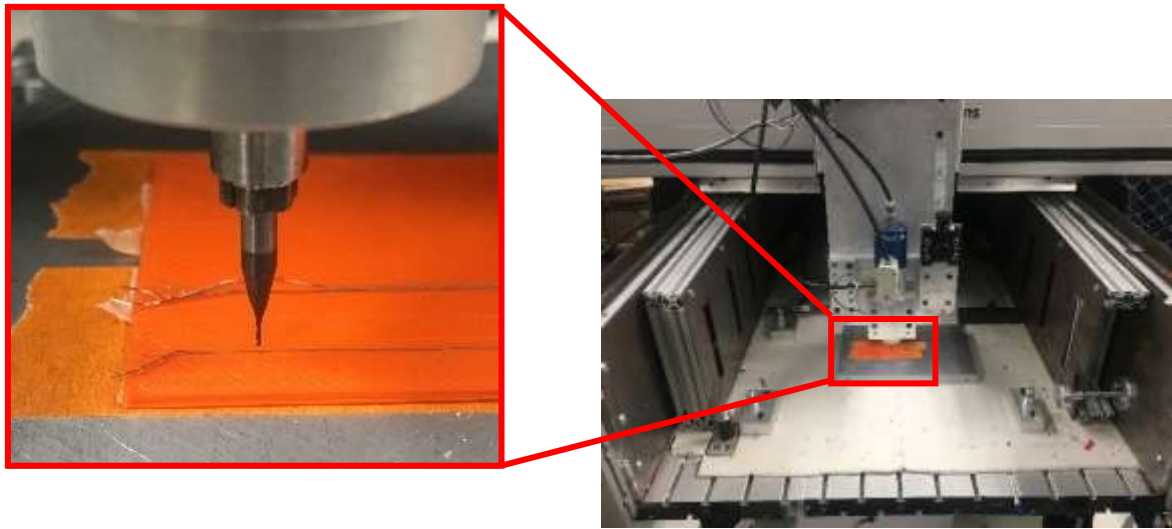
**Figure 18: (a)** Top view of 2 mm thick ABS test coupon with ultrasonically embedded wire, **(b)** ultrasonic horn embedding on 3D printed substrate.

after wire embedding to allow for manual placement on to component leads before soldering with a soldering iron during build interrupts. This chapter reviews initial methods investigated for electronics integration which complement existing methods used in the Multi<sup>3D</sup> system, while also allowing for a smoother implementation of a laser soldering tool. Subsequent sections aim to remove remaining manual steps in the Multi<sup>3D</sup> process plan; including the need to cut excess wire to size for placement onto device leads, by using the machining tool to cut through both embedded wire and substrate material to reveal cavities sized according to component dimensions, and determination of machined cavity sizes which allow for tight, press-fit placement of components within those cavities to avoid adhesive requirements. Additionally, experimentation with a semiconductor laser already available in-house was conducted with two common substrate materials used in FDM.

To resemble a plane, or pause in printing for electronic component insertion, a 50 x 76 x 2 mm thick test coupon of ABS was imprinted using a Fortus 400 mc FDM printer (Stratasys, Grand Prairie) and wire was embedded with 26 AWG copper wire of arbitrary circuit design (Figure 18). Process planning indicates that wire embedding of a potential circuit will be outlined first according to the predesigned cavity layout of its electronic components, followed by placement



(a)



(b)

**Figure 19: (a)** CNC spindle's toolpath on example coupon within Autodesk's Fusion 360 **(b)** front view of CNC routing station and test platform.

and soldering of components within their designated cavities. In order for this to be possible, milling of component cavities must be done via CNC over an embedded wire circuit, as the wire embedding process only allows for placement of a continuous string of wire. Milling of cavities on existing wire configurations means creation leads for laser soldering and integration of electronic components, but also creates the possibility of releasing the plastically embedded wire from its slot. This possibility made way for a machining test to ensure clean cuts and minimal

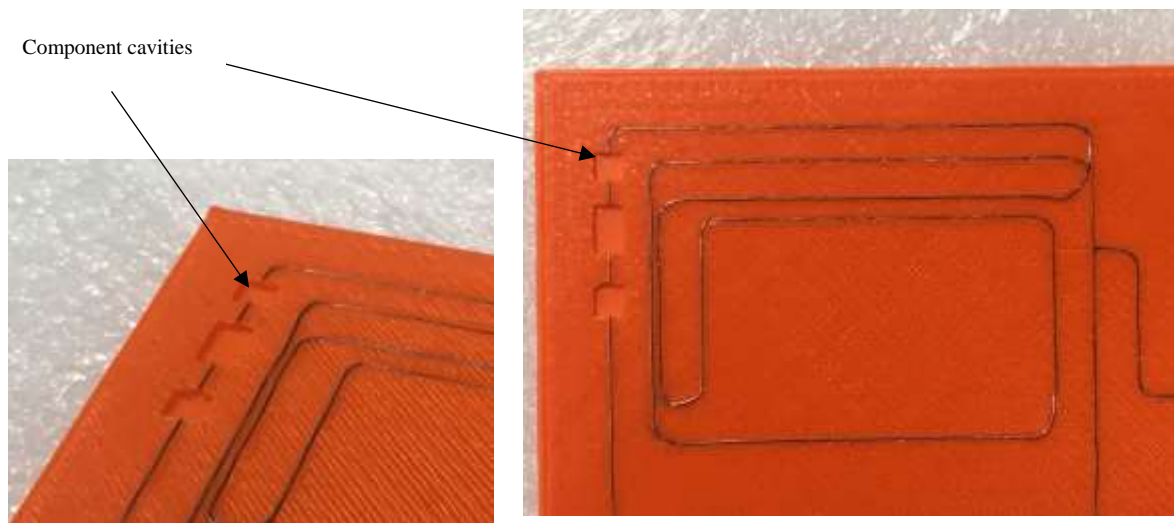


**Figure 20:** Milled cavities for electronic components on ABS 1.18 mm thick test coupon with ultrasonically embedded wire, with closely spaced cavity slots near wire.

invasiveness of embedded wire. Toolpaths for the machining test were created via G-code on Autodesk's Fusion 360 CAM feature and then transferred to the CNC routing station (Figure 19).

Characterization of this test consisted of components sized near the 4532 SMT chip package sizes slots machined directly through embedded wire to assess severed wire at the edge of newly created cavities. An uncoated, 4 flute LOC miniature end mill with 0.5 mm cutting diameter from Harvey Tools was used for machining. Larger component sizes were selected primarily as a starting point for component embedding research (3 x 3 x 0.5 mm, 4 x 3 x 0.8 mm), with the intent on machining gradually smaller slots for smaller SMT package sizes in later experimentation. The shallow machining depths (0.5 and 0.8 mm) were used as a means of assessing cavity quality for reasonably small electronic components at such thin layer thickness. Cavities were created substantially close to one another (5 and 3 mm) in order to determine any possible proximity limitations of milling cavities within such ranges on wire paths. Overall tests show that milling on all embedded wire paths exhibited rather clean cuts and minimal invasiveness of embedded wire along edges of end mill toolpaths. Embedded wire on small surfaces between cavities were also unaffected by the CNC milling (Figure 20). These results reinforce the notion

of successful milling of cavities on 3D-printed and wire embedded substrates for creation of functionalized circuits

### 3.2 Laser Soldering Tests with ABS, Passive SMT Components, and 450 nm Laser

To simulate conditions for accurately placed laser application, a 2000-milliwatt class IIIb blue diode laser of 450 nm wavelength was fastened to a Lulzbot Taz 6 gantry along with a red class-I infrared targeting laser for accuracy (Figure 21). Controlled via CURA software and step sizes of up to 0.3 mm, experimental distances and focal adjustments were made on ‘dummy’ coupons with puddles of solder paste/flux to determine the highest delivery of light energy while exhibiting the smallest possible laser diameter size to accurately hit such small component joint locations. The blue laser was adjusted to its smallest and most concentrated beam diameter (0.5 mm) at 100 mm from the substrate’s surface.

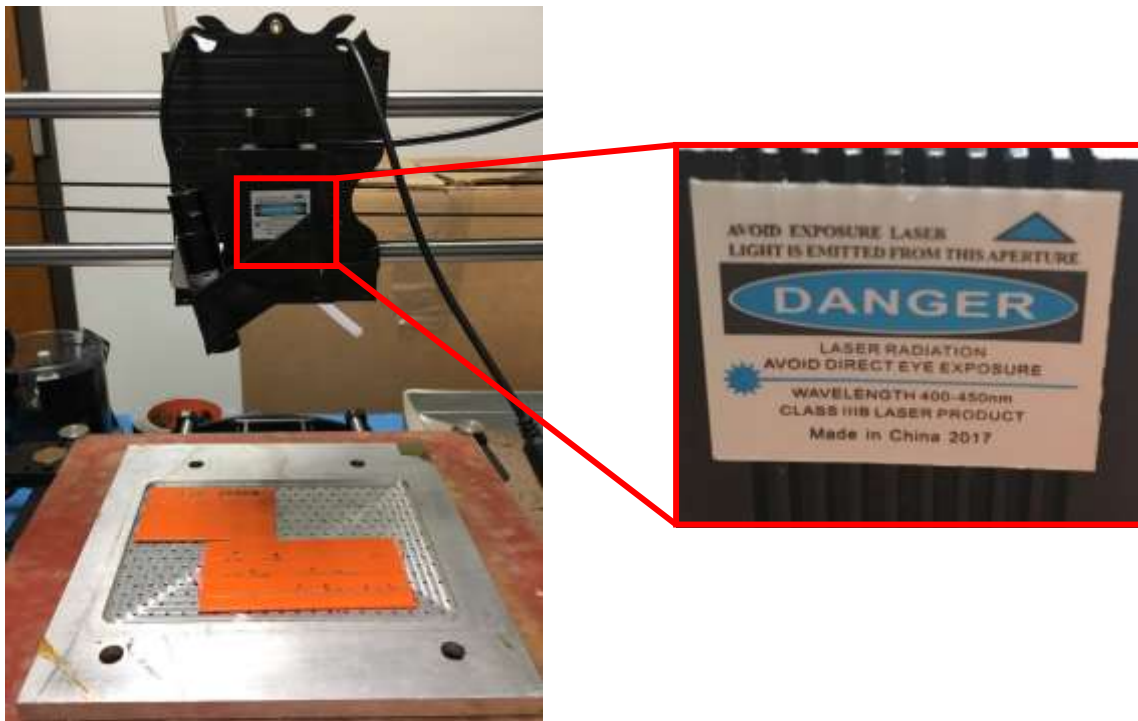


**Figure 21:** Lulzbot Taz-6 gantry with mounted diode and infrared lasers.

With the gantry’s laser and titanium platform placed below for build platform protection, cavities were machined to component dimensions within the 1608 package size (1.6 x 0.8 mm) on

an ABS test coupon 50 x 76 x 2 mm in size. The test coupons contained straight lines of 26 AWG embedded wire with machined cavities sized at 2 x 1 mm for simplicity. Toolpaths were once again generated on Fusion 360's CAM feature, and then transferred to a CNC Router. An uncoated, 4 flute miniature end mill with 0.5 mm cutting diameter was used to machine cavity depths of .35 mm (average height of some capacitors and resistors in the package size). Resulting cavities allowed for snug placement of components within slots (Figure 22). Reasonably small amounts of solder paste/flux were then gently applied on top of connection points via precision paint brushes

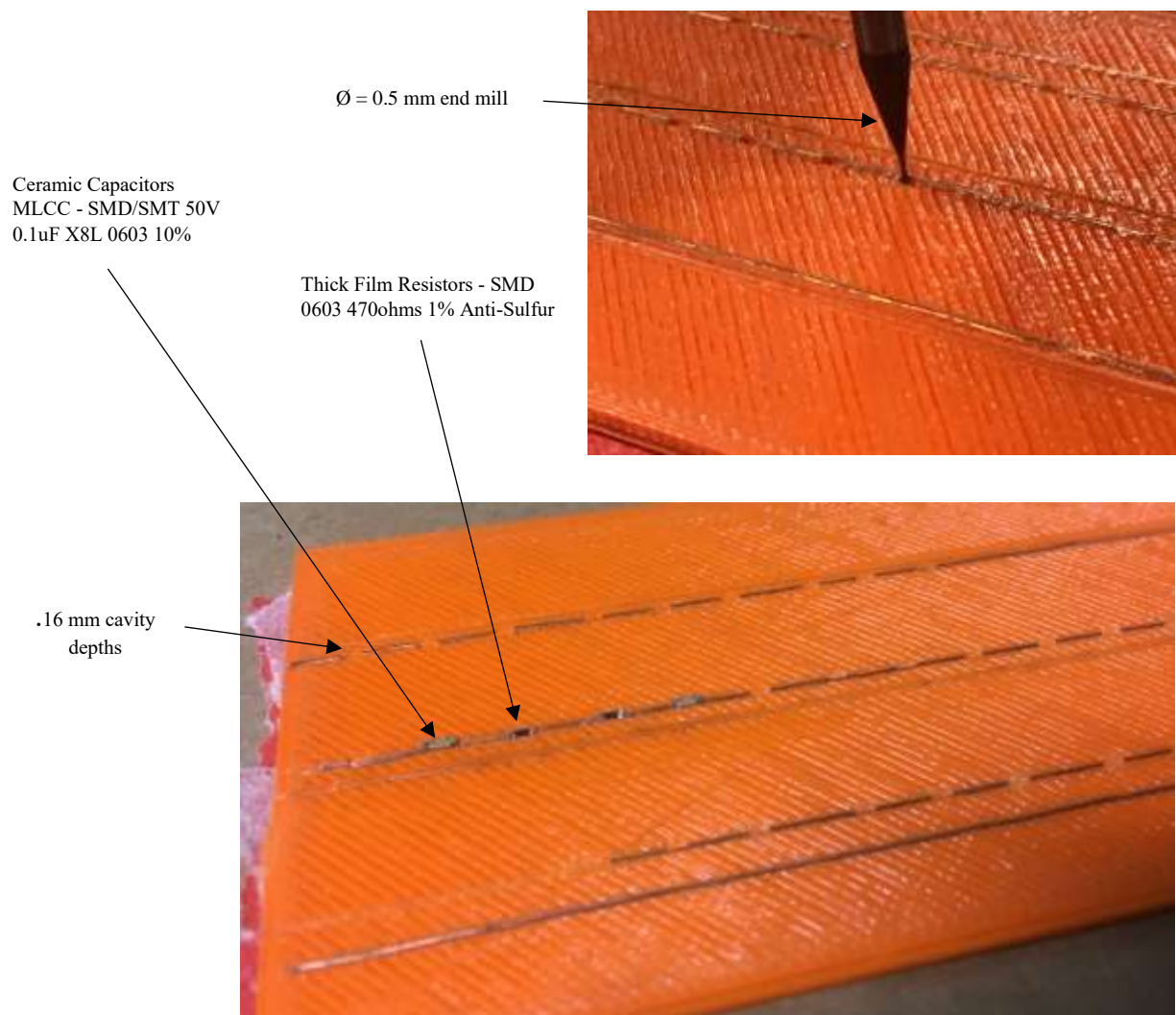


**Figure 22:** Machining of cavities with an  $\text{Ø} = 0.5$  mm end mill (top), placement of components within cavities for solder testing (bottom).



and thin steel rods/prongs in a dabbing fashion, as neat and as accurate as possible (Figure 23a). A second trial included application of paste/flux at inner edges within cavities before component insertion for experimentation (Figure 23b). RA Rosin Flux Paste from MG Chemicals was applied first, followed by CHIPQUIK Sn63/Pb37 T3 Solder Paste on top of the flux. The lead-based solder was selected due to its low melting point and known consistency in producing solder joints. Two tests with different process parameters were conducted, all at the 100 mm distance from the laser but at varying time intervals. Resulting solder joints were then tested for continuity across each termination, then tested for designated ratings of capacitance and resistance. Resulting solder attempts were then inspected on a Leica 7X-90X Microscope (Leica Inc., Buffalo, IL).

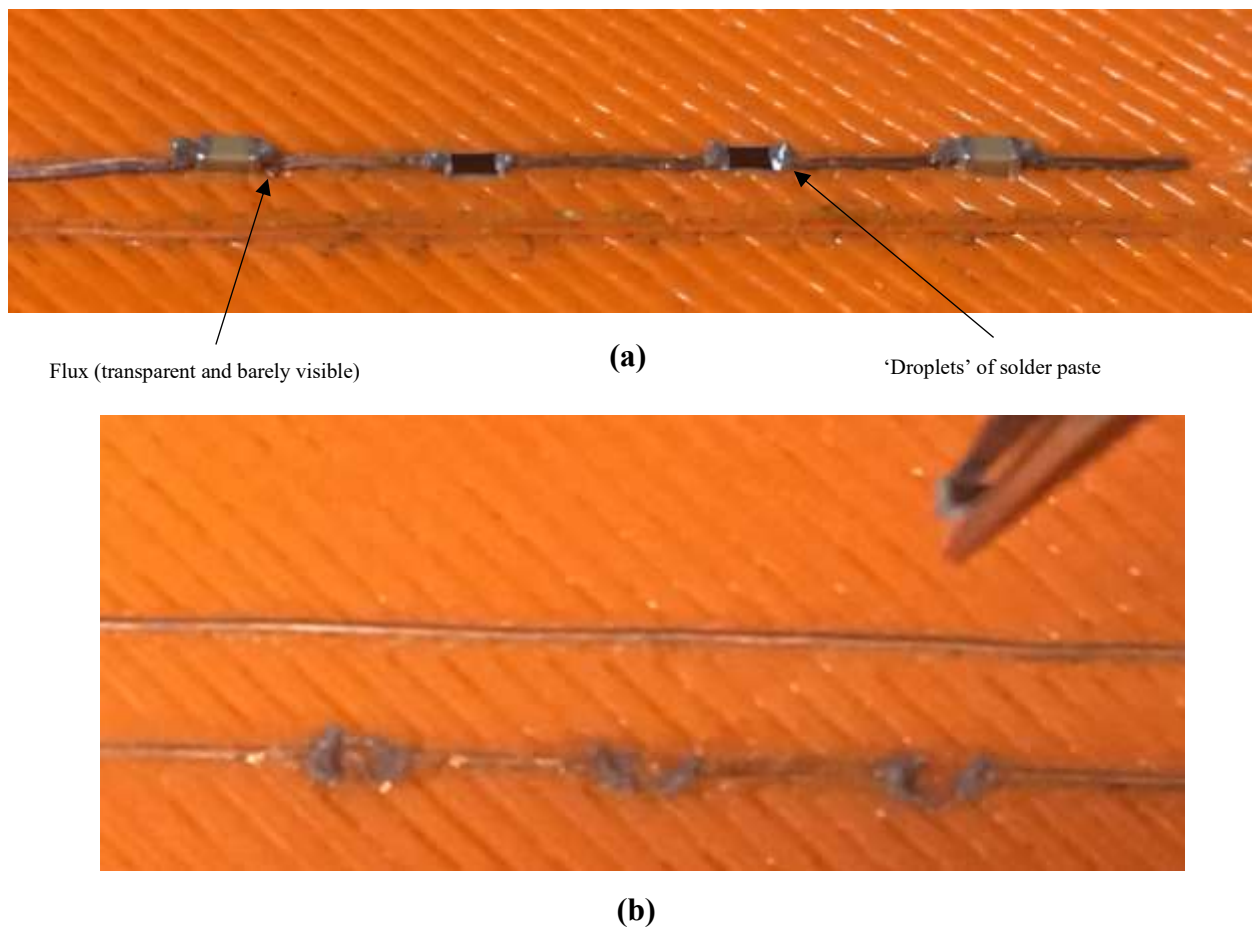


**Figure 23:** (a) Flux/solder paste placement at desired joint locations, (b) pre-applied flux and solder paste along cavity edges.

The first trial focused only on making accurate and complete solders, and because of this were not characterized in any particular manner. This preliminary test-run consisted of laser application duration varying between one and seven seconds, and practice with manual X-Y positioning of the Lulzbot platform and targeting laser. This explains the holes burnt into the substrate while aiming for solder joint locations shown below. Laser spot size was positioned so that one quarter of the beam would hit the components' outer edge, while the other three quarters would hit wire edges, with the intent of heating solder paste droplets and the metallic surfaces for joining. Laser application times over seven seconds were noted to severely damage the 3D-printed substrate, and so signs of reflow activity were closely monitored (shiny and metallic look) before reaching this time period. One second laser application (typical of higher wavelength lasers) was ultimately ineffective; solder particles were still visible with little to no volumes of reflowed solder present, which is indicative of insufficient heat delivery from the 2W laser or poor absorbance characteristics of the paste and metals at this wavelength (Figure 24a). Similarly, laser application times of three seconds performed slightly better but remained widely inconsistent with the majority of paste droplets exhibiting little to no signs of reflow.

At five second application times, only a handful of components were able to produce signs of reflow and multimeter readings, ranging from poor to acceptable solder joints. Figure 24b and Figure 24c show a capacitor and resistor which were able to create acceptable solder joints, albeit with discolorations or burning associated with excessive heat delivery. The right side of the resistor failed by showing characteristics of insufficient heat delivery. Cavities with paste deposited before component insertion were all unsuccessful and not shown, as most of these components either fell out (loose and non-reflowed solder) or were badly damaged potentially due to overheated joints caused by excessive solder paste. It also important to note that inaccurate placement of the laser beam will melt the substrate's surface instantaneously, which in turn requires the highest possible accuracy of beam placement solely on wire leads and component edges. The second test was conducted for repeatability of the better performing 5 second application time. A total of 12 components were tested (all capacitors and resistors), with only 7 of which giving multimeter

readings. Multimeter readings gave values relatively close to components ratings, within 5 ohms for resistors and exact values for capacitors. Aesthetically, resulting solder joints were not much different from solders already seen above.

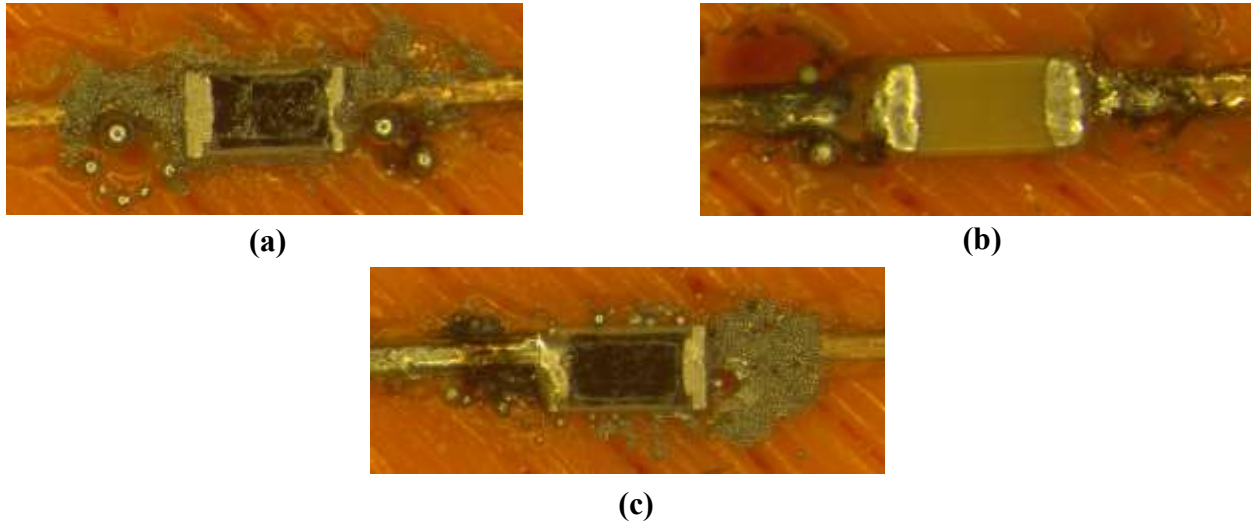


**Figure 24:** (a) Failed solder joint at left and right sides of 50  $\Omega$  resistor, (b) passing capacitor (100nF) with functional solder joints on both sides, (c) resistor failure with acceptable solder joint on left side but failed solder joint at right side.

Solder joint creation with a 450 nm laser was possible, although, highly inconsistent. The majority of attempts either damaged and burned the substrate or failed to coalesce the solder paste into one solid volume. Those which did exhibit signs of reflow, did so ineffectively by producing the solder balling effect (splatter or splitting of central solder volume) notorious for insufficient heat delivery or poor heat absorption of constituent metals to be joined. Solder volumes that were able to reflow and remain coalesced produced acceptable solder joints but showed poor wetting and dull discoloration. These results reinforced the requirement to utilize a laser of proven wavelength which could maximize heat absorption of metal materials while maximizing reflectivity of the organic substrate to improve reflow conditions and avoid substrate damage. Other notable conclusions from these experiments were the importance of machining cavities according to a components actual size which could pinch components in place for soldering, as the undesired capillary phenomena known as tombstoning (pulling of component towards bulk solder



on nearest metallic surface) frequently occurred to pull components away from opposite wire leads or out of cavities during reflow. Additionally, capacitors performed better than resistors, which implies partial protrusion of components from substrate surfaces is better as more surface area is exposed for solder joint creation.

### **3.2 Laser Soldering Tests with Polycarbonate (PC), Passive, and Active SMT Components**

Additional exploratory work involved experimentation with different substrate material and active electronic components for a research collaboration at the time. The same 2 W, 450 nm laser was used due to the long lead time experienced after ordering a new 808 nm laser system, and was mounted on the Multi<sup>3D</sup>'s CNC gantry to produce an orthogonal delivery of energy. The project involved fabrication of a sensor device consolidated from multiple PCB circuits in a housing to a monolithic FDM build which could stack the circuitry within its structure.

To resemble a plane, or pause in printing for electronic component insertion, two (35 x 30 x 4 mm thick) test coupons of white Polycarbonate were extruded and ultrasonically embedded with 26 AWG copper wire of arbitrary circuit design. White Polycarbonate was selected versus orange ABS due to its higher heat deflection temperature and its substantially lower tendency to thermally expand. The white color was selected due to its ability to better reflect irradiated laser energy to reduce the potential of substrate damage. Figure 25 depicts a top view of the two test coupons within SolidWorks, with black/blue circuit pathways concentrated within the upper half of the substrate to simulate actual allotted space for such a schematic; with bottom halves of each substrate meant to resemble space which could be used by other electronics. Rectangular cavities present in CAD images resemble the intended placements of SMD's while round cavities resemble plane interconnection VIA's seen within industrial PCB's. The smaller rectangular cavities were designed to press-fit and hold two 1608 50 V 0.1uF MLC capacitors and three 1608 49.9  $\Omega$  resistors, with the larger rectangular cavity to hold one high speed wideband operational amplifier with Stable FET-Input. The rectangular pockets along the left and right edges of the top plane are to serve as locations where free wire is to protrude off of the test coupons for the circuit testing.

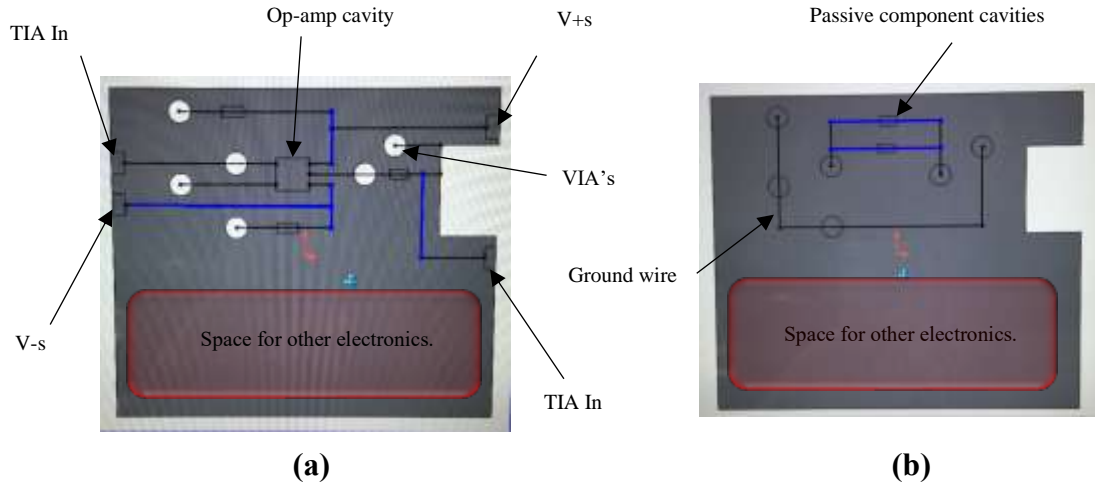


**Figure 25: (a) CAD of top plane of circuit, (b) CAD of bottom plane of circuit.**

The two on the left edge were TIA input and V-S connections while the two on the right edge were TIA output and V+S connections. These input and output feature locations were included during CAD and produced along with the print as opposed to machining.

In accordance with previous works, all cavities created via machining were preprocessed on Autodesk's Fusion 360 computer aided manufacturing software (CAM) to generate GCODE for the CNC, and all wire embedded traces generated on Solid work's DXF format to emulate the pathways needed to communicate to the CNC as well. Laser distances remained 100 mm from solder joint locations with five second application times. Multimeter tests were also performed in order to test solder joint connections (continuity, capacitance, resistance). Notable changes in the process plan included machining of 'junction cavities' 1 x 1 mm in size before wire embedding. The additional vacant cavities were to serve as node locations for wire joining, and the removal of dielectric material from these locations allows for less likelihood of plastic melting to contaminate or interfere with the localized heating process during reflow. Adjoining wire pathways travelling through these locations were subsequently embedded over one another to overlap and make contact for joining during laser soldering.

Figure 26 shows a comparison of the final results for a pair of the many top and bottom planes fabricated. The densely packed regions of circuitry proved difficult in replicating desired

pathways, as the orifice of the ultrasonic horn used at the time was of large diameter ( $\varnothing = 0.5 \text{ mm}$ ) and allowed for wire to stray from intended embedding lines. Additionally, wire frequently fell out during embedding of adjacent pathways as the ultrasonic thermal energy often moves substrate surfaces past their glass transition temperature, and with the combined heat and vibration activity, loosens and displaces wire. Ultrasonic embedding would also tend to darken the white polycarbonate substrate and smooth design features (cavity edges), and would worsen when multiple ‘rubbing’ passes were required. This is especially evident near the op-amp cavity, where the need to embed three closely spaced wire traces proved exceedingly difficult. Laser soldering results remained inconsistent, exhibiting much of the same behavior seen in the previous section. Some solder joint locations showed no signs of reflow and would only soften and disperse to contaminate the substrate as the binder (flux) was heated. Solder balling and splatter seemed more

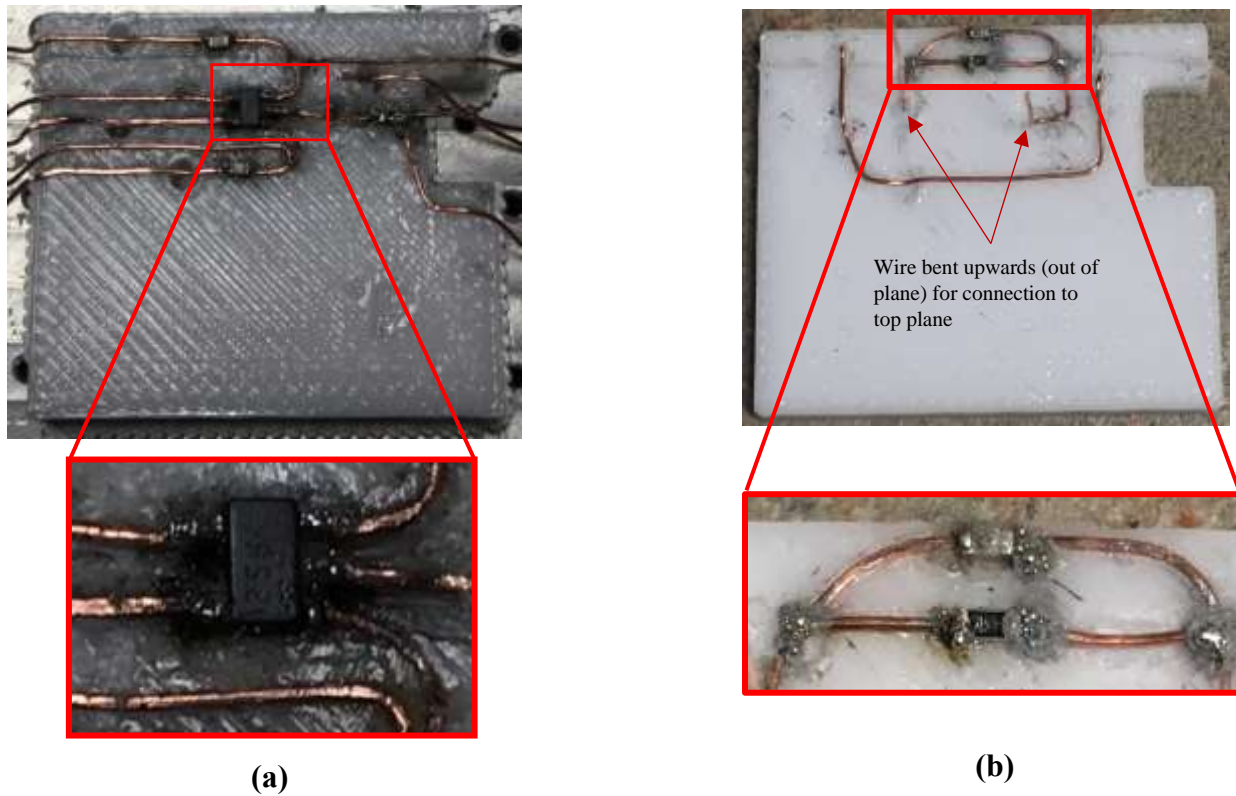


**Figure 26: (a)** Resulting top plane portion of circuit **(b)** resulting bottom plane portion of circuit.

frequent for solder joints which did reach reflow activity, which can be indicative of even less localized heating of the area due to the lower absorption characteristics of white polycarbonate, and thus less heat exuded near the solder paste and metal surfaces. Solder joints which did reflow into a single mass resulted in spherical joints, which although unified, indicates insufficient heat delivery for desirable wetting characteristics. Laser soldering of op-amp leads also proved difficult; despite accuracy in targeting solder joint locations, even less signs of reflow were present. Solder volumes at each leg required additional application times of seven seconds in order to form solder joints, likely due to the higher thermal mass of the larger leads.

Ultimately, laser soldering was possible to form solder joints for these circuits but were mechanically weak and exhibited undesirable reflow and wetting characteristics. Fortunately, the white polycarbonate material proved resilient to burning as little to no solder locations were damaged, leading to its use as the substrate material going forward in this research. The combination of the technologies used for these tools also proved unsatisfactory for this manufacturing system and inspired redesign of both tools and their methods for a more complementary process plan.

### **3.4 Process Plan Improvements**

By this stage of the project, the second version of the ultrasonic wire embedding tool had been developed for use in conjunction with a newly designed laser soldering system presented in Chapter 4. The exploratory work in this Chapter motivated changes in the process plan, with two minor yet impactful changes that substantially improved the flow and compatibility of the secondary operations performed within the CNC workspace.

The first involved preprinting of channels for copper wire placement, outlined according to a circuit's design within the CAD design of a part. This technique would address many of the issues faced during exploratory work, namely, the inaccuracy and inability to embed wire at a required location due to the wandering of copper wire within the orifice of an ultrasonic horn, and the tendency of wire to displace itself during the embedding process at higher ultrasonic

frequencies. The tight press-fit placement of wire within these channels was found to decrease the chances of wire falling out during the embedding process at higher ultrasonic frequencies, while also acting as a guide to embed wire in close proximity to previously embedded wire (Martinez, 2020). This would allow circuit designs comparative to the spacing between conductive pathways on conventional PCB's (in theory), enabling further miniaturization of the circuits used within the context of this application. Proximities may only be limited by the dimensional accuracy of FDM produced parts ( $\pm 0.254$  mm) in printing channels alongside one another. This change inspired redesign of the ultrasonic wire embedding tool to the version currently used, which utilizes a 'sewing' method to pulse the ultrasonic horn at a given frequency to heat and seal thermoplastic around a desired location of wire (every 0.5 seconds for PC) as it is mechanically embedded for improved grasp of wire while minimizing damage to substrate surfaces (Martinez, 2020). Similarly, the second change in the process plan involved preprinting of component cavities at designated locations along the length of wire channels, as machining through both copper wire and polycarbonate material proved difficult. Miniature end mills (0.254 mm and .5 mm) required for machining 1608 package sizes frequently break, and so inclusion of empty cavities within CAD tasked end mills with machining, or severing, only through thin copper wire routed through their center to reduce chances of breaking. Additionally, this technique helps address the dimensional inaccuracies inherent to material extrusion produced parts by machining rounded or tapered corners within the cavities to allow for better press-fitting of components; critical in pinching components during soldering.

## Chapter 4

### Tool Design

#### 4.1 Overview

Building upon insight developed during literature review and exploratory work, a new semiconductor laser system of suitable wavelength and power would be required for implementation within the Multi<sup>3D</sup> process plan and workspace for soldering embedded electronic components to respective conductors during build interrupts. This would require the selected laser system to have a laser head small in size and of low weight to mount to an already populated CNC gantry for positioning, an adjustable module/driver with analog modulation modes for computer control of supplied current, and an optical waveguide (optical fiber) to carry the diode beam from the driver located away from the CNC work space to the mounted laser head on the gantry. The next major requirement would be a computer control software which can accomplish detail programming of temperature-time profiles tailored to a solder joint's particular geometry and solder alloy used, along with a real-time controller to acquire or generate the analog control signals between the laser driver and computer. Lastly, a CCD camera would be needed to allow for co-axial targeting and viewing during laser beam application. Additional external focusing optics would be required if beam diameter is unable to culminate to desired spot sizes, fortunately, adjustment of the laser system's internal coupling optics within the head allowed focusing to desired beam sizes. Other additions to the system are not absolute requirements but would provide substantial increases in process stability, namely, implementation of a closed loop temperature control system for monitoring and control, typically utilizing a sensor to output signal proportional to the laser input for display on a meter. Some advanced diode laser systems will utilize a pyrometer to accomplish feedback control, and may also contain computer controlled galvanometers (positioning mirrors) which are programmed to adjust themselves to a particular components geometry. All aspects mentioned above were desired for integration within this system, although time constraints only allowed focus on implementation of fundamental

components within the tool and system developed within this work, with concerted efforts on providing this technology a basic form to accomplish its specified task repetitively for preliminary experimentation. Figure 27a shows a general view of the laser head mount in a CAD rendering alongside view of the finished product mounted on the CNC gantry (Figure 27b).



**Figure 27: (a)** CAD rendering of laser soldering tool alongside other tools on CNC gantry, **(b)** finished laser soldering tool alongside IR thermography camera used for process evaluation.

## 4.2 Semiconductor Laser and Power Supply

With overwhelming use for laser soldering applications in literature, a low-power, diode-pumped, solid-state 808 ( $\pm 5$ ) nm infrared (IR) semiconductor laser system from Naku Technology Co., Ltd. was purchased from Civil Laser Suppliers. The system features a 100 x 40 x 50 mm<sup>3</sup> fan-cooled laser head of heat sink design, with 4 ft. armor jacketed fiber cable connection to a 4W, LSR-PS-II lab adjustable power supply sized 179 x 148 x 56 mm<sup>3</sup>. The laser head features output coupling optics which collimated to a red near-visible, 5 x 5 mm square spot size at aperture. The driver features a continuous wave (CW) working mode with TTL or analog (30 kHz) modulation modes along with internal output coupling optics and a temperature stabilizing thermoelectric device (TEC). Other features included on the driver were an LED display with a current adjustment dial, which allowed for control of output power by adjusting current supply. The system also features a 10,000 hour MTTF (mean time to failure) and emergency safety key for switch off during analog modulation. Figure 28 shows an image of the IR semiconductor laser system.



**Figure 28:** 808 nm 2W - 4W low power IR semiconductor laser system used for this research (courtesy of CivilLaser Suppliers)



### 4.3 Gantry Mount

The nature of the experimentation in this work aimed to position a laser beam's diameter such that one half of the beam would hit a copper wire's lead while the other half hit a components termination, regardless of the height differences between each material. The beam's center would align with the deposited solder paste's volume. To accomplish this, the laser head need only be mounted orthogonally to a substrate's surface while the CNC's gantry movement could position it at desired locations. Despite this, the need to be able to adjust the head at any angle was deemed necessary in the event the mounted laser's beam dimensions were not uniform and needed adjustment. Additionally, the desire to adjust the laser head for laser beam application at various angles for later experimentation was discussed, and so a series of tilt stages were implemented as part of the overall gantry mount. Figure 29a shows an exploded CAD view of the assembly of the laser soldering tool. Three spacers were 3D printed in PC using an FDM 400mc printing machine (Stratasys, Eden Prairie, MN) with customized features in order to interface and fasten all items to one another before mounting on the central plate. A PR01-M6 high-precision 360° rotation stage and a PY003 2-dof "pitch and yaw" kinematic stage ( $\pm 5^\circ$ ) were selected to provide manual adjustment of laser angle, both provided by Thorlabs. The stages featured precision micrometer head actuators adjustable via thumbscrew knobs, and contained 8-32 (M4) and 1/4"-20 (M6) taps.

Assembly consisted of fastening the pitch and yaw stage to the mount-to-tilt spacer first, then fastening of the tilt-to-rotation spacer onto both, etc., working outwards until completion using a combination M4 and M6 black-oxide alloy steel socket head screws. Aside from four through-hole features on the outer edge of the tilt-to-rotation spacer, 3D printed through-holes were unthreaded. The overall assembly would then be fastened to a two part, screw-style locking MC-16 tool changer (ATI Industrial Automation, Apex, NC) with the "master" side mounted to the CNC's central plate and the "tool" side fastened to the assembly's mount-to-tilt spacer. The manual twist-knob locking mechanism on the tool changer provides a repeatable and high-strength mounting of the assembly, using steel locking ball bearings driven by sideways cams to sustain a 35 lb. payload and large moment capacity (220 lbf-in). The final addition to the laser soldering

tool was implementation of CMOS camera, coaxially aligned to leave targeting regions in view. An acA2500-14uc-Basler ace camera (Basler Inc., Exton, PA) was mounted to the laser-to-rotation spacer with a two-link mechanism which could allow angling of the camera and Z-direction movement along a shelf. Overall, the laser soldering tool is relatively compact and weighs only 10 lbs. Overall dimensions of the tool is 200 x 76 x 95 mm, and is easily mounted and removed to accommodate other equipment if need be. The tool is positioned at the left most position on the central CNC plate. Figure 29b shows an image of the assembled CAD for reference.

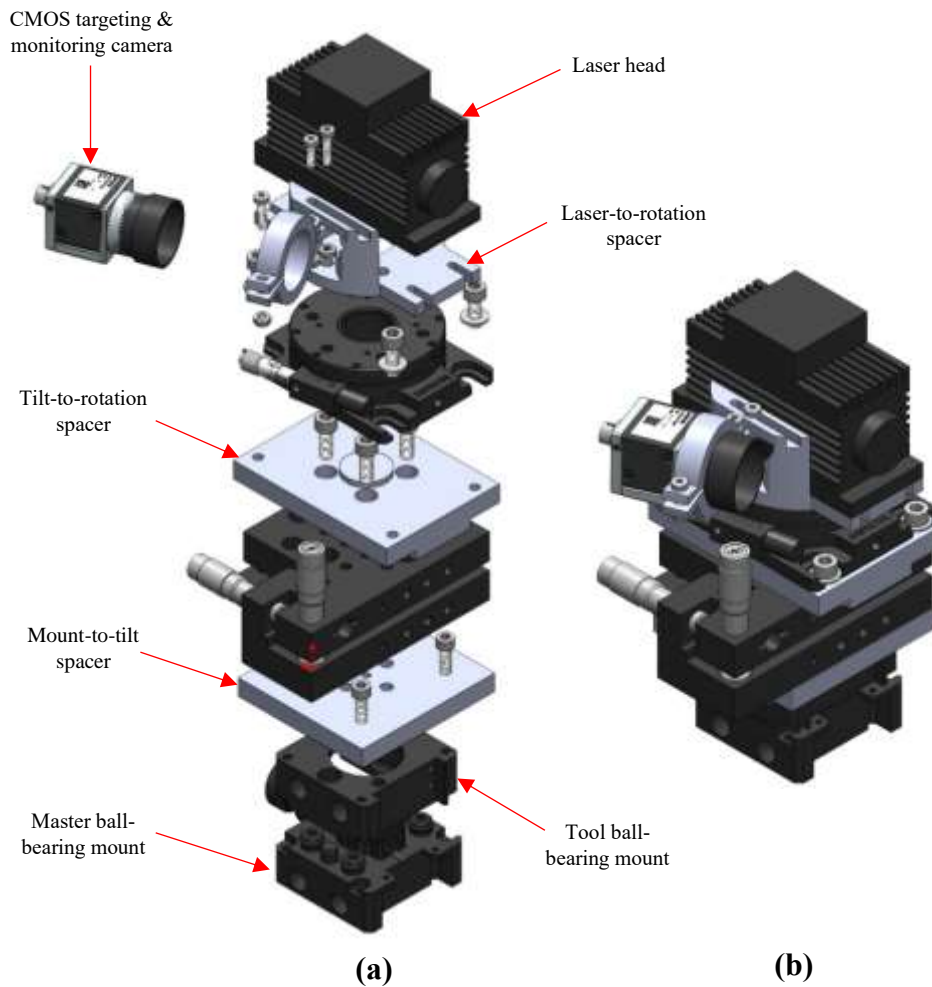


**Figure 29: (a) CAD image of laser soldering tool in exploded view (b) CAD image of laser soldering tool assembly.**

#### 4.4 Controller and Software

Briefly discussed in Chapter 1, the Multi<sup>3D</sup> utilizes a Yaskawa Motoman MH50 to mechanically lock onto customized build platforms within either of the two Fortus 450mc industrial printers before pulling them out and transferring them to a CNC router (Techno CNC systems, Ronkonkoma, NY) where all secondary additive or subtractive processes take place. The clamping mechanism on the end-effector of the robot arm and build platform receptacles within each station (FDM1, FDM2, and Techno CNC) rely on pneumatics for automation to maintain vacuum of build sheets which contain printed parts, and are precisely aligned in place by mechanical means (pucks on threaded screws) to maintain specific coordinates to allow for accuracy in print continuation once returned to the FDM build chambers (Coronel, 2015). The highly automated process requires a programming interface utilizing a root library containing multiple sub programs to control all movements. LabVIEW (NI, Austin, TX), the default programming interface which came with the Yaskawa robot arm, provided a library to facilitate its implementation. LabVIEW was also used to accomplish control of the laser soldering tool and detail programming of laser outputs for specific temperature-time profiles.

LabVIEW is an interactive program development/execution system utilizing a graphical programming environment to use programs called virtual instruments (VI's) to carry out controls, measurements, or data acquisition operations. The program allows for direct test and measurement of automated systems for monitoring, control, and communication with programmable logic controllers (PLC's), or supervisory control and data acquisition in real-time, real-time scan, and FPGA programming modes. The program commands plug-in data acquisition (DAQ) devices/modules to acquire or generate signals to and from connected sensors, where they are conditioned and return that information to the computer for processing, analysis, storage, or other data manipulation (Travis and Kring, 2013). The DAQ devices can be inserted within a single chassis with direct USB connection to a computer for use, or several within an embedded controller chassis capable of data-logging, embedded monitoring, and control in and of itself. Figure 30 shows the 8-slot cRIO-9047 CompactRIO Controller with Intel Atom quad-core processing was

used to provide signal communication between the laser driver and the Multi<sup>3D</sup> operation computer (NI, Austin, TX). The controller features a 1.60 GHz CPU to provide precise and synchronized timing for deterministic communications using Time Sensitive Networking (TSN), which is ideal for highly distributed measurements. The cRIO can be considered to be the ‘brain’ of all auxiliary tooling and processes performed on the Techno CNC’s platform, as it is used to control or acquire data from the many sensors the other technologies utilize for operation (e.g., wire embedding tool, alignment cameras, pick-and-place, etc.). The NI modules used for conditioning of signals from sensors combine common I/O circuitry within, and are available for numerous applications depending on the sensor requirements needed. A 12 Bit, 0 to 5V, NI-9381 C-series multifunction I/O module with 8 AI/8 AO/4 DIO was used for communication and current output control to the laser driver (NI, Austin, TX). Figure 30 shows the cRIO controller along with the NI-9381 module inserted within, alongside others. Able only to supply 1 mA current outputs per AO pin from its DSUB connection, a parallel connection was made to allow for a total 2 mA output from the module to the driver for full range current outputs to the laser head.

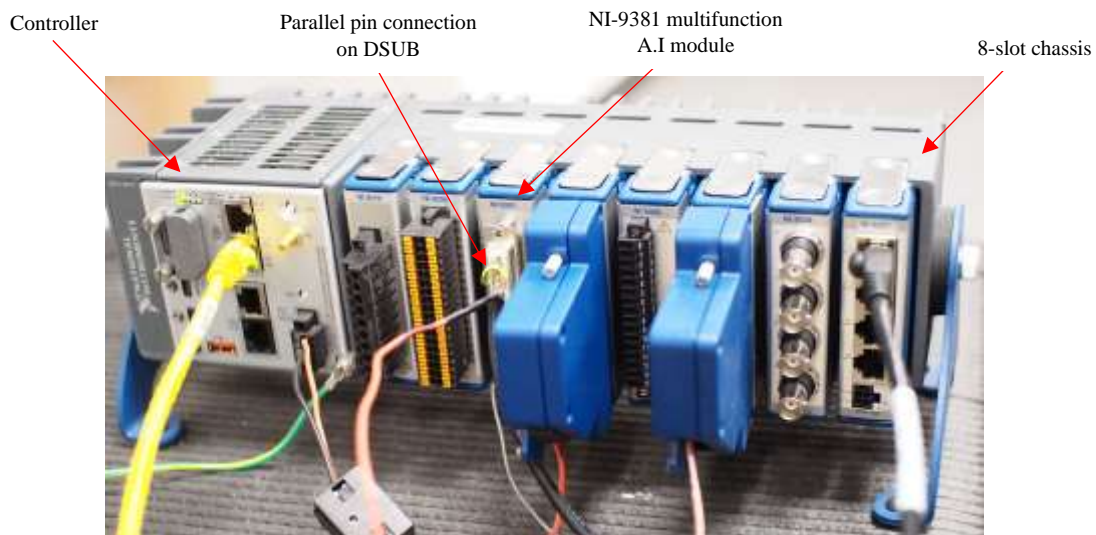


**Figure 30:** 8-slot cRIO-9047 CompactRIO Controller with C-Series Modules inserted within its chassis.

Within LabVIEW, projects are used to store configuration, build, and deployment information. It is here where multiple VI's can be created and organized for deployment, and where external devices such as the cRIO and its many modules must be connected. Within a VI, a functional graphical code is created within a 'block diagram' window by connecting functional nodes via wires through which data flows, and it is here where a module's analog and digital channels are assigned for use. A second window within the VI known as the 'front panel' acts as the user interface and is used to display and simulate the physical instruments used with sensors. The front panel will contain the knobs, push buttons, etc., to adjust user input values and 'run' the VI to display program outputs on indicators which are available as graphs, charts, LED's, etc. The project for this work utilizes two central VI's consisting of the laser control VI and the targeting camera VI. Figure 31a shows the front panel and block diagram for the laser control VI and Figure 31b shows the front panel and block diagram for the targeting camera VI.

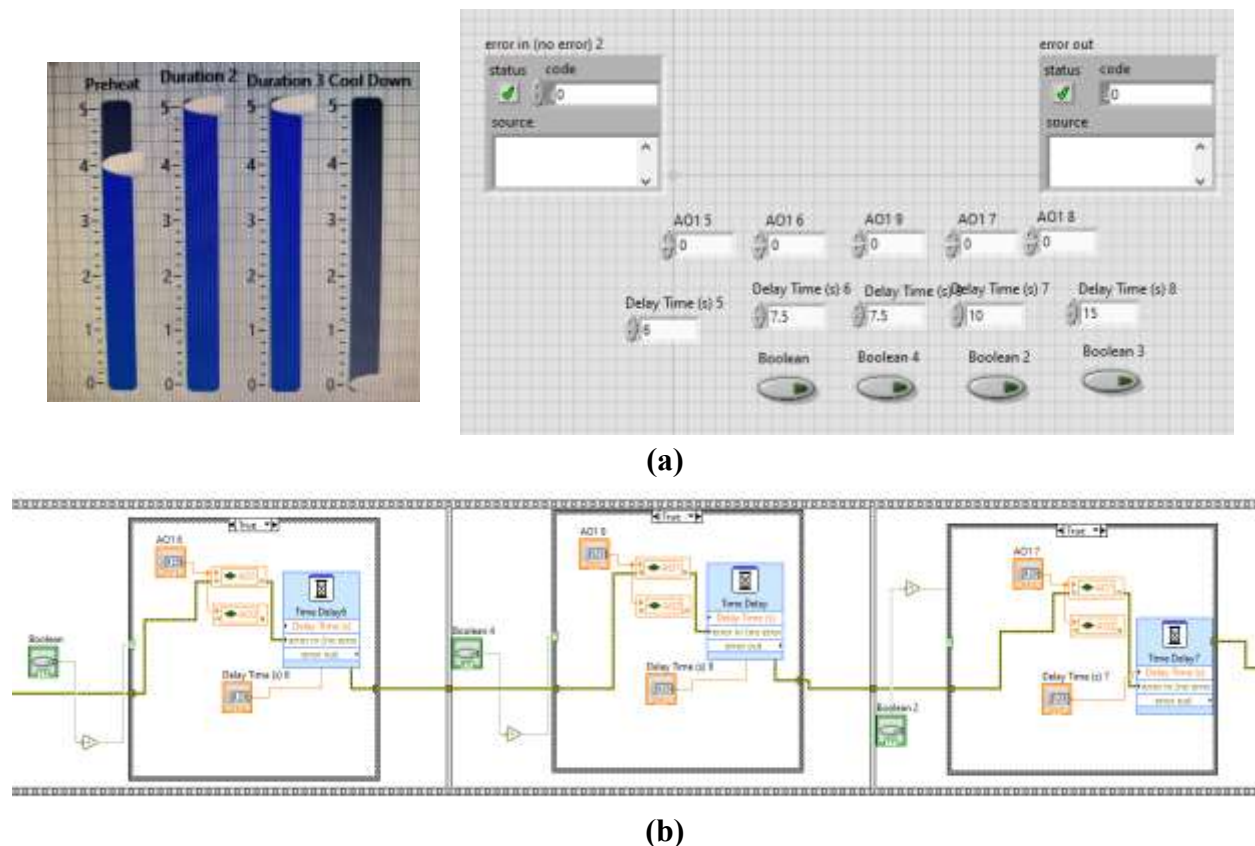
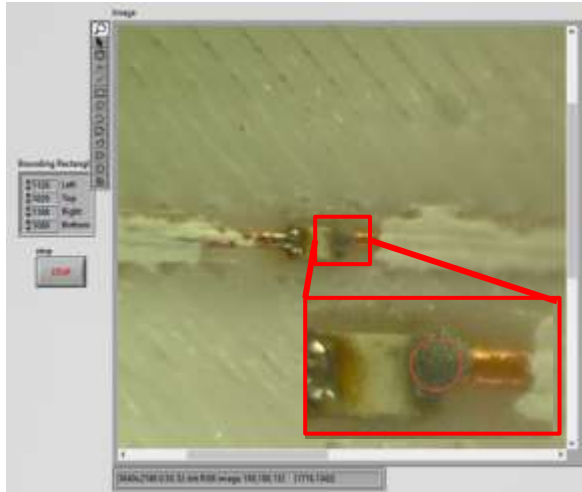
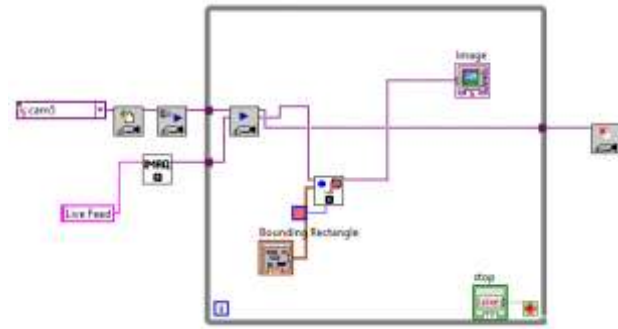


**Figure 31:** Partial views of (a) front panel and (b) block diagram for the laser control VI.

Within the block diagram of the laser control VI, a series of time-delays are placed within case structures. The case structures act to allow data flow with a TRUE or FALSE from a Boolean operator, only allowing data flow if certain conditions are met. The time delays are linked to the two designated analog output channels of the NI-9381 module, which are linked to the series of vertical slider bars shown within the front panel and their designated input value bars for time duration. The current output of the laser driver and duration of laser application are controlled here, and thus allow for tuning of a solder alloys time-temperature profile. The targeting camera VI is a digital image processing VI, in which an imaging sensor converts an image into a discrete number of pixels using image acquisition commands known as IMAQ Vision nodes (Figure 32). The imaging sensor, in this case the CMOS camera provided by Basler, assigns to each pixel a numeric location and a gray level or color value that specifies the brightness or color of the pixel to produce a digitized image. The three basic properties of a digitized image consist of the sensor's resolution, definition, and number of planes. Within the front panel of this VI, a window displays the image produced by the CMOS camera, which is a 32-bit, Red-Green-Blue (full-color image), 3,840 x 2,748 pixel image. The block diagram of the targeting camera VI shows a series of IMAQ Vision nodes which call on and deploy connectivity to the CMOS camera, to which culminate within a while loop to allow for continuous live feed imaging while the VI is running. The data flow bridges off within the while loop to a "bounding rectangle" node which allows for display of a circular bounding region of interest (ROI), used to target solder volumes as seen on the front panel of the targeting camera VI. The targeting reticle is adjusted based off the location of beam application, measured by hitting a sheet of laser paper to mark the beam's circular burn mark after laser turn on, and then defined within the bounding rectangle control seen on the front panel. In the case of Figure 32a, the bounding reticle is a 60 x 60 pixel area which is positioned via CNC gantry above solder joint locations.



(a)



(b)

**Figure 32: (a) Front panel and (b) block diagram for the targeting camera VI.**

## **Chapter 5**

### **Methodology**

#### **5.1 Overview**

The research presented in this work focuses on successfully and repetitively reproducing solder joints at fundamental locations for electronic functionality within thermoplastic substrates. This meant focus on soldering discrete, passive SMT components (resistors) to embedded wire, as they often form the bulk of components seen in electronic circuits. The other fundamental solder joint location(s) is the many nodes seen in a typical circuit, necessary for electrical connectivity between circuit elements. To facilitate a repeatable laser soldering technique for each of these locations, adjustment and testing of process parameters inherent to laser processing is performed, which include laser power, process time, and geometry of the laser beam's spot size. Various combinations of power and duration for laser application are tested, with intent on reproducing reflow cycle time requirements provided by a solder paste's manufacturer, preserving all components and materials, and producing mechanically and electrically sound solder joints.

#### **5.2 Materials**

- Substrate material - Polycarbonate FDM Thermoplastic Filament (Stratasys, Grand Prairie, MN)
- Solder – Sn 63/Pb 37 No-Clean Solder paste (Chip Quik, Niagara Falls, NY)
- Flux – RA Rosin Flux Paste (MG Chemicals, Ontario, Canada)
- Electric wire – Bare, polished, 26 AWG gage copper wire
- Thick Film Resistors - SMD 1608 49.9  $\Omega$  1% Anti-Sulfur (Mouser, Mansfield, TX)
- Correction fluid – BiC WITE-OUT Correction fluids (BIC USA Inc., Shelton, CT)
- Isopropyl Alcohol – Laboratory-grade, 99% (hBARSCI LLC, Victor, NY)



### 5.3 Experimental Setup

Laser soldering tests were performed on parts fabricated with Polycarbonate thermoplastic within an Fortus 400mc FDM industrial 3D printing machine (Stratasys, Eden Prairie, MN), then transferred to the CNC router used within the Multi<sup>3D</sup> workspace (Techno CNC Systems, Ronkonkoma, NY). Parts were processed on Stratasys slicing software (Insight) and then positioned on build platforms within Stratasys Control Center software. To simulate conditions during pauses, parts were left on build sheets and cut out to the dimensions of a vacuum plate for secure placement. The vacuum plate contained set screws at each corner which were used to level its top surface. Figure 33 shows the general setup at the CNC routing station for laser soldering experimentation. IR thermography was used for evaluation of pseudo temperature history in an attempt to recreate reflow oven temperature vs. time profiles provided by manufacturers to scale effective parameter sets for laser soldering in this application. A Fluke RSE600 Mounted Infrared Camera with 640 x 480 resolution and SmartView desktop IR analysis software was used (Fluke

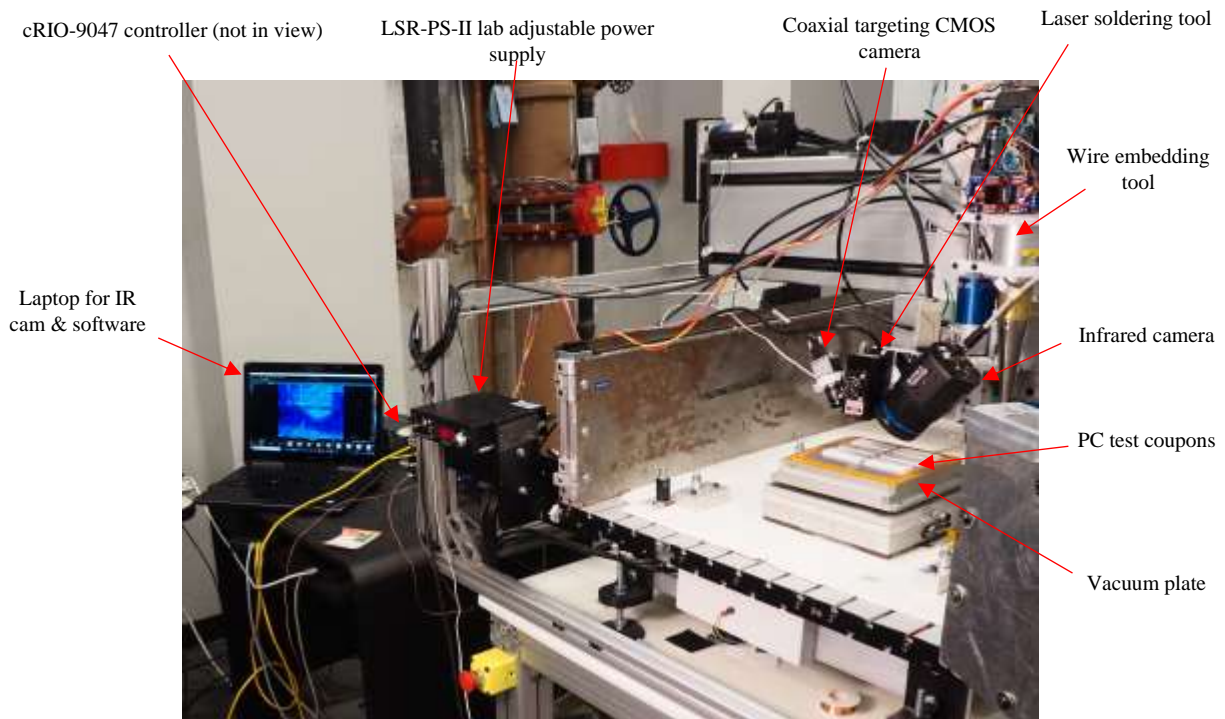


**Figure 33:** General setup at CNC routing station for laser soldering experimentation.

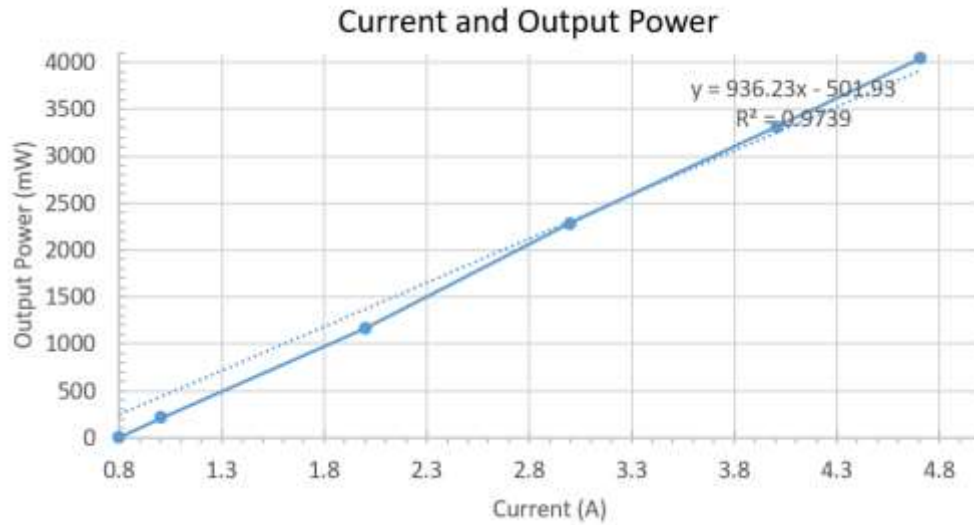


**Figure 35:** Current to power curve fitted to manufacturer power settings.

Corp., Everett, WA). Figure 34 shows a current to power curve fitted to the laser system's power outputs provided by the manufacturer (CivilLaser Supplier, HangZhou, China). These current values were used as inputs within the LabVIEW Laser Control VI in an attempt to follow the Sn 63/Pb 37 solder paste time vs. temperature profile provided by the solder paste manufacturer (Chip Quik, Niagara Falls, NY). The temperature profile, shown in Figure 35a, is divided into four key phases which occur during reflow and are numbered and labeled respective to their duration and

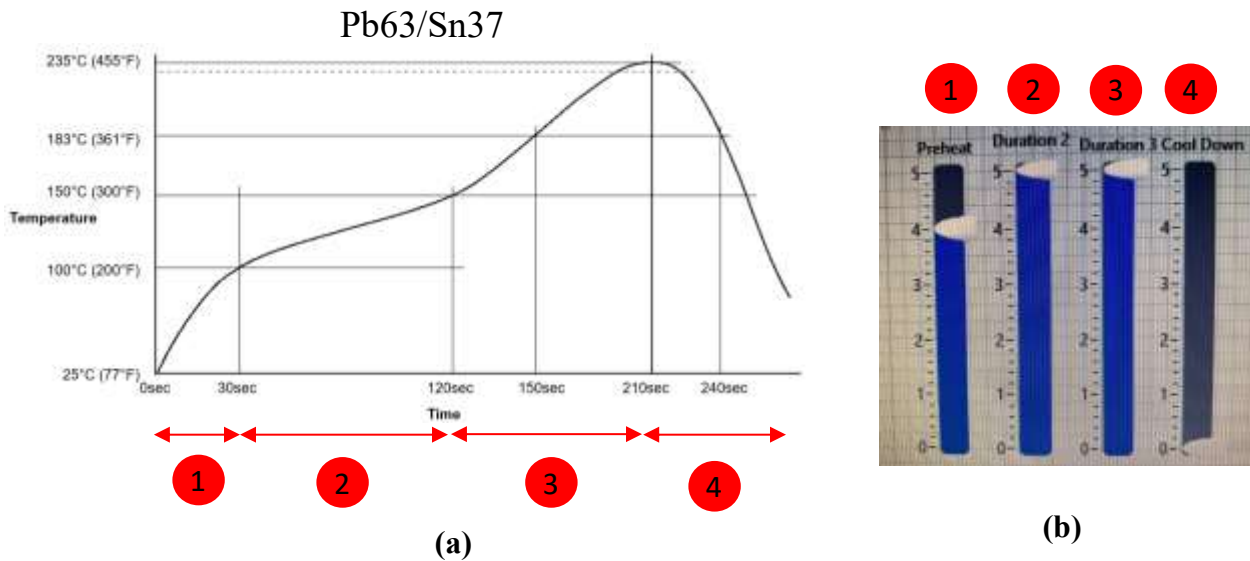


**Figure 34:** (a) Temperature vs. time reflow profile for Pb 63/Sn 37 solder paste alloy (b) partial view of Laser Control VI's front panel depicting current output controls.

power settings. Figure 35b shows a partial view of the Laser Control VI's front panel, which depicts a series of vertical slider bars which represent the current outputs from the laser driver to the laser head for soldering. A targeting CMOS camera was used to target all solder volumes within a LabVIEW Targeting Camera VI, and the laser head was positioned in the X-Y directions via CNC gantry. The laser head was adjusted in the Z-direction to produce a desired laser beam spot size depending on the solder volume. Targeting VI feed and IR thermography capture was recorded during laser soldering. As the 808 near-infrared wavelength cannot be visibly observed by the CMOS camera, a secondary High-Definition Olympus OM-D camera was fitted with a colored lens rated to filter 808 nm light for recording and observation during reflow (Laser Safety Industries, Minneapolis, MN). Polycarbonate laser safety glasses fitted with lenses of the same rating were worn during all experimentation. Resulting soldering attempts were inspected on a Leica 7X-90X Microscope.

#### **5.4 Temperature Observations using Thermocouple, IR Thermography, and HD Camera**

Fundamental to all electronic circuits, wire-to-wire joining would be necessary to facilitate electronic nodes for current flow through the circuits intended for fabrication in this application. This motivated the implementation of a preprinted square cavity feature to allow for minimal contact with the polymer substrate while providing adequate space and depth for subsequent 'bridging' wire pathways to be pressed over previous wire within these small cavities via wire embedding tool for simplicity and soft contact in preparation for solder joint welding. The intent of this design is to reach sufficient surface tension via capillary motion (wicking) during reflow, such that solder flows into the narrow spaces between and around both a top and bottom wires' cross section to envelop the wires and form a sound solder joint within a cavity. Figure 36a shows a conceptual side view of a solder junction prepped for laser soldering, and Figure 36b shows a top view image of a junction with flux (not visible) and solder paste deposited above crossing wire.

Initial laser soldering experimentation focused on determination of a feasible emissivity ( $\epsilon$ ) range which could be used for all constituent materials during infrared thermography recording,

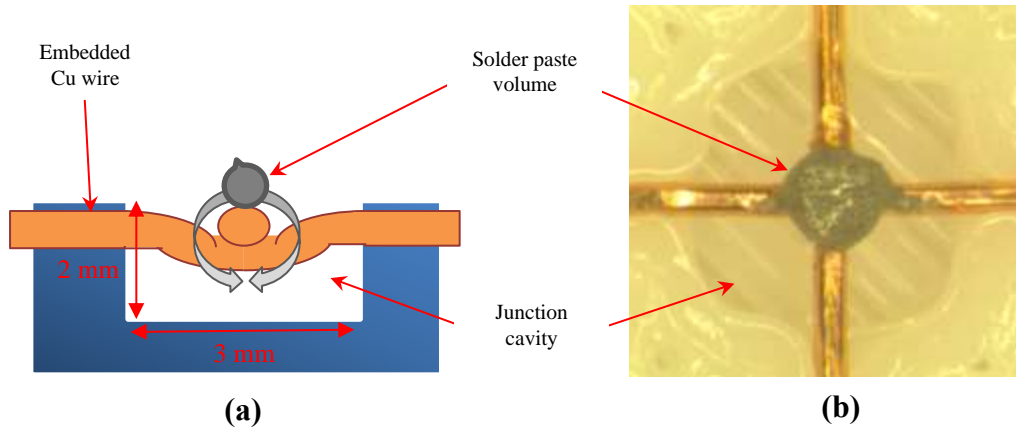


**Figure 36: (a)** Conceptual side view of a solder junction point prepped for laser soldering, **(b)** image of solder junction point with flux (barely visible) and solder paste.

and proved challenging as emissivity values for metallic surfaces are exceedingly small (e.g., polished copper:  $\epsilon = 0.02 - 0.05$ ) while emissivity of polycarbonate polymer material is substantially higher ( $\epsilon = 0.90 - 0.97$ ). Additionally, the emissivity of solder paste is variable and difficult to determine as alloy composition and flux (binder) amounts can change within each deposited volume. Along with phase changes of solder paste during heat application, determination of absolute temperature of a solder paste volume was not possible. Being in intimate contact with solder paste volumes and in direct exposure to the laser beam, an attempt to determine a pseudo temperature vs. time profile for the copper wire being joined was conducted. As mating metallic surfaces are required to be heated enough to allow for wetting during reflow, ideally, as close to the eutectic temperature as possible, it was assumed that solder paste which properly adheres and establishes a sound solder joint would signify that heat being supplied to its volume reaches its eutectic melting point at minimum (183°C for Pb 37/ Sn 63). As such, the maximum temperature value on a copper wire's IR temperature vs. time profile for an acceptable solder joining should lie near the eutectic point.

In an attempt to demonstrate this, a material with known emissivity was used to coat copper 26 AWG wire nearest solder joint locations to produce more insightful representations of pseudo temperature profiles. With an emissivity of  $\epsilon = 0.95$ , BiC Correction fluid (BIC USA Inc., Shelton,

CT) was brushed onto wire, enough to allow for placement of rectangular regions of interest (ROI's) 2 x 7 pixels in size centered along a wire within IR analysis software. Within the software, emissivity values would be set to that of the correction fluid's during IR recordings, while outputting minimum, maximum, and average temperatures for each ROI. In an attempt to validate reported pseudo temperatures, two J-type thermocouples were used to make contact with the surface of copper wire at locations where correction fluid was present and where an ROI would be placed within the IR software. Figure 37 shows the coupon design used for this preliminary experiment, which is a variation of the test coupons used for wire-to-wire parameterization and repeatability tests, with machined channels for thermocouple placement. Two separate 35 x 35 x 3 mm polycarbonate coupons were fabricated with two preprinted channels sized 0.36 x 0.36 mm (for wire embedding) perpendicular to each other, and a single cavity sized 3 x 3 x 2 (solder junction cavity) at the coupon's center cross section. Figure 37a shows two thermocouples making contact with a horizontal bottom wire, with one positioned underneath the crossing wire within a junction cavity, and another roughly 6 mm away from the crossing wire section. Figure 37b shows a deposited solder paste volume on top of the crossing wire, with correction fluid on each wire at cavity edges. Figure 37c shows an IR image as seen on IR analysis software at room temperature, with breaks in the wire representing correction fluid coatings and two ROI's positioned on these gaps accordingly. Wire within each junction cavity was cleaned with isopropyl alcohol before manually dabbing flux and paste using a precision scraping pick. The method for determining solder paste amount is discussed in Section 5.5.

Based on the scaling technique used in Section 5.5, two arbitrary parameter sets were used, acquired during early experimentation which produced what appeared to be formidable solder joints. One coupon was subject to a 2 W for 10 seconds (preheating), 3.3 W for 30 seconds (ramp duration 2), 3.7 W for 30 seconds (ramp duration 3), and 0 W to emulate cool down at laser shut off. The second coupon was subject to 3.3 W for 15 seconds, 3.3 W for 45 seconds, and 3.7 W for 45 seconds. Time vs. temperature profiles from both thermocouples and IR software for each ROI

were plotted and analyzed, with focus on evaluating if pseudo values reported temperature peaks near the solder paste's eutectic melting point.

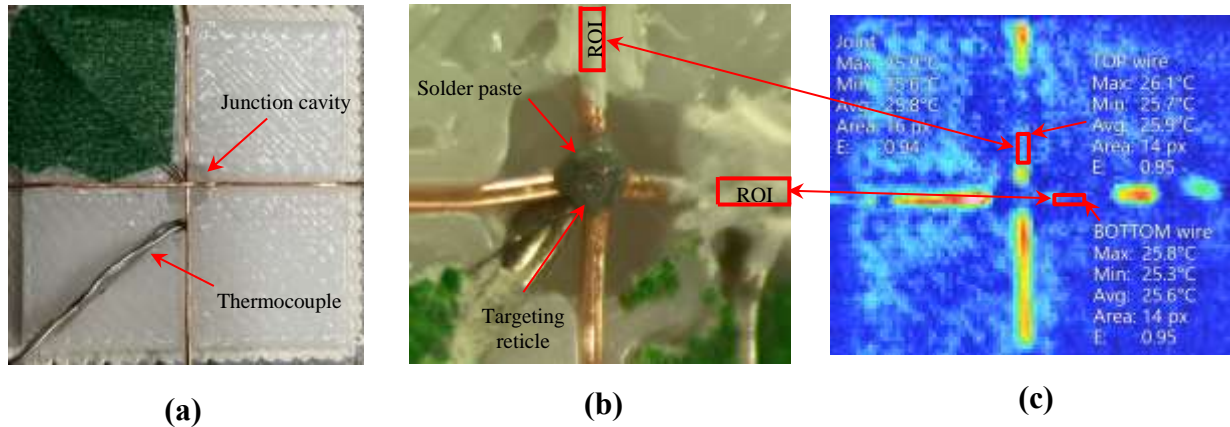


**Figure 37:** (a) Initial wire-to-wire test coupons (PC) used for IR pseudo temperature evaluation, (b) deposited solder paste volume on crossing wire with correction fluid coating on wire, (c) IR image as seen on IR analysis software with designated ROI's on correction fluid coating.

## 5.5 Wire-to-Wire Joining: Parameterization and Repeatability

Reflow profiles given by a solder paste manufacturer are designed as a starting point for process optimization, particularly for use within convection ovens for mass soldering. As previously discussed in Chapter 2.6, the heating zones within these ovens are kept at the temperatures suggested in these reflow profiles, and conveyor equipment traverses SMT assemblies through each zone with speeds tailored for adequate heat transfer with respect to an assembly format's solder paste amount, the number of SMD components involved, and the overall thermal mass expected to be overcome during heat soaking. The temperatures reached and total duration of heat exposure depend on the solder alloy used and the expected thermal mass of an overall PCB assembly. The total time duration for the lead-based composition used in this work suggests 4 minute long heat exposure (Figure 34a), but since the rapid method of heat delivery via laser is near instantaneous, must be either scaled to resemble the general temperature profile for shorter laser soldering times, or have laser power adjusted to recreate a similar profile to keep the same 4 min duration.

As the tool designed in this work acts to solder one solder joint location at a time, scaling laser power to maintain a 4 min duration would substantially prolong the soldering process of a simple circuit. The Multi<sup>3D</sup> process favors completion of all secondary processes at the CNC station as quickly as possible in order to return builds back to the Fortus 400mc print chamber to avoid severe thermal contraction of substrate material and thus retain dimensional accuracy of a build for print continuation. As such, attempts to scale the reflow profile for shorter laser application times was attempted, with the intent of determining a suitable parameter set for a repeatable soldering practice. Similar to the test coupons seen in Section 5.3, three 34 x 100 x 2 mm long coupons were fabricated containing 10 solder junction cavities on each. The preprinted solder junction cavities were positioned 17 mm away from each other in the X-direction and 15 mm in the Y-direction, with preprinted channels interconnecting each column and row for wire embedding. Copper wire was embedded and press-fit manually, with use of a tapered steel rod of similar geometry as the ultrasonic horn's tip. The cavities and channels remained the same dimensions as in Section 5.3, but test coupons included additional cavities sized 3 x 5 x 2 mm in between junction cavities to allow for severing of wire via cutters to avoid premature heating of wire between junction cavities during laser soldering experimentation. Figure 38a shows a partial view of a wire-to-wire test coupon with embedded wire. Figure 38b shows a corner of a test coupon with severed wire within the additional cavities along with flux and a solder paste volume placed

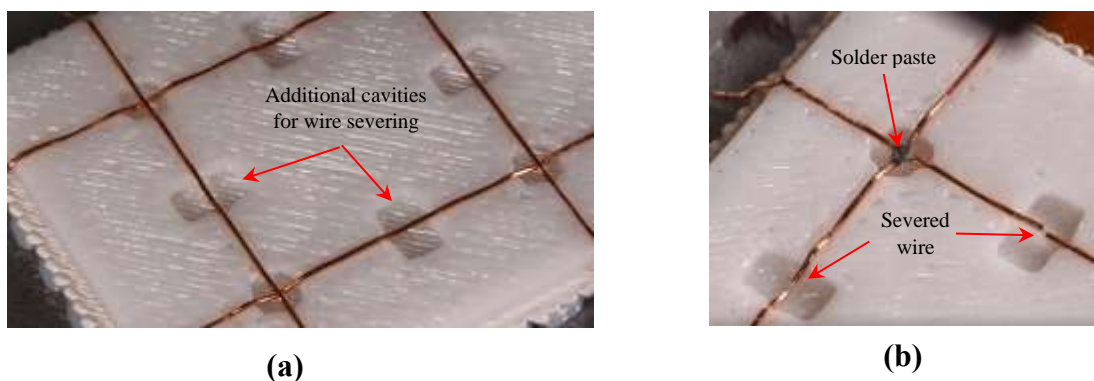


**Figure 38:** (a) Partial view of wire-to-wire test coupon (PC) used for wire joining tests, (b) corner of a test coupon with severed wire within additional cavities along with flux and solder paste placed at intersecting wire locations.



at an intersecting wire location within a junction cavity after cleaning of wire with isopropyl alcohol.

Flux and solder paste was manually dabbed at desired locations with use of a precision metal scraping pick. The amount of paste deposited was based on the wire gage dimension used, wherein just enough paste would touch only metallic surfaces while avoiding polymer substrate material. Avoiding excess amounts of paste and flux is paramount in limiting flow of either material to the polymer substrate during reflow, or in the case of the test coupon design used, drip off wire and fall to a cavity's bottom surface. The weight of an intended solder paste volume was approximated with the calculation shown below; where  $r_{\text{Cu-wire}}$  is the radius of

$$\begin{aligned}\text{weight} &= \text{volume of a sphere} \times \text{density of solder paste alloy}; \\ &= \frac{4}{3} \times \pi \times 2(r_{\text{Cu-wire}} \text{ cm})^3 \times \rho_{\text{Pb37/Sn63}} \frac{\text{g}}{\text{cm}^3}; \\ &= \frac{4}{3} \times \pi \times 2 \times (0.020 \text{ cm})^3 \times 8.34 \frac{\text{g}}{\text{cm}^3} = \mathbf{0.0023 \text{ g}};\end{aligned}$$

the 26-AWG gage copper wire ( $0.020 \text{ cm}^3$ ) and  $\rho_{\text{Pb37/Sn63}}$  is the density of solder paste ( $8.34 \frac{\text{g}}{\text{cm}^3}$ ). Deposited solder paste droplets typically resemble small spheres, and so the volume of a sphere was used for simplicity. As two wires would be joined, the radius of the wire was doubled. The amount of flux remained unknown, as it should lightly coat surfaces and be  $\leq 5\%$  of the total paste amount. This guideline for flux amount is one that can be followed, although, remains lenient as some solder paste compositions already contain a percentage flux within its binder contents and would therefore require less additional flux. Flux effectively preps heavily oxidized surfaces for soldering and excess amounts of flux would only be required in this instance. A substantially excessive amount of flux may drown a solder joint location and create difficulty in heating at recommended temperatures, or leave large amounts of residue which would make for more clean-up post soldering before service. In general, too little flux is far more detrimental than too much, and so a light coat of flux was brushed onto crossing wire locations within junction cavities. Figure 39 shows a reference image of the amount of solder paste deposited onto solder



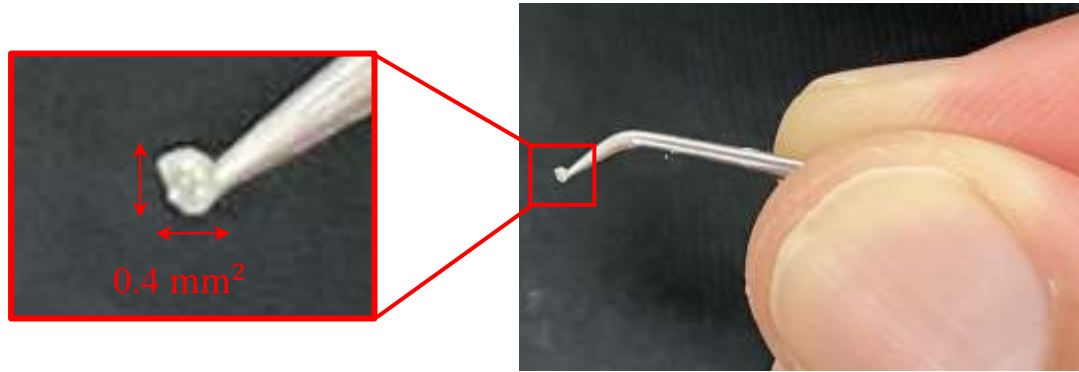


**Figure 39:** Reference image of the amount of solder paste deposited onto solder joint locations using a precision scraping tool, attempting to remain within the copper wire's diameter.

joint locations using a precision scraping tool. Wire was coated with correction fluid in the same locations as in Section 5.3, and was also recorded in IR software, targeting VI feed, along with a HD camera fitted with an 808-nm lens for comparison.

An array of 20 joints were prepared, followed by immediate laser processing. No dwell time was allowed between prep and creation of joints. Four different power intensity sets were used in combination with four different time duration sets, scaled down in  $1/5^{\text{th}}$  for each phase's time interval. Table 5.1 lists the various combinations of laser power and time durations used for determination of a suitable parameter set. During targeting of each solder joint location, the lasers beam was positioned such that one half would hit a top wire and the other half a bottom wire, with a beam diameter of 2 mm at 158 mm from the work piece in the Z-direction. Figure 40 shows an image of a solder joint location being targeted as seen on the Targeting Camera VI screen, with an inner red circle the representing the bounding targeting reticle and the dashed outer circle the approximated affected area. Resulting solder joints were cleaned of flux residue and excess, un-reflowed solder paste, which also acted to serve as a precursor method for testing mechanical integrity before lightly scraping and tugging of joined wire with a separate scraping tool. Solder joints that did not survive the cleaning, scraping, and tugging tests were considered failures which were not analyzed. Remaining intact joints were visually inspected for a smooth and shiny surface appearance and measured for resistance. Out of 20 solder joints, only 10 passed to remain intact

**Table 7:** Array of laser power and time duration combinations used for laser soldering with Sn 63/Pb 37 solder paste alloy's manufacturer temperature profile

Row	Power Intensity Set	Duration/5	Duration/4	Duration/3	Duration/2	Full Duration
1	0.3 W, 0.34 W, 2 W, 0 W	Joint 1	Joint 2	Joint 3	Joint 4	Joint 5
2	0.34 W, 2 W, 3.3 W, 0 W	Joint 6	Joint 7	Joint 8	Joint 9	Joint 10
3	2 W, 3.3 W, 3.7 W, 0 W	Joint 11	Joint 12	Joint 13	Joint 14	Joint 15
4	3.3 W, 3.7 W, 3.7 W, 0 W	Joint 16	Joint 17	Joint 18	Joint 19	Joint 20

and report resistance values in the milliohm range (close to zero). The third and final coupon was used for repeatability tests, in which two of the better performing parameter sets which produced the best solder joints were each fabricated 5 times (two different power settings). Observations were made of all resulting solder joints, with comparisons of fillet wetting angle, wetting length, solder joint thickness, and IR thermography-produced time vs. temperature profiles.

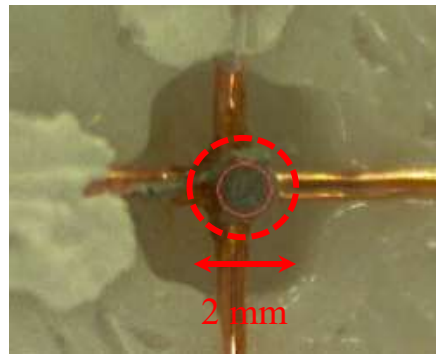


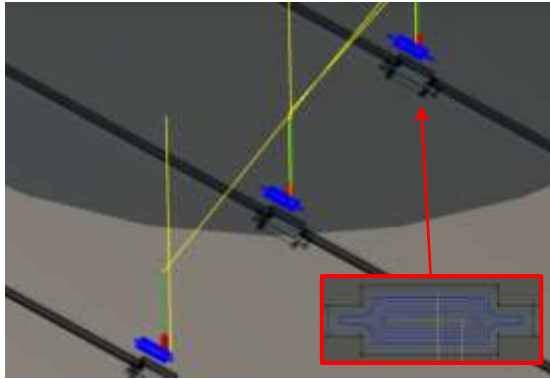
**Figure 40:** Solder joint location being targeted as seen on the Targeting Camera VI screen, with an inner red circle the bounding target reticle and the dashed outer circle the approximated affected area.

## 5.6 Wire-to-Component Joining: Parameterization and Repeatability

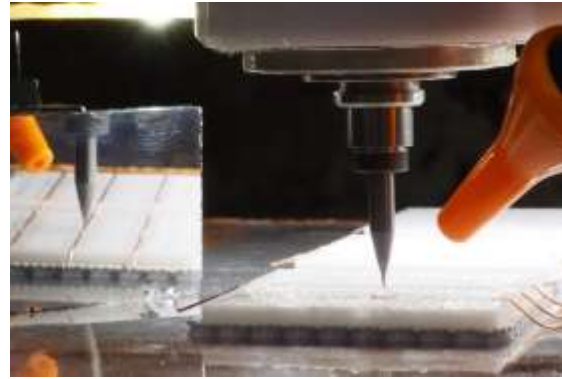
Forming the bulk of electronic components which populate a PCB circuit, focus on the embedding and laser soldering of passive surface mount components (SMC's) within polymer substrates remained paramount to the success in producing electrically multifunctional parts. With

wide-ranging SMT component package sizes (0402 – 6332, roughly 10 different metric case codes) which can make up the assortment of components seen on any given PCB, the fourth smallest package size 1608 was selected for testing in order to allow for high-density component embedding within a printed part during a build interrupt if the laser soldering process proved successful. This would require a means of quickly and efficiently prepping an empty space of a polymer's surface for a circuit design by routing all copper wire pathways through all preprinted cavity geometries, machining (severing) of wire within cavities intended for electronic component placement, and placement of all components and soldering materials (flux and solder paste) before laser soldering and returning to a 3D printer.

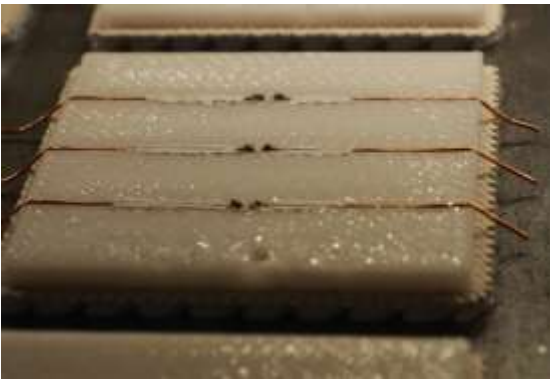
Using the same methodology as the wire-to-wire test coupon preparation, twelve 35 x 35 x 2 mm coupons were fabricated within the Fortus 400mc and secured to a vacuum plate via build sheets. Each coupon contained three rows of 0.36 x 0.36 mm preprinted channels for wire embedding and three 1.6 x 0.9 x 0.36 mm cavities centered along each wire for placement of SMD 1608 50  $\Omega$  resistors, for a total of 18 components on a single sheet. Two sheets were used for testing (36 total solder joint trials). As the machining tool would be utilized to sever wire within cavities and assist in shaping each cavity for manual press-fits in order to pinch component sides and avoid tombstoning during soldering, toolpaths for machining were created via G-code on Autodesk's Fusion 360 CAM feature. A technique integrated during exploratory work involved alteration of the cutter's toolpath within the CAM software which would slightly move the cutter into the preprinted channels at each side to cut away wire and leave a 0.1 mm spacing to allow reflowed solder to fill these gaps via capillary action for a more mechanically sound solder joint. The G-code file was then transferred to the Techno CNC's central operating computer and executed using an uncoated, 4-flute LOC miniature end mill with 0.5 mm cutting diameter from Harvey Tools at 50,000 RPM. A 50  $\Omega$  resistor was then inserted within each cavity (face-down), cleaned at termination edges along with copper wire, and then manually dabbed with RA rosin flux and solder paste on both termination and wire on each side of the resistor. Correction fluid was also used to coat wire on both sides for IR evaluation.



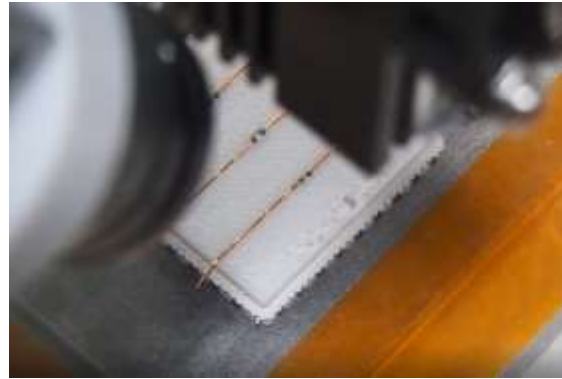
(a)



(b)



(c)



(d)

**Figure 41:** (a) Toolpath generation in Fusion 360 CAM (b) machining through wire within cavities, (c) component, flux, solderpaste, and whiteout placement (d) targeting of solder paste.

With substantially smaller surface area in contact with solder paste and in close proximity of polymer substrate material to a solder joint location, the amount of solder paste was determined using the same formula in Section 5.4, which aimed to be roughly half the amount of flux and paste deposited for wire-to-wire joining (0.0012 g) as only a single wire would be used. Figure 41 shows a series of images encompassing test coupon preparation for wire-to-component joining before laser soldering, and Figure 42 shows the steps taken to prepare each component once placed within a cavity, as seen on a Leica 7X-90X Microscope. Figure 42a shows a resistor tightly press fit within a cavity after machining, which also exemplifies the challenge in leaving 0.1 mm spacing between component terminations and wire as the Techno CNC's backlash during operation somewhat inhibits feature creation at this scale. The left side remained closed off in close

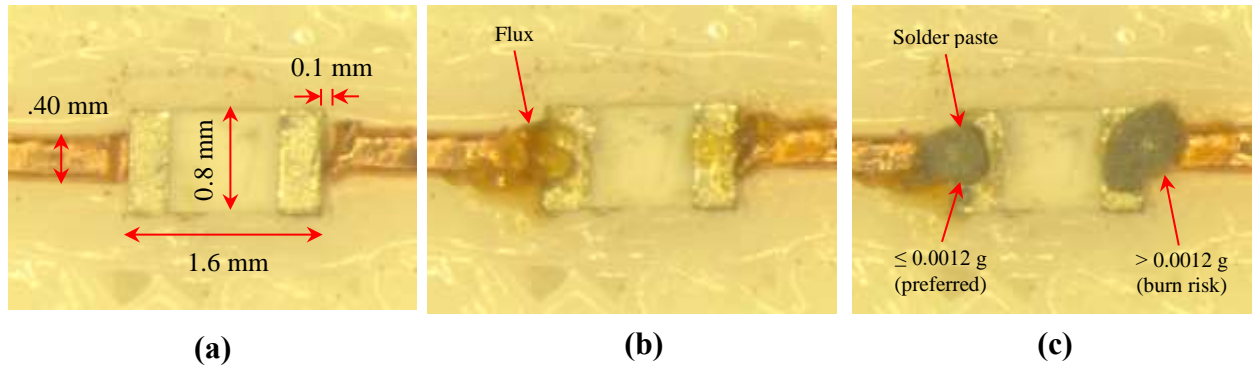
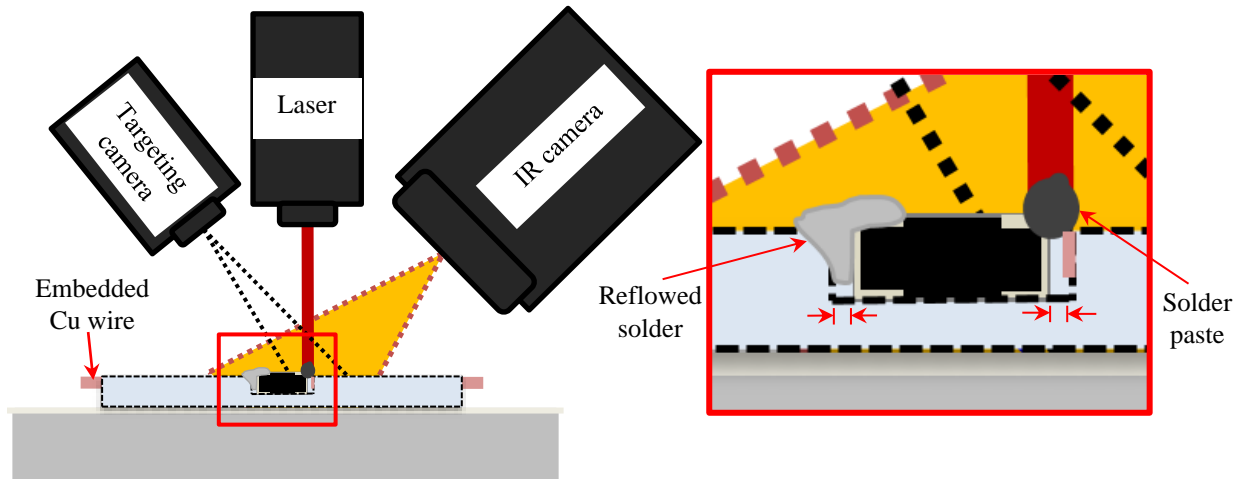


**Figure 42:** (a) Press-fit placement into cavity, cleaned with Isopropyl Alcohol (b) Dabbing of flux at intersections (termination & wire edges) (c) Dabbing of solder paste at intersections above flux

**Figure 43:** Conceptual drawing of setup used for wire-to-component joining with close up view of resistor being targeted at its right side termination.

wire. The spacing which was not able to be created was still acceptable for soldering, as the 0.1 mm spacing was only a guideline to follow and does not dictate solderability of a solder joint location as mating surfaces in close contact with one another still allow for adequate solder joint creation. Figure 42b shows a light coat of flux brushed onto interconnecting solder joint locations, and Figure 42c shows droplets of solder paste deposited above flux. As pastes were manually placed at each location, the absolute amount remained variable, although, a concerted effort to remain consistent with paste amounts was practiced.

Similar to the targeting technique seen in wire-to-wire joining, the laser head's beam was positioned such that one half would hit wire, and the other half the termination, with the beam's center focused on the solder paste volume. With a much smaller beam diameter required to avoid hitting substrate material to induce charring, the laser's head was positioned 152 mm from the work piece in the Z-direction (closer than wire-to-wire) to produce a 0.5 mm beam diameter. Figure 43 shows a conceptual drawing of the setup used for wire-to-component joining, which was the same tooling configuration for wire-to-wire joining albeit at a closer distance. The concept also shows a close up view of a resistor being targeted at its right side termination, with its termination at its left side having already been soldered. The shape of a soldered joint is expected to look similar to the solder joint shown at the left side termination. Figure 44 shows two images; the left



side depicting an image of an embedded component being targeted within the Targeting Camera VI video feed (a), and the right side image showing an image as seen on IR analysis software (b). Figure 44a shows the targeting reticle, which represents the 0.5 mm affected area of the laser beam. Figure 44b shows one horizontal wire crossing a coupon with two ROI's present, and IR heat seen generated at the instant of laser turn on. Similar to the ROI's used in wire-to-wire joining, a single 2 x 7 pixel ROI is placed on correction fluid coating, centered along the wire nearest a solder joint location. This rectangular ROI would be recreated and placed on each wire respective of the side

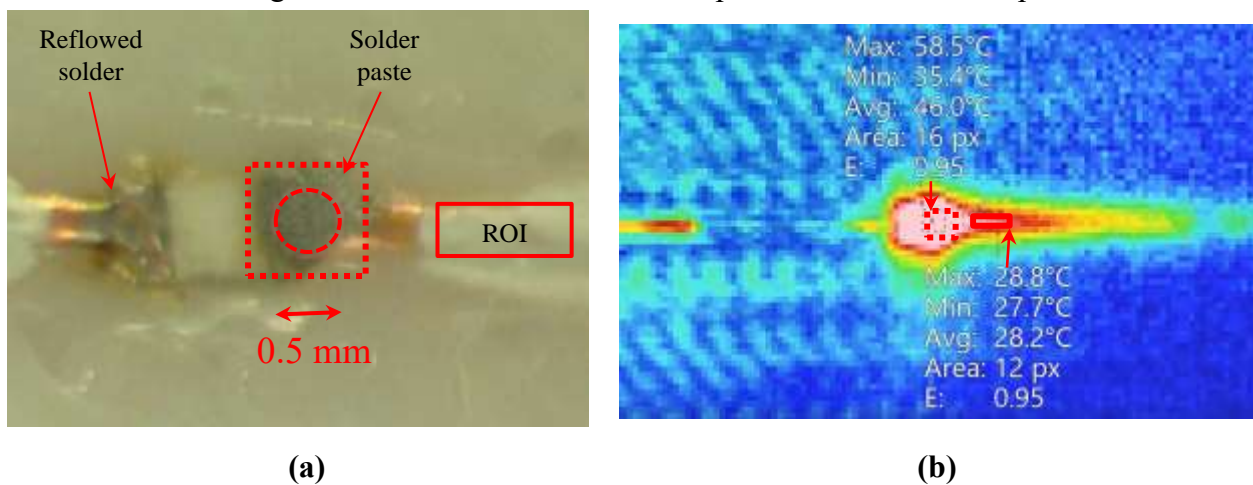


**Figure 44:** (a) Embedded resistor being targeted within the Targeting Camera VI video feed (b) image of component, wire, and ROI's as seen in IR software, with heat seen at laser turn on.

of the component being soldered, i.e., one for the left side laser soldering recording, and then another for the right side laser soldering recording. The second, dashed square ROI seen in the image is indicative of the solder paste location, but was not used as the emissivity of solder paste was unknown and therefore would not report accurate pseudo temperature readings. Within the software, emissivity values would be set to that of the correction fluid's during IR recordings, while outputting minimum, maximum, and average temperatures for each ROI.

Variable tests at different power settings and time durations were conducted on sheet 1 after attempting to use the parameters developed during wire-to-wire joining, which did not translate to wire-to-component joining due to near instantaneous burning/damaging of substrate material at solder joint locations (excessive power and time durations for much less paste and surface area). As such, the lowest power settings and shortest time durations seen from wire-to-wire joining were used for this experimentation. The parameter settings used are shown in Table 5.2. During variability testing on sheet 1, time durations were adjusted based off resulting solders as experimentation went on; those solders which did not induce reflow had time durations increased, and those which damaged the substrate had time durations shortened. Of the 18 components tested, only 5 resistors were successfully soldered (on both sides) to produce desirable soldering aesthetics and accurate resistance values. All components processed at power setting 2 failed (damaged), as did those in power setting 1 with time duration 2. Power setting 1 with an adjusted duration of phase 3 within time setting 1 (18 s, 18 s, 12 s, laser off) performed best and was used for repeatability testing on sheet 2, where 10 of the 18 resistors passed to produce desirable solder joints with accurate resistance values with little to no damage. As in testing of wire-to-wire solder joints, resulting component solders were wiped clean of loose and excess solder paste, lightly scraped and tugged on, and measured for resistance before inspection under a microscope. Only solder joints which passed on both sides of a component were considered successful, and had their time vs. temperature profiles analyzed via IR software for insight.

**Table 8:** Laser power and time duration combinations used for laser soldering of wire-to-component joining, respective of phases during reflow.

Setting	Phase: Dur 1 (preheat), Dur 2, Dur 3, Dur 4 (cool down)
Power 1	0.341 W, 2 W, 3.3 W, 0 W
Power 2	2 W, 3.3 W, 3.7 W, 0 W
Time 1	18 s, 18 s, 6 s, <i>t</i> (laser off)
Time 2	30 s, 30 s, 10 s, <i>t</i> (laser off)



## Chapter 6

### Results and Discussion

#### 6.1 Temperature Observations using Thermocouple, IR Thermography, and HD Camera

As stated in the previous chapter, two polycarbonate coupons each containing a single solder junction point were prepped for laser soldering experimentation at two different parameter settings to evaluate use of IR thermography in generating pseudo (apparent) temperature profiles for a copper wire nearest a solder joint location. The need to determine true temperature during key phases of a solder paste's temperature history is important for laser programming parameter adjustment to achieve the greatest solderability and bring forth insight for temperatures being reached by this combination of constituent materials during reflow soldering. The IR camera's use was also based off its ability to instantly output a temperature vs. time profile, which would allow a first look at the profiles the laser soldering system was producing as well as provide insight on max apparent temperatures being reached. Two J-type thermocouples were embedded within machined channels to make contact with copper wire within adjacent preprinted channels on each coupon; one in contact with a bottom wire within the solder junction cavity (just underneath intersecting wire), and another roughly 6 mm away from the junction cavity and in contact with the same bottom wire. Correction fluid and an emissivity setting of  $\varepsilon = 0.95$  were used for ROI's within IR software, placed on both top and bottom wire. Time vs. temperature profiles for both thermocouples and from IR software for each ROI were plotted and analyzed, with focus on evaluating if pseudo values reported temperature peaks near the solder paste's eutectic melting point. Video feed from an HD camera fitted with an 808 nm lens was referred to for analysis.

Figure 45 shows the before and after images of the two solder junctions tested. Figure 45a shows the resulting solder joint for the first coupon which was subject to 2 W for 10 seconds (preheating), 3.3 W for 30 seconds (ramp duration 2), 3.7 W for 30 seconds (ramp duration 3), and 0 W to emulate cool down at laser shut off. This first parameter setting was of low power and short duration, which ultimately failed to produce a desirable solder joint. The solder joint

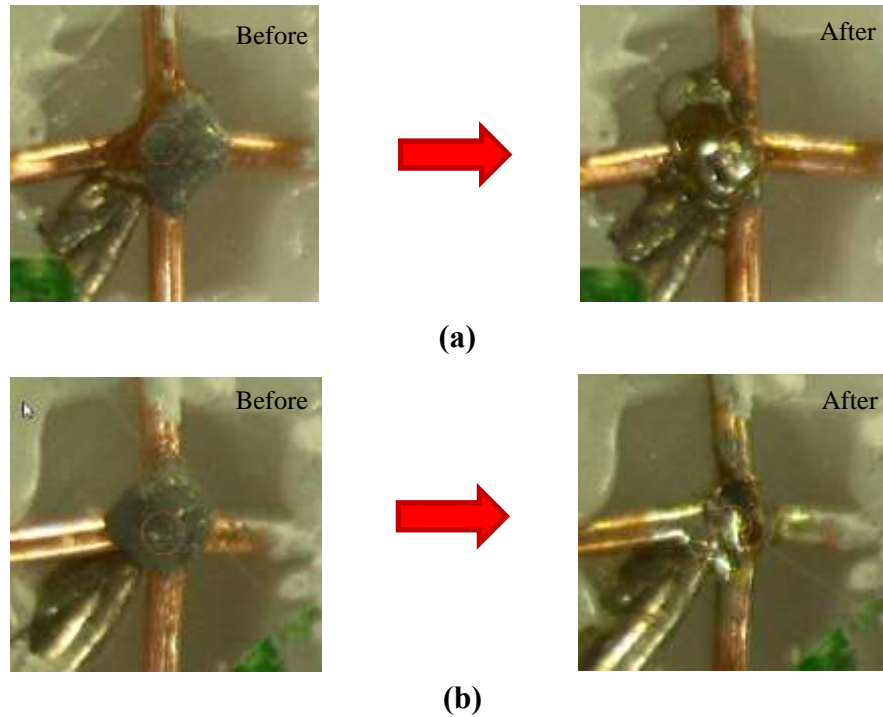


**Figure 45:** a) Before & after images of first coupon at 2 W for 10 s, 3.3 W for 30 s, 3.7 W for 30 s b) Before & after images of second coupon at 3.3 W for 15 s, 3.3 W for 45 s, 3.7 W for 45 s.

exhibited a jagged texture, no uniformity, poor wetting, and little coalescence of the general solder volume despite showing suitable smoothness and brightness (color) characteristics on separate coalesced volumes. The parameter settings used also failed to induce reflow of a portion of the solder paste, leaving excess solder paste residue. Along with solder balling formation, overall characteristics of this solder joint were indicative of insufficient heat delivery, due mostly to a low localized temperature of joining surfaces, and partly to excessive flux used during preparation of this test coupon. Additionally, the thermocouple's contact with the bottom wire ultimately adds to the thermal mass of the solder joint area, and may have contributed to heat losses of the joining surfaces as a portion of the reflowed solder paste cooled and adhered to the thermocouple's wires.

Figure 45b shows the resulting solder joint for the second coupon, which was subjected to 3.3 W for 15 seconds, 3.3 W for 45 seconds, and 3.7 W for 45 seconds. This solder joint was of desirable aesthetic and produced a zero-resistance value between wires via multimeter despite what appeared to be charring of flux early on during the preheating and ramp duration 1 phases.

Flux charring is an undesirable yet benign cosmetic defect which can be attributed to excessive dwell time and the overheating of flux (past its boiling point), but does not hurt or degrade the solder joint if left on surfaces and can be easily cleaned off with a compatible solvent. Flux charring is more common in robotic solder applications where a default program is run without considering the type of flux being used. The additional flux added for this experiment would require adjusting time and temperature to account for the differences in flux chemistry to that of the flux present in the solder paste, or usage of a different flux, or less flux to avoid this phenomenon.

The solder joint demonstrated all necessary actions during reflow, observed via the HD video recording but shown as a sequence of images in Figure 46. Figure 46a shows the solder paste droplet before laser turn on, and 46b the instant of laser turn-on for the preheating phase. The almost instantaneous dispersion of solder into separate reflowed solder ball volumes, evaporation of solvent, and flux activation at laser turn-on was indicative of a violent preheating; the power used to provide this intensity of heat delivery was too sudden and too high, as crucial actions required to occur separately during the first three phases of a solder paste's temperature profile (in moderation) occurred within seconds of laser turn-on. Figures 46b, 6.2.c, and 46d alone account

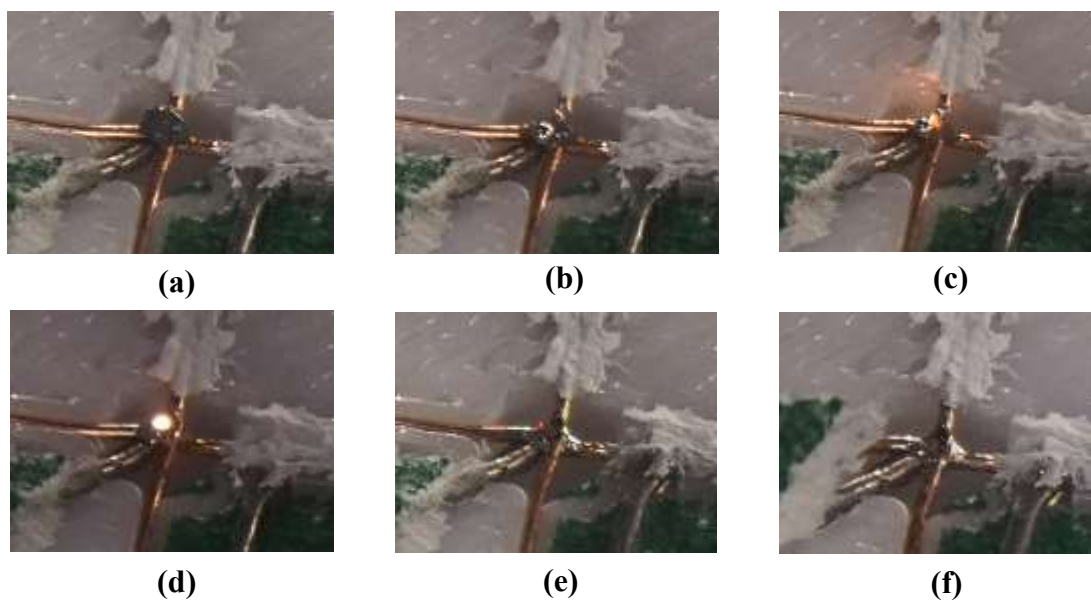


**Figure 46:** Sequence of images depicting actions observed during reflow of solder paste for solder junction test coupon 2 as seen in video recording.

for such actions during the preheating phase, which included the dispersion of solder paste into reflowed spherical volumes and solvent evaporation in 46b, and the burning and charring of flux in 46c and 46d. Figure 46e accounts for events during ramp duration 3; remaining flux evaporated out of the general solder volume while reflowed solder volumes melted and coalesced into a unified volume through surface tension, and during wetting and wicking of solder around the copper wire. Figure 46f shows the resulting solder joint after laser turn-off, and accounts for the final cool-down phase. Having been the only acceptable solder joint of the two tested, the time vs. temperature profile for test coupon 2 is shown in Figure 47.

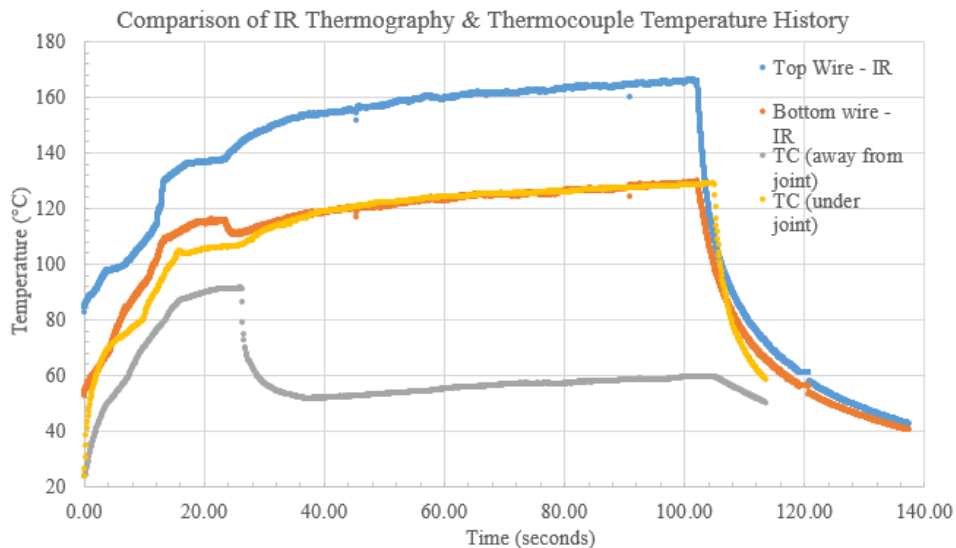


**Figure 47:** Plot comparing IR thermography and thermocouple temperature history.

At first glance, the profiles produced by IR camera looked similar in design to that of the thermocouples which assured proper function of the IR camera. Profiles produced from both methods of evaluation remained exceptionally different compared to the traditional temperature profile suggested by the manufacturer (Figure 34), which is inevitably due to the rapid manner of heat energy delivery created via laser beam application. Per video recording, solder balling, solvent evaporation, flux activation and melting (cleaning) occurred instantly at the start of and during phase 1, which lasted 15 seconds, and explains the early ramp in temperatures for all profiles. Flux began to burn and add localized heat at 7 seconds, and accounts for a second steep ramp in

temperature near end of phase 1. In reference to Table 6.1, which lists temperature values for all sensors at start and finish of each phase, this solder paste and mating surfaces should preheat to 100°C at the end the first phase, according to the manufacturer. Values for IR reached 130°C for the top wire and 110°C for the bottom wire, which surpassed but fulfilled manufacturer requirement. Thermocouple values reported 95°C at the solder junction location (in contact with bottom wire) and 80°C away from solder junction (also in contact with bottom wire), which was below the bottom wire value from IR (-15°C) and well below the requirement at the thermocouple away from the solder joint area (-20°C). Reassuringly, IR values for the bottom wire remained somewhat near values for the thermocouple just underneath the bottom wire and within the junction cavity (-15°C), and that deviation lessened to  $\pm 5^\circ\text{C}$  throughout phases 2 and 3 which may suggest accuracy in temperature representation for the bottom wire. The thermocouple located

**Table 9:** Laser power and time duration combinations used for initial laser soldering of wire-to-wire joining, respective of phases during reflow.

Sensor	Phase 1: 15 s (T °C)	Phase 2: 45 s (T °C)	Phase 3: 45 s (T °C)	Phase 4: n (T °C)
Oven (manufacturer)	25S – 100F; 75	100S – 150F; 50	150S – 230F; 80	230S – 25F; n
IR (top wire)	82S – 130F; 48	130S – 160F; 30	160S – 165F; 5	165S – 25F; n
IR (bottom wire)	54S – 110F; 56	110S – 123F; 13	123S – 130F; 7	130S – 25F; n
TC under joint	40S – 95F; 55	95S – 122F; 27	122S – 128F; 6	128S – 25F; n
TC away from joint	25S – 80F; 55	null	null	null

S = start, F = finish, n = arbitrary number

away from the junction was also expected to report a value similar to these series', but unfortunately did not, perhaps due to poor contact between thermocouple bead and wire surface (secured by tape, but should have been secured with thermally conductive grease or epoxy), or the delay in thermal conduction through the wire from the solder joint area to the adjacent point 6 mm away. Slope non-uniformity of all profiles during the transient preheat phase may also have been the result of light reflectance off of solder spheres as they formed, which ultimately reflected incoming laser light to concentrate portions of the beam onto some areas of the solder volume more than others.

The first signs of coalescence and wetting began immediately at the start of ramp phase 2 (16 seconds), which saw a slope decrease in all profiles into a brief thermal soak before upending into a second gradual slope increase for the remainder of the phase's duration. As the power remained the same for both the preheat phase 1 and ramp phase 2, the brief laser shut off in between phases (laser driver programming) may explain the sudden flattening of curves before continuing upwards in slope, but more likely represents the phase change occurring within portions of the solder paste (there is no temperature change until a phase change is complete). At the 20 second mark, more flux began to escape as more solder balls began to melt, which produced the first signs of surface tension and thus growing heat localization of the solder joint area. At 26 seconds, enough solder paste had reflowed as mating surfaces grew hot enough to induce unified reflow once surface tension had taken over. At this mark, the second slope increase can be seen, which may also have been the result of the growing rate of heat conduction achievable by an amalgamating solder volume during reflow. Full coalescence of all solder volumes into a single volume enveloping both wires was achieved instantly thereafter (end of phase change). At 28 seconds, the thermocouple located away from the junction area broke off due to localized heating of surrounding areas on the substrate, melting tape adhesive to cause it to release while correction fluid seethed, seen on the graph as the sudden dip and slope change for "TC away from joint". All other profiles saw a steady rise in temperature for the remainder of ramp duration 2, ending the duration at 163°C, 123°C, and 122°C for "IR top wire, IR bottom wire, and TC under joint"

respectively, whereas manufacturer settings suggest reaching 150°C at minimum. Only a reading from the IR camera for the top wire met such requirement. With correction fluid also placed 6 mm away from the joining area, this may suggest that the top wire may have been even hotter than 163°C. This assumption can be followed by suggestion that the solder paste itself is even hotter than the top wire, and as reflow was clearly achieved, suggests temperatures well above the eutectic point were achieved by the solder paste to form a joint.

As the power increased from 3.3 W to 3.7 W (maximum allowable power available from the laser driver) from duration 2 to duration 3, a slight increase in slope is seen but is not much different than that of duration 2. In reference to the manufacturer's time-temperature profile, a second rise in slope similar to that of duration 1 should be produced to reach temperatures above 200°C, which was clearly not the case as reported by IR thermography or thermocouple. Pseudo temperatures from start to finish for duration 3 saw less than 10°C changes for all profiles, whereas manufacturer requires an 80°C rise. The highest temperature recorded was the apparent pseudo temperature of 165°C for the top wire, which again can be assumed to be higher for the solder paste volume itself as adequate reflow was observed, and wire surfaces must have been hot enough within the junction cavity to demonstrate such desirable wetting and wicking characteristics, with wetting lengths along each wire spanning near the junction cavity's edges. A slight aesthetic change of the solder joint was observed at the moment of laser shut off (105 seconds), where the color of the solder instantly changed from shiny in its reflowed state to a somewhat duller look at the instant of phase change to solid, which may be the result of a violent ramp rate change as the start of duration 4 (cool down phase) began, and to where an additional time delay set for a lower power may help to decrease the cooling rate. However, the change in surface finish appeared miniscule, as the solder joint appeared to remain mostly shiny in appearance, and suggests adequate solder joint creation by the laser soldering system.

As for the pseudo temperatures of the surfaces, which were found to be much less than the solder paste, are recommended to be at or above the eutectic point for an optimal solder joint. This proved challenging as the maximum power (3.7 W) used for a 45 second heat soak was still not

enough to reach the 183°C mark for the top wire, and even less so for the bottom wire as heat must be conducted from the paste through to the top wire's boundary layer, and with little contact (cylindrical) through to the bottom wire. The need to conduct through the bottom wire and into the thermocouple may report an even lower temperature value. Although the laser's beam diameter was adjusted such that 1/3rd of each wire was targeted, the absorption in copper for this wavelength of laser energy may not be as suitable as it was for this composition of solder paste alloy. During time span of 30s to 75s, ten measurements were analyzed, equally spaced by 5 seconds. The average difference in pseudo temperature between the top and bottom wire IR measurements was  $36^{\circ}\text{C} \pm 1^{\circ}\text{C}$  ( $\sigma$ ), which confirms the inability of the 808 nm laser to heat copper mating surfaces, making the solder paste the only viable heat source for heating wire below it as it absorbs heat energy from the laser beam. Despite this, the challenge of determining true temperature of the solder paste and the area of wires directly beneath it remains (in the junction cavity), as the solder joint formed was clearly of desirable aesthetic and remained intact despite tugging and scraping of the joint area with a precision tool, and produced a zero resistance value between each wire when measured with a multimeter.

Ultimately, the assumptions made above are dependent on the accuracy of the tools used for temperature evaluation and the degree to which they were properly prepared (i.e., calibration of IR camera, non-conductive epoxy to secure thermocouples). The accuracy of the IR camera in reporting apparent temperatures for locations coated with correction fluid was confirmed, which proved unreliable during transient, sudden changes of temperature (response time of camera, variable emissivity, flashing, solder reflective, etc.), but aligned "Bottom wire – IR" with "TC under joint" values during a steady heating condition. The large pseudo temperature difference between each wire as reported by IR camera (36°C) remained concerning, but can be used to evaluate temperature differences in further experimentation. Intended to provide insight on temperature differences between a solder joint location (in cavity) and areas where correction fluid is placed, the "TC away from joint" suggests a 24.6°C difference between each location (before being displaced). Potential remedies for the heating of copper wire may be to acquire a higher



powered laser (5 – 10 W) and increasing beam diameter such that more surface area is hit, or optimizing laser program parameters in combination with less solder paste, or even use of a different flux.

## **6.2 Wire-to-Wire Joining: Parameterization and Repeatability**

Prior testing with a limited number of parameter settings and with little understanding of the global and local events occurring between constituent materials brought the need to conduct testing of multiple parameter settings to better understand the process and determine a suitable parameter set which can be used repeatedly for creating electrical nodes for circuitry fabricated within the M3DMS as quickly as possible. The settings involved pairing various laser powers with time durations taken from the manufacturer temperature-time profile, scaled down in 1/5ths in order to recreate a similar time-temperature profile within a fraction of the time. The experiment included IR thermography and video recording during laser soldering tests, mechanical testing (cleaning and dislodging attempts), and visual observations of resulting solder joints. Visual observations were based on establishing relationships between wetting lengths (WL) from the center of a solder joint out towards the junction cavity's edges and the general size of solder joint measured diagonally across its volume (SJS), such that a numerical representation for a fillet thickness is achieved. The wetting angle (WA) of a solder joint's fillet measured orthogonally from the surface of a wire was also documented. Additionally, the current vs. power plot presented in Section 5.1 was used to determine the total energy delivered for parameter settings, which was then analyzed along with fillet thickness values. Only solder joints which survived cleaning and mechanical testing were considered successful and used for analysis of time vs. temperature profiles, to which the better performing solder joint from each of two power settings were down-selected and used for repeatability tests.

Figure 48 shows an array of before (top) and after (bottom) images for the four rows of 20 solder joints tested, or two coupons used for parameter testing, which began at the lowest power settings (Row 1) and finished at the highest available power settings available from the laser driver

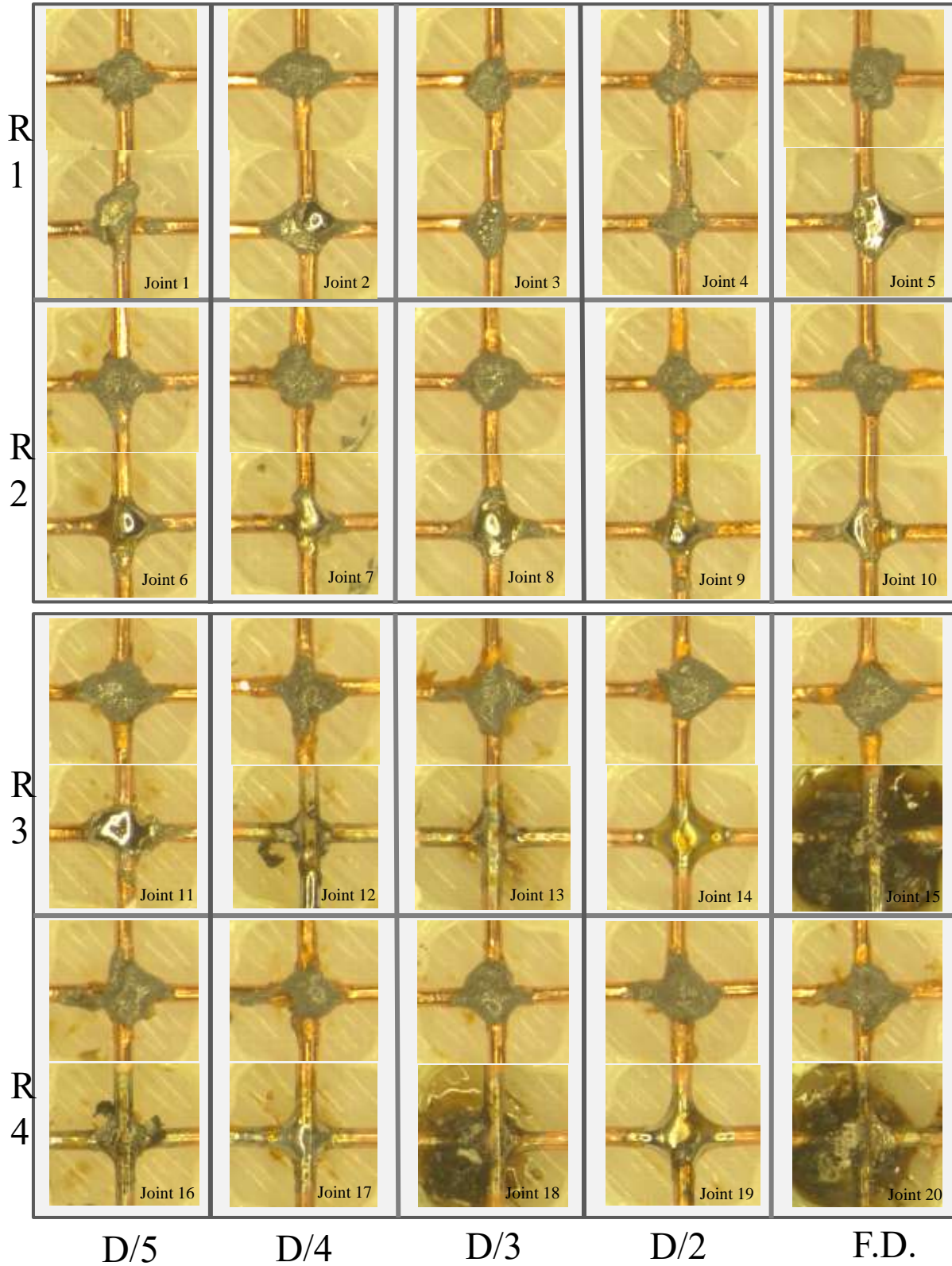


**Figure 48:** Before and after images for 4 rows of 20 solder joints tested (parameter testing).

(Row 4). Figure 49 shows an array containing images of the same solder joints post-scraping and

cleaning processes, with each image enclosed in red to represent failed solder joints attempts or in green to denote successful solder joint attempts. Each setting was paired with five different durations including the manufacturer's oven time settings (full duration, F.D.). Row 1 was set to 0.248 W (0.8 W) for preheat duration 1, 0.341 W (0.9 A) for duration 2, and 2 W (2.67 A) for duration 3 before laser turn-off for cooling duration 4. The left-most junction cavity (Joint 1) was exposed to the laser for the shortest duration (6 s, 18 s, and 18 s) and progressed to the right-most cavity which was subjected to the longest duration of (30 s, 90 s, and 90 s). The large degree of unreflowed solder paste and inactivated flux evident in the first row established this power setting a failure as little to no signs of reflow were observed, due largely to the low power used for all durations. As time of application increased for this power setting, increased signs of reflow were

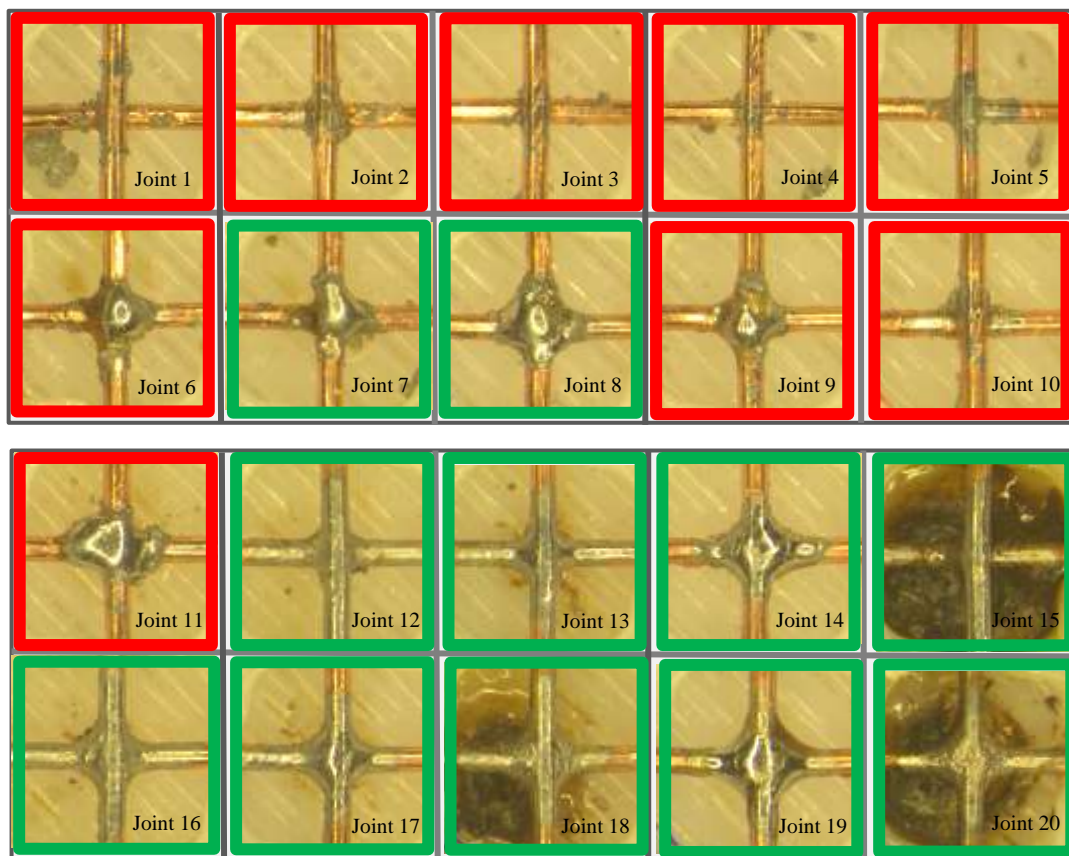


**Figure 49:** Images of solder joints post-scraping and cleaning processes, with each image enclosed in red to represent failed solder joints attempts and in green to denote successful solder joint attempts.

observed; the full duration (Joint 5) provided the highest degree of coalescence due to a larger thermal soaking window. Joint 2 was the outlier, as it was subjected to the second quickest time duration (7.5 s, 23.5 s, and 23.5 s) and appeared to induce reflow for a formidable portion of the solder paste, perhaps due to unintended positioning of the laser beam mostly on the top wire (CNC backlash). Joint 2 and Joint 5 resulted in failure nonetheless, as only the surface of these solder paste volumes achieved reflow and were easily displaced and removed during the scraping and cleaning processes (Figure 49). Only Joint 5 exhibited a thin, wetted layer of solder on the surface of the copper wire, which was ultimately not enough to alloy or bridge the space between wires.

Set to 0.341 W, 2 W, and 3.307 W, Row 2 demonstrated further signs of reflow and coalescence of solder paste, or reflowed deeper portions of each solder volume as time of application was extended. Larger quantities of flux were also activated as time of application extended, but joining's remained largely unsuccessful as all reflowed volumes produced cold solder joints, or joints that failed to melt entirely and flow to form ideal solder joints, and typically only "picked" top wires upon cooling as they were the hottest and closest surfaces. From this row, only Joints 7 and 8 made bridging connections and passed the scraping and cleaning tests. Joint 7 established a bridging connection from the top wire down to the bottom wire on only one side (right side), while Joint 8 established connection downwards to the bottom wire on both sides. These joining's were passed but not considered acceptable as they exhibited poor wetting and surface characteristics, and produced resistance values of 5 and 4  $\Omega$  respectively. For all solder joints in this row, the higher prevalence of adhered solder (mostly to top wire) post scraping and cleaning operations signified greater alloying between solder paste and the surface of copper wire due to the reaching of higher temperatures, which also confirms greater wetting and wicking of paste onto wire surfaces with the slight increase in laser power settings.

Set to 2 W, 3.307 W, and 3.717 W, Row 3 exhibited greater success to produce 4 of 5 passing solder joints, and provided the initial metrics for success. Subjected to the shortest duration of laser application, Joint 11 was the only failure and displayed similar characteristics to that of joints in Row 3; the solder joint established what appeared to be full connection between both

wires despite appearing as a cold solder joint, remained intact during cleaning and light scraping tests, but failed during the mechanical tugging test (broke area of solder joint at point of contact). Joint 12 resulted in what is believed to be the lower limit of a fully acceptable solder joint for wire joining; the solder volume melted in its entirety, wetted and flowed into and around the point of contact between both wires, induced activation of all flux content and allowed it to escape (residue can be seen above solder surfaces), and produced a sound solder joint which passed all mechanical and electrical tests (0  $\Omega$  resistance value). The solder joint did exhibit signs of flux charring, which can be seen as dark streaks on the joint's surface as well charred residue which managed to fall into the junction cavity. Having used the same RMA Flux (rosin mildly activated) for all experimentation, its residuals may be left on the assembly or removed, and was easily removed to leave the aesthetically acceptable solder joint shown in Figure 49. Joint 13 produced near similar characteristics, having produced an even thicker solder joint fillet around the point of contact with slightly less wetting distances traveled outwards along wire by the reflowed solder. The slightly thicker solder fillets seen in each quadrant of joined wire for Joint 13 suggests greater mechanical integrity and strength of the joint, and was considered a hallmark solder joint as the surfaces of the wire remained discernible. Joint's 14 and 15 on the other hand, each represent an extremity for each end of a spectrum which pits Joint 13 directly in between. Joint 14 embodies uneven heating of the solder joint area, which despite having achieved full reflow of the solder volume, exhibited a somewhat rough surface and a short wetting length as a result of having one wire hotter than the other. Joint 15 embodies excessive heating and wetting lengths, a result of a long thermal soaking period and the dripping of reflowed solder and/or boiling flux down into the junction cavity, to which then burnt the polycarbonate substrate below causing it to melt and produce additional heat below the solder joint. The excessive heating conditions and perhaps unwarranted amount of flux allowed the reflowed solder to travel the extensive distances due to low surface tension, which may also have allowed the pastes to fall into the cavity. Joint 15 passed all cleaning and mechanical tests, but was not considered acceptable as the damaging of the substrate is paramount to avoid.

Figure 51 shows the time vs. temperature profiles for Joints 13, 14, and 15, along with the total energy delivered and the dimensionless fillet thickness number,  $n$  for each. Appendix B lists results for all successful solder joints not shown in section for reference. The total energy delivered was calculated by multiplying the power (W) used by each phase's particular duration (s), then summing all phases to give the total energy delivered in joules (J) for each solder joint trial. The fillet thickness number  $n$  was calculated by measuring a solder joint's size (SJS) in Fusion 360 by assigning distances to the pixels of an image using a scale bar, then subtracting and dividing this value by the diagonal distance measured from each corner of what would be bare, adjoining wires (e.g., from quadrant 1 to quadrant 3) as shown in Figure 50. The fillet thickness number, which ranges from 0 to 1.2, was designed to represent a balance between solder joint size (SJS) and wetting length (WL), into which an  $n$  value near zero implies “too much” wetting has occurred and to where a small solder joint size was produced (i.e., solder volume spread too thin) and suggests a weak mechanical joining between wires. A value near 1.2 implies insufficient wetting has occurred, in to which a solder volume remains centered around the wire's point of contact,

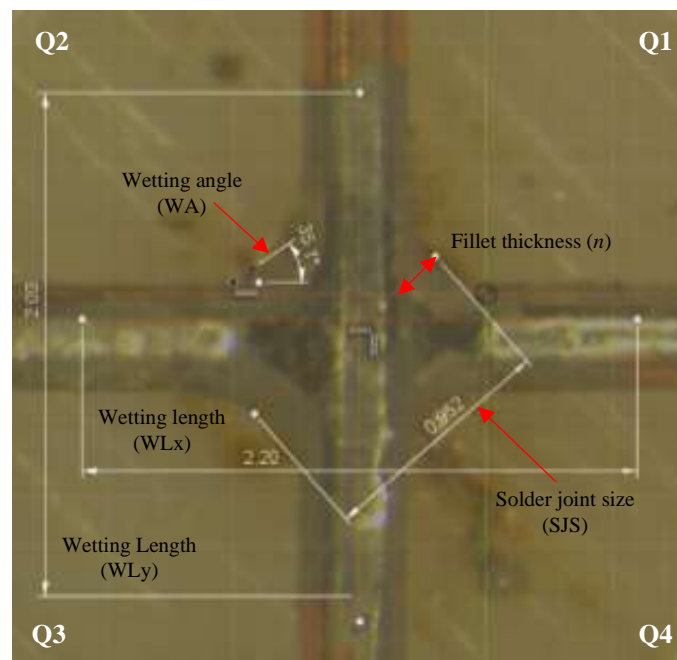


**Figure 50:** Metrology of solder Joint 13 within Fusion 360 for calculation of fillet thickness ( $n$ ).

excessively enveloping the solder joint area which would likely signify a cold joint that did not exhibit sufficient alloying between the solder and copper surfaces. Values for  $n$  nearest 0.6 embody what is believed to be a suitable balance between both extremes.

The profiles shown in Figure 51 helped to confirm the observations discussed above; the profile for Joint 13 shows a mostly even distribution of temperature between top and bottom wires, with apparent temperature values well around the eutectic temperature of 183°C which resulted in a desirable balance between wetting length and solder joint size. Per manufacturer time-temperature profile, Joint 13 fulfilled requirements for the preheat period and ramp duration 2; 100°C was reached at the end of preheating, 150°C was reached at the end of duration 2, and reached the paste's eutectic temperature (at least) by end of ramp duration 3. Similar to the profiles analyzed in Ch. 6.1, the suggested max, or "peak" temperature of 235°C was not reached. The profile for Joint 14 confirmed uneven heating between top and bottom wire to produce little wetting and a thicker solder joint; which is believed to be due to poor positioning of the laser beam mostly on the top wire, which in turn retained most of the solder upon cooling to produce a bulky solder joint with little wetting and a higher fillet thickness number of  $n = 0.73$ , and was the only wire to reach a near eutectic pseudo value of 178°C. The profile for Joint 15 shows a mostly even distribution of temperature between both wires, with the top wire's peak temperature reaching 260°C and the bottom wire the suggested temperature of 235°C. The curve for the preheat portion of the graph coincides with that of Joint 13, but exhibited a rather flattened curve for duration 2, believed to be due to the dripping of solder into the cavity for heat losses up until the incineration of the polycarbonate substrate material below at the second of laser energy amplification for the start of duration 3, causing temperatures to spike to such peaks and produced the near zero value of  $n = 0.02$  for fillet thickness.

Row 4, subjected to 3.307 W (4A) for preheat duration 1 and 3.717 W (4.5 A) for both ramp durations 2 and 3, produced sound solder joints for all trials but also increased the likelihood of damage to substrate material as durations were extended at a higher power setting. Joint 16 performed similar to Joint 13 to produce a near 0.60 value, but was noticeably duller in color as



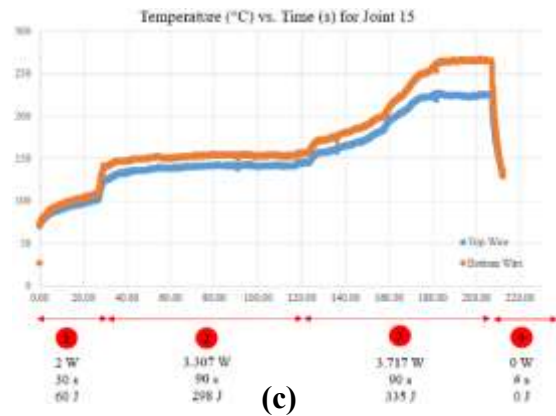
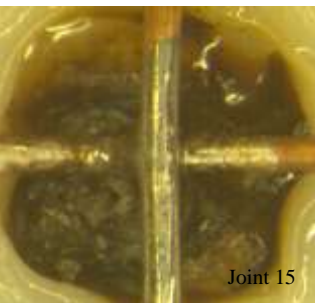
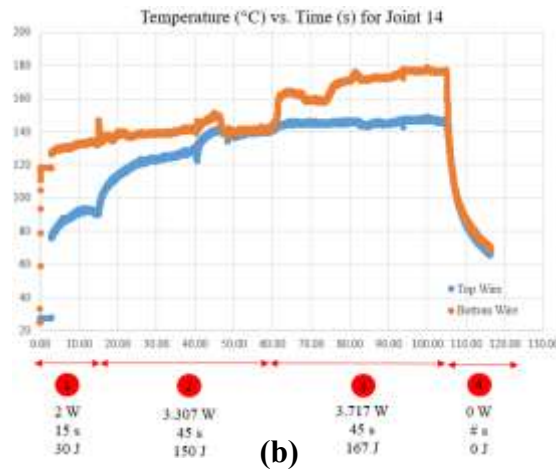
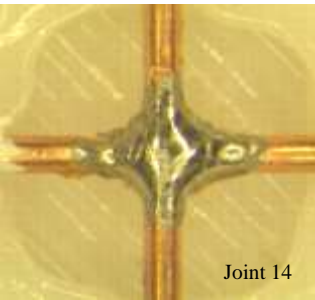
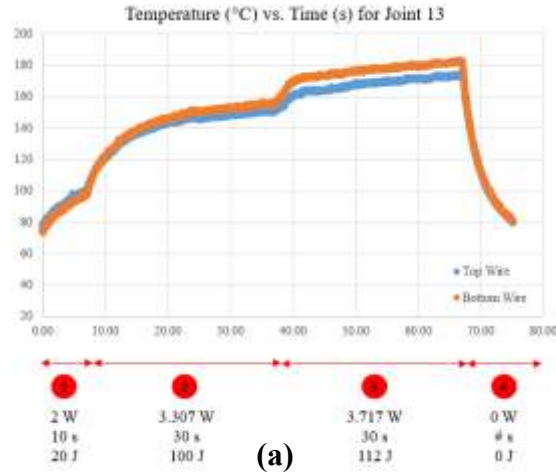
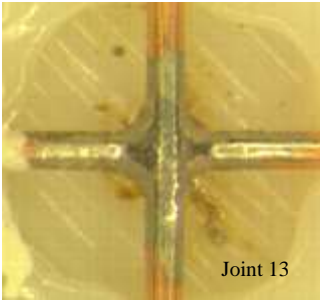
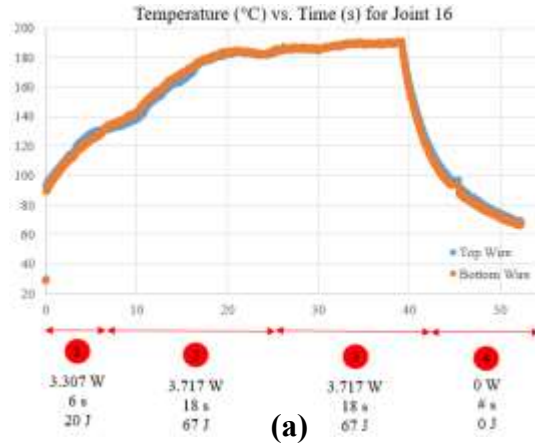
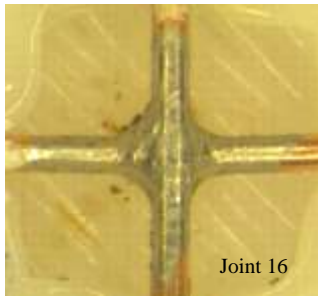


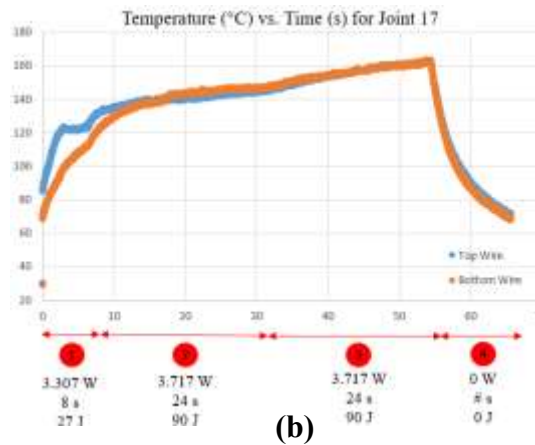
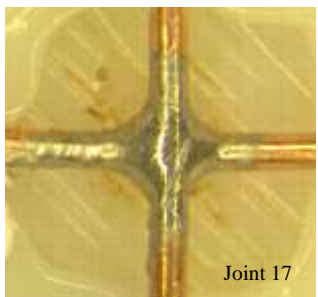
**Figure 51:** Time-temperature profile, total energy delivered, fillet thickness number, and reported resistance values between for a) Joint 13 b) Joint 14 and c) Joint 15.

seen in Figure 52. This is believed to be due to shorter durations of application which did not allow sufficient time for solvent evaporation and flux activation, or for heat to be localized and produced the surface discoloration seen on cold joints. Joint 17, which produced near identical values in

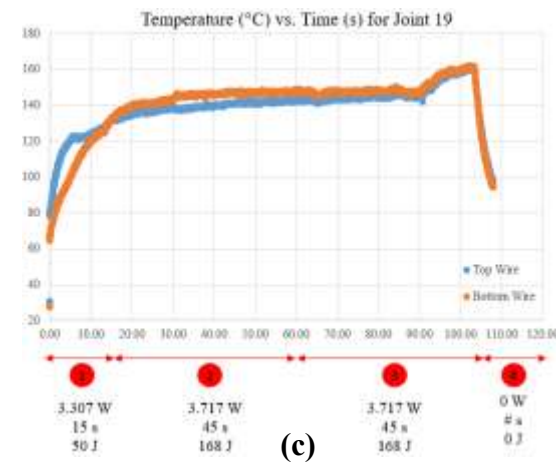
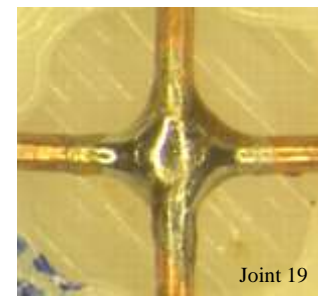




Time duration: **42 s**  
 Total E delivered: **154 J**  
 Fillet  $n$ : **0.58**  
 Wetting angle: **36°**  
 Resistance value: **0  $\Omega$**



Time duration: **54 s**  
 Total E delivered: **205 J**  
 Fillet  $n$ : **0.68**  
 Wetting angle: **24°**  
 Resistance value: **0  $\Omega$**



Time duration: **105 s**  
 Total E delivered: **385 J**  
 Fillet  $n$ : **1.1**  
 Wetting angle: **38°**  
 Resistance value: **0  $\Omega$**

**Figure 52:** Time-temperature profile, total energy delivered, fillet thickness number, and reported resistance values for **a) Joint 16 b) Joint 17 and c) Joint 19.**

terms of fillet thickness number and energy delivered ( $n = 0.68$  and 205 J delivered), was deemed the hallmark solder joint for Row 4 and fulfilled manufacturer recommendations for preheating duration 1 and ramp duration 2 despite the inability of the joint in reaching eutectic temperatures

for both wires (162°C) during ramp duration 3 (Figure 52). Joint 18 saw damage to the substrate below it and produced a rough, dull solder joint. This profile surpassed manufacturer temperatures by 20°C or more for durations 1 (120°C at end of preheating duration) and 2 (180°C at end of duration 2), while reaching just below the recommended temperature for peak duration 3 (220°C). This joint was believed to have performed better had solder and flux not fallen off of the mating surfaces. Joint 19 was an interesting case, as it produced the highest fillet thickness number of all series', surpassed manufacturer settings as did Joint 18, saw a profile which experienced virtually no temperature changes throughout ramp durations 2 and 3, topped out at only 160°C as its peak temperature, yet produced the most desirable surface aesthetics of any joint tested and was felt to be the most mechanically strong bonding (the joint could not be destroyed even with what seemed like double the tugging force) and exhibited wetting lengths just under Joints 13 and 17. Joint 20 was the second and final trial to damage substrate material in this row, which was unsurprising as it was subjected to the highest available power setting for the longest duration.

Upon analysis of parametrization results, it was found that profiles for solder joints in Row 4 remained similar to those in Row 3, with the most obvious comparisons being the increase in slope upon laser application for preheating in Row 4 at a higher power early on, and the more subtle changes in slope between preheat duration 1 and ramp duration 2 in Row 4. Figure 53 shows the original time-temperature profile provided by the manufacturer alongside hallmarked Joints 13 and 17 from each row alongside. The sharper changes in slope for Row 3 were more easily observed when amplifying laser power by 1.307 W as opposed to the 0.41 W change between said durations for joints in Row 4. Ideally, producing a profile which can recreate the rise in slope seen in Joint 17 for durations 1 and 2 combined with the rise in slope seen at start of Joint 13's duration 3, but maintaining that ramp rate consistently through to the solder's eutectic point (183°C) and beyond to the suggested temperature peak of (235°C), would likely ensure optimal solder joint creation as suggested by the paste's manufacturer. Fortunately, it appears that with further customization of laser programming controls, i.e., shortening or extending time durations paired

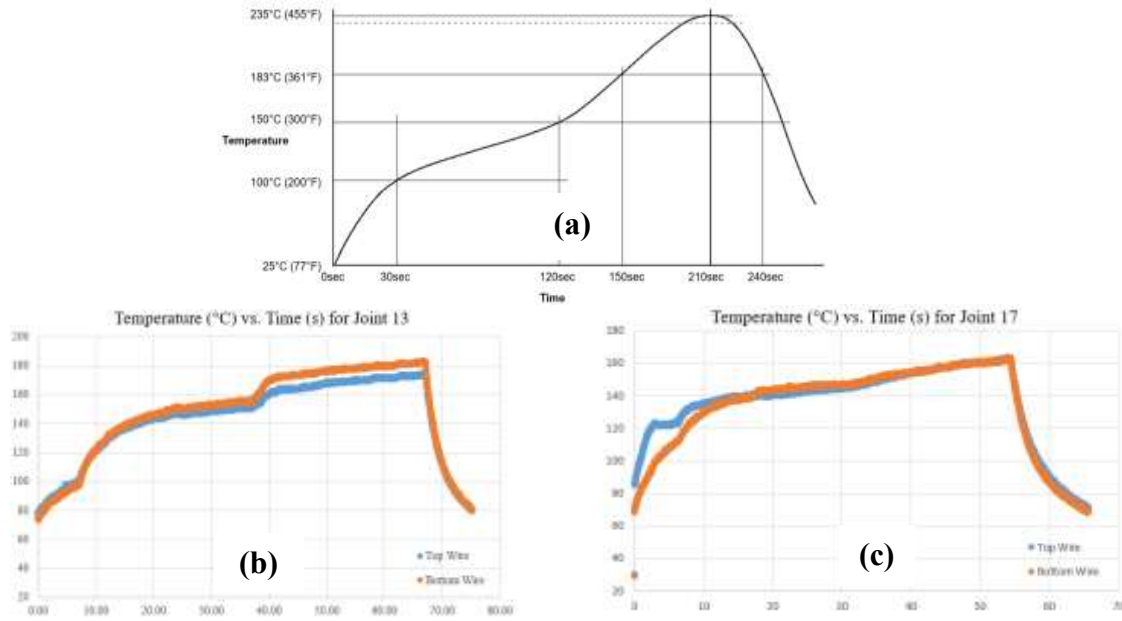


**Figure 53:** a) Original time-temperature profile provided by the manufacturer alongside hallmarked Joints 13 of Row 3 (b) and 17 of Row 4 (c) for comparison.

with additional time delay windows at mediating power settings, the fine tuning of ramp rates can be achieved to reach desired temperatures (with further parametrization testing of course). This was evident as Joint 17 performed similar to Joint 13 at a shorter application time but with increased power settings. The issue in reaching peak temperatures above 200°C in duration 3 for any particular parameter setting can be easily attributed to a low powered laser driver of 4.5 W (3.7 A), in which case can be modified by Al-doping the semiconductor plates used within the laser driver or implementing an additional semiconductor plate to widen reachable power levels. Although, contrary to what was believed only to be due to the additional heat produced by burning/charring substrate material, Joint 12, which produced the first fully acceptable solder joint, induced a large degree of wetting and allegedly reached temperatures of 220°C for its top wire and 200°C despite the second fastest time settings (54 s) and the lowest successful power setting of Row 3 (Figure 54). This is believed to be due to the preparation of Joint 12, which saw unintended application of flux further away from the solder joint area and a volume of solder paste which was unintentionally ‘flattened’ to spread over the joining area. Consequently, the solder volume was

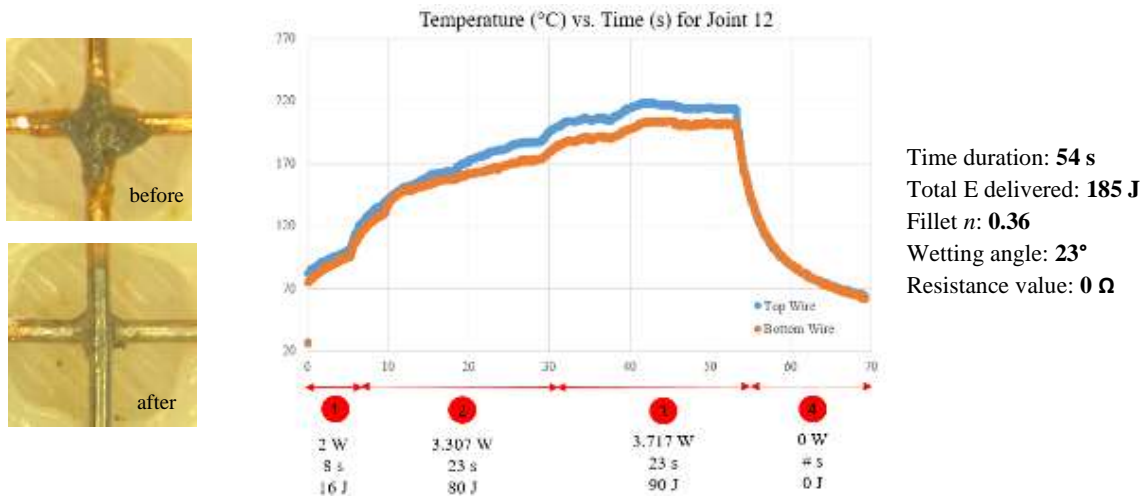


**Figure 54:** Time-temperature profile, total energy delivered, fillet thickness number, and reported resistance values for Joint 12.

better able to absorb heat irradiation from the laser within a quicker heating period while the vehicle (flux) provided longer pathways for the solder volume to spread and heat the areas closer to the ROI's used to acquire pseudo temperature, and reinforces the notion that the true temperatures being reached in the joining areas are indeed hotter than being reported from the location of correction fluid placement (just outside the cavity).

Originally meant for hallmarked Joints 13 and 17 in repeatability testing, parameter settings for Joint 13 and Joint 19 were down-selected for repeatability trials due to their superior aesthetics and the particularly high strength seen with Joint 19. Figure 55 shows an array of images for the 10 solder joints tested post cleaning, with the five tested for Joint 13 in Row 5 and the five tested for Joint 19 in Row 6. These solder joints were prepared in the same fashion as their counterparts in parametrization tests, and were all considered successful (enclosed in green) with respect to mechanical and electrical tests, although it was apparent that many of these solder joints would not traditionally be considered acceptable cosmetically as four joints exhibited cold joint phenomena (poor wetting and surface characteristics) and three junction cavities were damaged. Arguably the better performing parameter setting, joints in Row 5 produced four of five sound solder joints which saw formidable solder joint sizes and wetting lengths, and produced desirable aesthetics despite the charring of the junction cavities containing Joint's 24 and 25. Joint 21

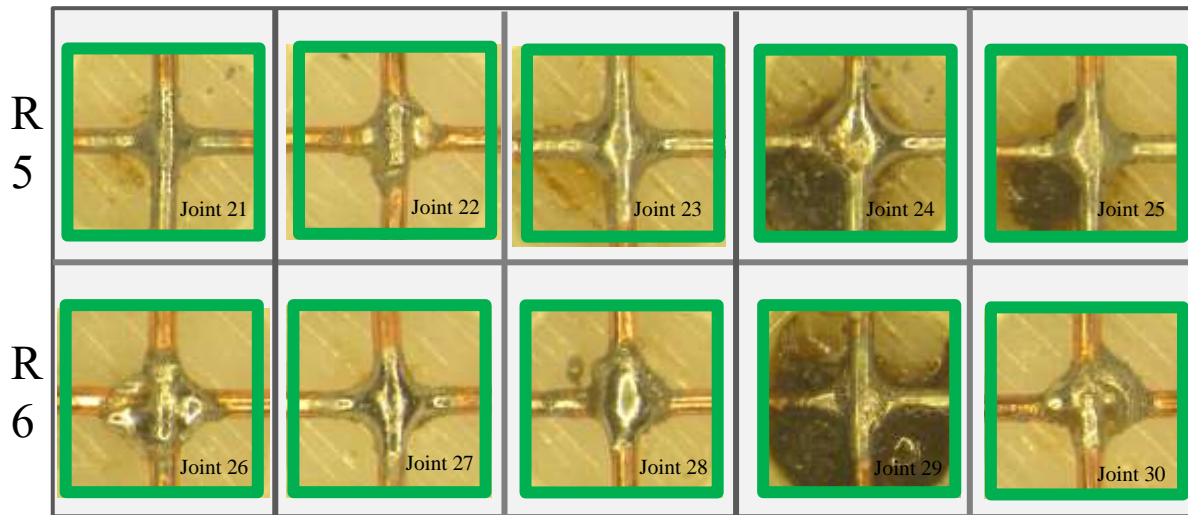


**Figure 55:** Images of the 10 solder joints produced during repeatability testing, with parameter settings for Joint 13 in Row 5 and settings for Joint 19 in Row 6.

reproduced the hallmarked Joint 13, exhibiting a similar value for  $n = 0.6$  which denoted a suitable balance between wetting lengths and solder joint size, while having also revealed clean, shiny, and discernible surfaces around both wires. Joint 27 was the only trial to reproduce traits seen in Joint 19, while the rest of the solder joints in this row exhibited little to no wetting, unreflowed solder paste, and undesirable surface characteristics, all of which indicative of uneven heating between wires (poor localized heat) and inactivated flux residue. As Joint 19's parameter settings consist of higher power settings and longer durations of application, it was incomprehensible to observe characteristics representative of low localized heat and insufficient heat delivery. With further review of all 30 solder joints tested, it was concluded that reaching temperatures near or above the eutectic point, and that of temperature peaks suggested by manufacturer, were not as important as ensuring suggested temperatures within the preheating and initial ramp durations as the proper evaporation of solvents and activation of flux is paramount in allowing proper reflow of a solder volume. The surpassing of temperatures early on in the initial phases of a soldering profile will entrap flux and solvents and complicate temperature localization of the joint area regardless of

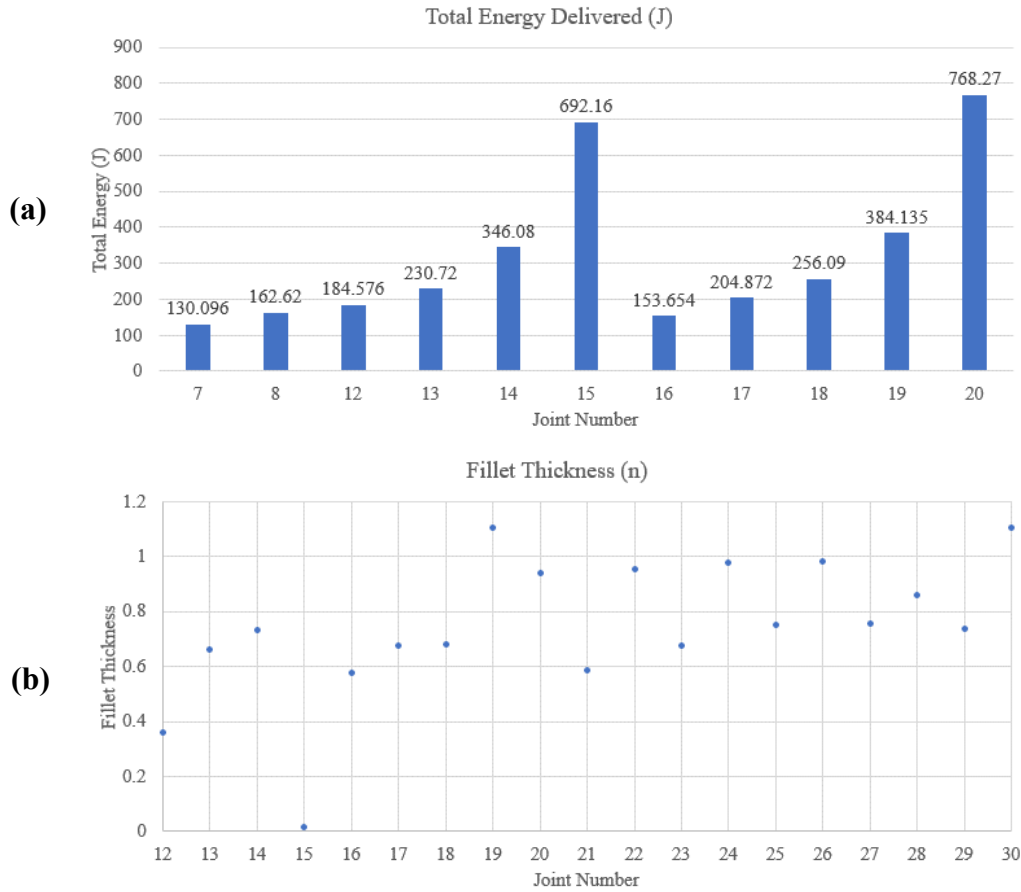


**Figure 56: a)** Total energy delivered to each passing solder joint and **(b)** values calculated for fillet thickness (n) of all passing solder joints.

lengthy time durations, and increases the likelihood of solder paste ‘spatter’ which can further complicate the soldering process as seen in Row 6.

Ultimately, it was found that proper preparation of solder joint areas with constituent materials, strict adherence to manufacturer recommendations in key phases of solvent evaporation and flux activation (preheating duration 1 and ramp duration 2), and the particular threshold of parameter settings which were able to deliver between 185 - 385 J of laser energy within 50 s and 70 s durations produced the highest quality solder joints. Figure 56a shows values calculated for the total energy delivered to each passing solder joint (excluding repeatability joints as they were delivered the same energy) and Figure 56b the fillet thickness n for all passing solder joints (excluding aesthetics and substrate damage). While wetting length distances and fillet thickness

sizes aren't critical in dictating the quality of a solder joint, their use assisted in quantifying solder joint behavior during parameter testing. Fillet thickness values appeared to increase as the total energy delivered decreased, and wetting length values increased as the total energy delivered increased. Fillet thickness values between  $n = 0.50 - 0.8$  were found to be the better quality solder joints. Solder Joint 12 was the only outlier, which may have proved that it is indeed possible to reach temperatures above  $200^{\circ}\text{C}$  with this laser system so long as preparation of the solder joint area and fine-tuning of a laser program is properly conducted. This particular combination of constituent materials paired with the 808 nm wavelength proved successful, as the low absorption of heat energy by the organic material (polycarbonate substrate) allowed for a high energy delivery mostly to the metallic solder paste and partially to copper wire with a low likelihood of substrate damage at the right parameter settings. The poor absorption of heat energy in copper at this particular wavelength remains a challenge, as a fundamental rule in general filament soldering requires joining surfaces to be heated before its introduction in order to establish good bonding. Although, the high thermal conductivity of copper proved mitigating; as the copper wires relied on heat transfer mostly via conduction and radiation from a heated and/or reflowing solder paste volume, each wire would quickly conduct heat from any solder paste in contact, and could promote better heat transfer to ensure adequate localization of heat between both wires so long as more of the solder paste's volume makes equal contact with both top and bottom wires (such as the flattening and pushing of more solder down onto the bottom wire of Joint 12). As for the accuracy of the IR camera in reporting pseudo temperature, the experimentation in Section 6.1 suggested accuracy in reporting a correction fluid coated wire's pseudo temperature values, but not the true temperature of the materials in the solder joint area. As such, the pseudo temperatures seen in the time-temperature profiles above are ultimately the temperatures of the copper wire 6 mm away from the solder joint area, in which case may suggest a  $15\text{-}20^{\circ}\text{C}$  increase to the actual solder joint area.

### **6.3 Wire-to-Component Joining: Parameterization and Repeatability**

With success in wire-to-wire laser soldering, the next area of investigation focused on successfully embedding and terminating surface mounted components (SMC's) to copper wire within a polycarbonate surface in order to enable full electrical functionality of a 3D printed part between builds. Originally intended for both capacitors and resistors of the 1608 package size, the fundamental passive components required for most circuitry, a particular difficulty in completing adequate solder joints between resistors and copper wire in exploratory works (most capacitors produced passable joints) presented the need to focus on developing parameter settings for passive resistors of this size. As the Multi3D's current process plan requires components to be fully embedded within the substrate before returning to a Fortus 400mc machine, such that the top of conductive materials are flush with a surface of a paused print or at least within one layer thickness value of 0.254 mm above it (to avoid print head collision), termination of the relatively small components while in close proximity to surrounding substrate material proved challenging. A result of further simplification of the process plan, these components were mechanically press-fit into their respective cavities for fixation to avoid tombstoning (component displacement linked to thermal differences between joining surfaces at each end of a component). This created an inability to position both component and wire away from the polymer substrate as in wire-to-wire joining (in junction cavities), and presented the challenge of delivering laser energy to constituent materials within a much smaller and sensitive area without damaging materials. Moreover, unorthodox positioning of components adjacent to a wire's tip differs from traditional SMT copper pad soldering, which forces creation of 'straight' or 'butt' joints between the items as opposed to the curvilinear solder joints seen between component terminations lapped onto a PCB's copper pads. Along with addition of a third metallic material to the solder joint area (the terminations on resistors are coated in mostly pure tin), localizing heat delivered by this laser system evenly between adjoining surfaces with different absorption and heat conduction characteristics at this particular wavelength also proved challenging.



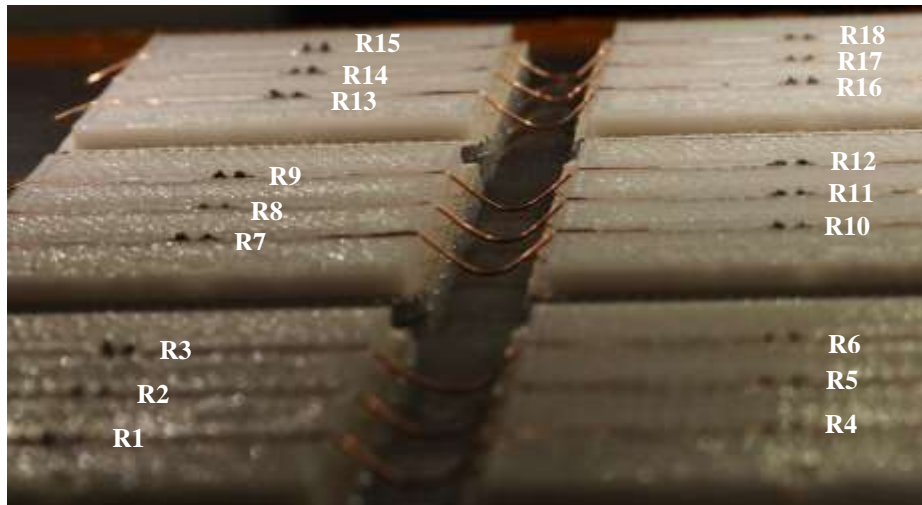


**Figure 57:** Single sheet containing coupons prepped for variability testing, with each row labeled R1 to R18 (resistor number 1, resistor number 2, etc.) to denote order of execution.

As with wire-to-wire joining, the soldering of components to wire involved investigation of parameter settings at varying laser powers and time durations. A single sheet containing 6 coupons with 3 cavities on each (18 total components) was first utilized for variability tests. Figure 57 shows a single sheet containing coupons prepped for testing, with each row labeled R1 to R18 (resistor number 1, resistor number 2, etc.) to denote the order of laser soldering. Each resistor number was further grouped into either its left (L) or right (R) side termination, to account for 36 total solder joint trials which were conducted from left to right. Originally intended to be conducted in a similar manner to that of wire-to-wire experimentation (preplanned, down-scaled parameters of manufacturer's time-temp profile), this set of components forced adjustment of predesignated parameter settings as testing ensued, largely due to ablation of the solder joint area with smaller paste amounts and the inexperience in laser soldering SMT components at higher powers. As such, repetitive failure early on required an exploratory method of testing which based a solder joint's testing settings off of a previous trial.

A successful parameter setting determined in wire-to-wire joining experimentation became attractive in testing first, but ultimately failed to translate to wire-to-component joining. Figure 58

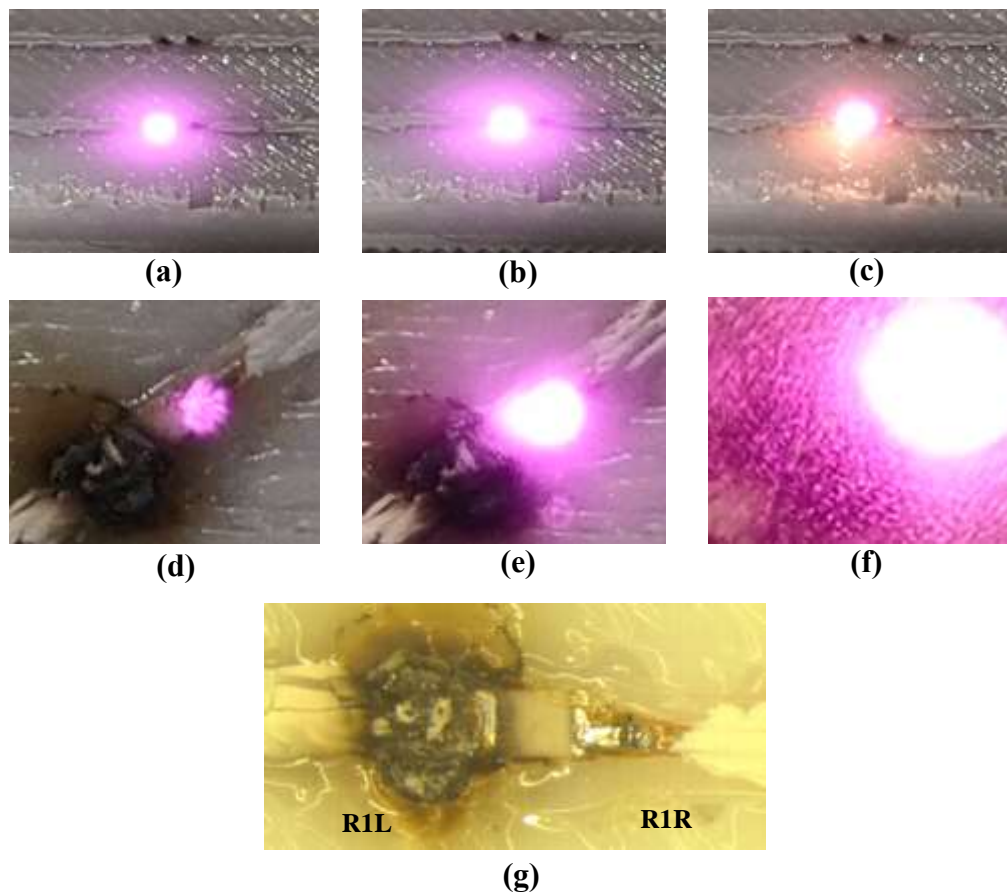


**Figure 58:** Series of images for resistor 1 during testing of Power-2 and Time-2 at 2 W for 10 s in preheat duration 1 (a), 3.3 W for 30 s in ramp duration 2 (b), and 3.7 W for 30 s in ramp duration 3 (c) at its left side termination; Power-1 and Time-1 for right.

shows a series of images for Resistor 1 during testing (without 808 nm lens for reference) of Power setting 2 (P2, from Table 5.2) with Time duration 2 (T2) at 2 W for 10 s in preheat duration 1 (6.14.a), 3.3 W for 30 s in ramp duration 2 (6.14.b), and 3.7 W for 30 s in ramp duration 3 (6.14.c) at the left side's termination. Taken from Joint 13 in wire joining, these settings began with steady laser application to the solder paste volume, wire's edge, and resistor termination in durations 1 and 2 (note increase in brightness of area), but induced burning of the joint area by start of duration 3 (6.14.g). Indicative of extreme power at too long a duration which would continue to char the substrate, the less intense power setting 1 (P1) was conducted on the right side's termination at time setting 1 (T1); at 0.3 W for 6 s in preheat duration 1 (6.14.d), 2 W for 18 s in duration 2 (6.14.e), and 18 s for ramp duration 3 (6.14.f) to produce the cold yet intact solder joint in Figure

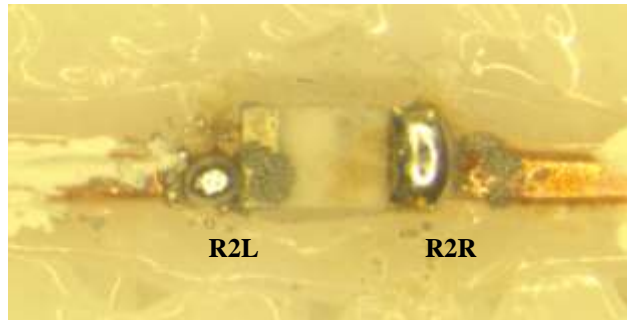


**Figure 59:** Image of failed solder joints for resistor 2 post laser soldering and before cleaning; at 6 s for duration 1, 18 s for duration 2, 18 s for duration 3.

58g. Having believed the settings for R1R to be the next suitable starting point, both R2L and R2R of resistor 2 were subjected to the same settings. Figure 59 shows an image of resistor 2 post laser soldering and before cleaning, which depicts a spherical solder volume sitting mostly on wire's edge and in light contact with the left side's termination. Along with traces of paste spatter and unreflowed paste on the top surface of the termination, this solder joint failed to receive enough heat to localize and induce unified reflow of the entire solder volume, and may have had a larger portion of the laser's beam diameter positioned above the wire (unintentionally) as the solder sphere adhered mostly to a hotter copper wire upon cooling, or may simply have conducted heat from the heated solder paste faster than the tin coating on the resistor's termination. The right side's termination did not perform much better, although, exhibited increased signs of coalescence and wetting with slightly less unreflowed solder paste or spatter.

As R1R had produced a better solder joining at the same settings used for both sides, it was concluded that it had only done so due to the already received heat for additional preheating time during soldering (and burning of) R1L, and why R2R had performed slightly better than R2L. An additional pair of components, Resistor 3 and Resistor 4, were each tested at matching parameter settings P1-T1 and P2-T2, respectively, to confirm that these settings indeed produced inadequate heat energy delivered with the first pair or excessive heat delivery with the second. Figure 60 shows images corroborating said observations, with Figure 60a showing Resistor 3 having exhibited near identical results to that of Resistor 2 (inefficient heating to eventually fall out during

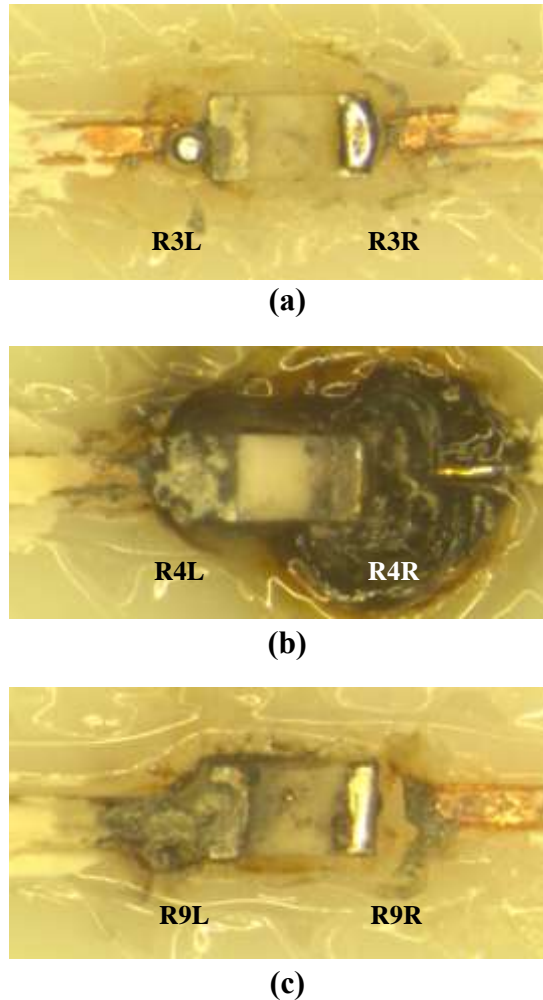


**Figure 60:** **a)** Image of failed solder joints for Resistor 3 at P1-P1 post laser soldering and before cleaning, **b)** image of failed solder joints for Resistor 4 at P2-P2 post laser soldering and before cleaning, **c)** Image of failed solder joints for Resistor 9 at P2-T1 with tombstoning

cleaning), and Figure 60b showing Resistor 4 which had experienced burning conditions at R4L and extreme charring in R4R and what was clearly to violent a parameter setting. This led to testing the next series of components in various combinations between parameter settings (P1, P2, T1, T2), in which case ended in overall failure, as either one side of a resistor would fail whilst the other would pass, or would produce cold joints at both sides with fluctuating resistance values across solder joint from termination to wire (indicative of improper solder joint connection) if a resistor managed to pass cleaning and mechanical testing. Some components were placed in poorly machined cavities as a result of CNC backlash, held loosely within cavities to allow for

tombstoning and render an opposite end of the resistor unusable, as the component would be pulled to far away from a wire's end (Figure 60c).

Having a limited number of coupons remaining for testing on this sheet, belief that perhaps adjustment of time settings at the lowly powered setting P1 could potentially produce better results. Taking findings from wire-to-wire experimentation which highlighted the importance of allowing sufficient time for preheating duration 1 and ramp duration 2, along with observations of repetitive burning frequently occurring during lengthy application times for duration 3, time setting T1 had its preheating and duration 3 values swapped. This would allow a longer preheating time to dispel solvent and activate flux, and limit higher laser intensities in ramp duration 3 to a smaller window. Figure 61 shows a set of images for 4 subsequent resistors tested, which ultimately allowed determination of a parameter set which could be investigated in repeatability tests. The adjustment trial began with P1 of 0.3 W, 2 W, and 3.3 W for an adjusted 18 s, 18 s, and 6 s (respectively), and had the newly adjusted time setting renamed T1.1. Figure 61a shows Resistor 11 having been subjected to these settings on both sides. Reminiscent in characteristic to P1-T1 resistors, this component also featured insufficient heat delivery overall. This led to the slight increase in time of duration 3 to 10 s for Resistor 12, shown in Figure 61b as T1.2. This component produced the initial metrics for success, which produced structurally sound solder joints at both terminations (survived scraping and cleaning tests) and produced a non-fluctuating, accurate resistance value of  $49.9\ \Omega$  on the multimeter. Although, it was evident that R12R had performed substantially better than R12L to produce one of two hallmarked solder joints on this sheet, and was again believed to be due to the already present heat from soldering R12L.

In an attempt to improve soldering of both sides of a resistor with one parameter setting to avoid implementation of a secondary time setting for opposing terminations, time settings saw adjustment of duration 3 to 12 s for Resistor 13 (Figure 61c). Reassuringly, the left side of this resistor featured traits to that of R12R and produced the second hallmarked solder joint of this series, labeled as T1.3 in Figure 61d. These hallmarked solder joints exhibited superior wetting and wicking characteristics, such that reflowed solder flowed into the space between termination

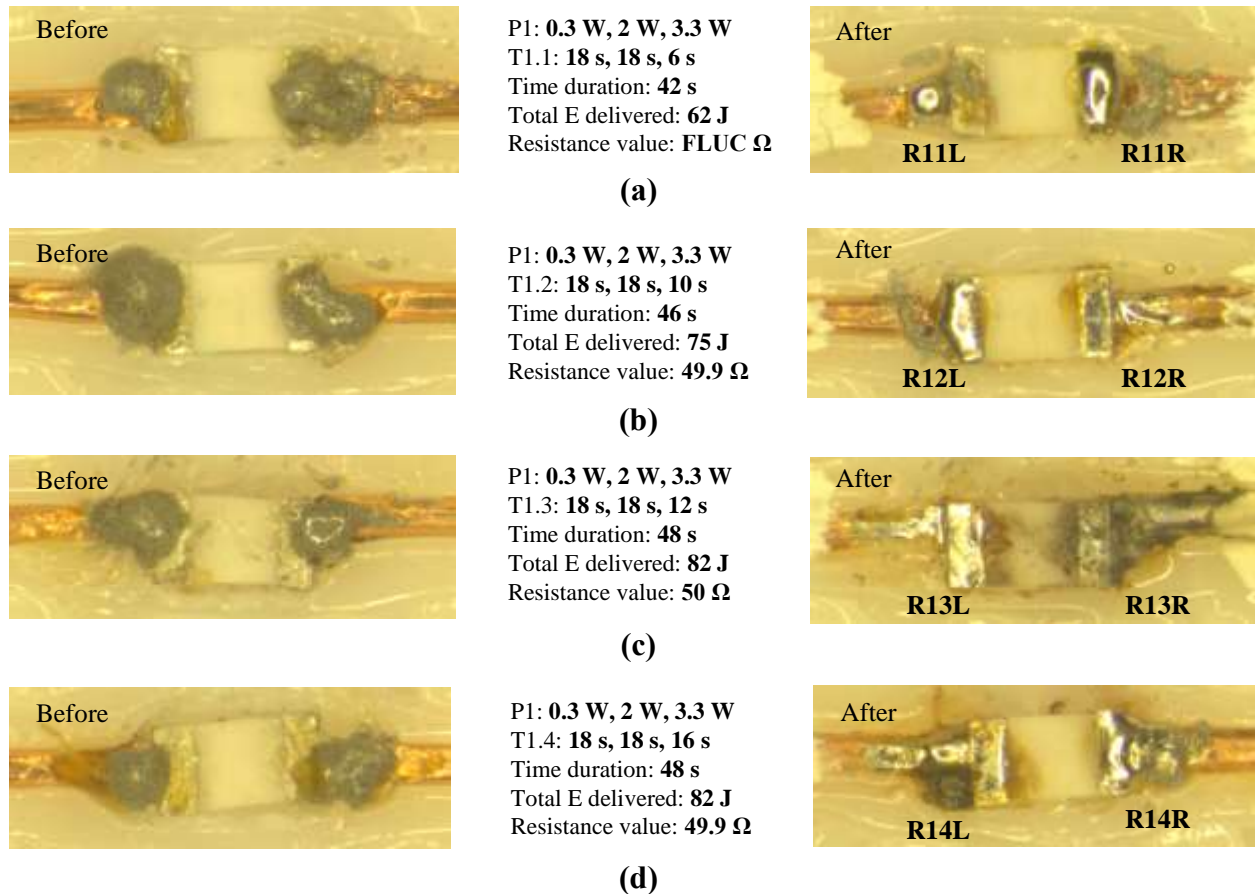


**Figure 61:** Images of resistors subjected to adjusted time settings, along with power settings, time duration, total energy delivered, and reported resistance values.

and wire, and engulfed the exterior of both items. These joints also exhibited minimal splatter and adequate aesthetics in terms of bright and shiny exteriors. The right side of Resistor 12 however, did not replicate the same characteristics as it experienced burning and thus damage to the component. This was believed to be due to ill positioning of the wire and component (poor machining and component placement), which had the wire touching the outer edge of the termination. Curiosity in exploring additional parameter adjustments of duration 3 with few components remaining led to the testing of Resistor 14 at 16 s for its duration 3 and Resistor 15 with a similar adjustment of time setting 2 (30 s, 30 s, 10 s instead of 10 s, 30 s, 30 s), with only R14 shown as T1.4 in Figure 61d. Resistor 14 produced passing solder joints on both sides, although appeared to have experienced slightly excessive heat delivery as charring occurred on R14L and both joints exhibited rough surface characteristics. Resistor 15 failed on both sides

unsurprisingly, as R15L formed a subpar solder joint followed by soldering and extreme charring of R15R. Resistors 12, 13, and 14 were the only components to survive scraping and cleaning tests, and produce accurate resistance values via multimeter despite burning or charring. Overall, components processed at power setting (P2) failed, as did those in power setting 1 with time duration 2.

As this laser soldering system is young and in development, its ability to only target and produce one solder joint at a time will continue to create temperature gradients between each side being targeted, and ultimately, require a slightly adjusted parameter setting tailored to each termination if not redesigned (e.g., splitting beam to target each side at once). The second termination targeted may require slightly more or less power depending on the overall power intensity being used and the overall size of the component being targeted (larger components act as larger heat sinks and thus need higher powers), or could use the same parameter settings on each side so long as a longer pause between each termination is undergone to alleviate temperature gradients (cooling) before conducting a subsequent solder joint. As quickly completing the laser soldering process at the CNC routing station is important, and all other secondary auxiliary processes therein, to avoid thermal contractions in the dimensions of a part, pauses for cooling or secondary parameter settings is unfeasible. As such, hallmarked solder joints R12R and R13L appeared to have established a suitable yet thin threshold between power and duration in which time setting T1.3 seemed adept in successfully soldering the first side of a resistor, and potentially less likely to damage the opposite side of a resistor if properly oriented. Parameter settings for Resistor 13 were ultimately selected for repeatability testing on both sides of 18 resistors on sheet 2, and were prepared identically to that of sheet 1 with no dwell time between preparation of specimens and laser soldering.

Figure 62 shows an array of images for all resulting terminations of 18 resistors post laser soldering and before cleaning to highlight the messiness of unreflowed paste with insufficient heat delivery or substrate damage with excessive heating. All components were tested in the same order as in sheet 1 but labeled “2R” for sheet 2. Of the 18 resistors tested, 12 resistors survived scraping





**Figure 62:** 18 resistors tested on sheet 2 at 0.3 W, 2 W, 3.3 W for 18 s, 18 s, 12 s.

and cleaning tests to reveal fundamentally sound and functional solder joints and produced



relatively accurate resistance values (enclosed in green). Six resistors failed during laser soldering or subsequent testing and are enclosed in red. Five resistors which did remarkably well in terms of desired visuals, fully reflowed and wetted solder volumes on both ends (with minimal splatter), and zero damage were considered of exemplary quality and hallmarked with a three-star rating (2R1, 2R4, RR5, 2R8, and 2R11) . Two resistors which exhibited moderately less acceptable solder joint qualities of either poor surface characteristics on one or both sides, or any sign of damage to the component, are marked with a two-star rating (2R3 and 2R9) as they produced adequate solder joints with little to no splatter and a mostly reflowed solder volume. All other resistors that survived soldering and evaluation tests but exhibited overwhelmingly unacceptable solder joint characteristics (obvious cold joints, excessive paste residue, damaged solder joint area, etc.) are marked with a one-star rating. In reality, the only solder joints which were considered fully passable for circuitry within a part are only those marked with a three-star rating, in which case all others would be considered unacceptable in application (with the exception of 2R3).

Figure 63 shows the time-temperature profiles for 2R4 (6.19.a) and 2R11 (6.19.b) of the three-star category along with their images before and after laser soldering, including their preparation. A frame from IR camera recordings showing the maximum temperature reached by each side is also included in Figure 63 for reference. Profiles for 2R4 and 2R11 featured near identical slope behavior and highlight the difficulty in localizing temperature between adjoining surfaces; substantially flatter curves consistently produced by the low preheating ramp rate concluded the phase at 40°C (10°C below manufacturer suggestion) for both components, saw sharp increases in slope between durations 1 and 2 (poorly reproduced due to camera response time in transience), a near identical trend in slope for durations 2 and 3 with a relatively consistent 40°C difference between each side, and slightly smaller deviation in pseudo temperature between the two sides in duration 3 to reach near eutectic temperatures. Originally believed to be an assisting factor in reaching higher temperatures at right-side terminations, temperature values at duration 2's end for resistor 2R4 backed this assumption with a higher maximum temperature of 175°C at 2R4R as opposed to the 153°C reported at 2R4L. Although, this assumption was short-

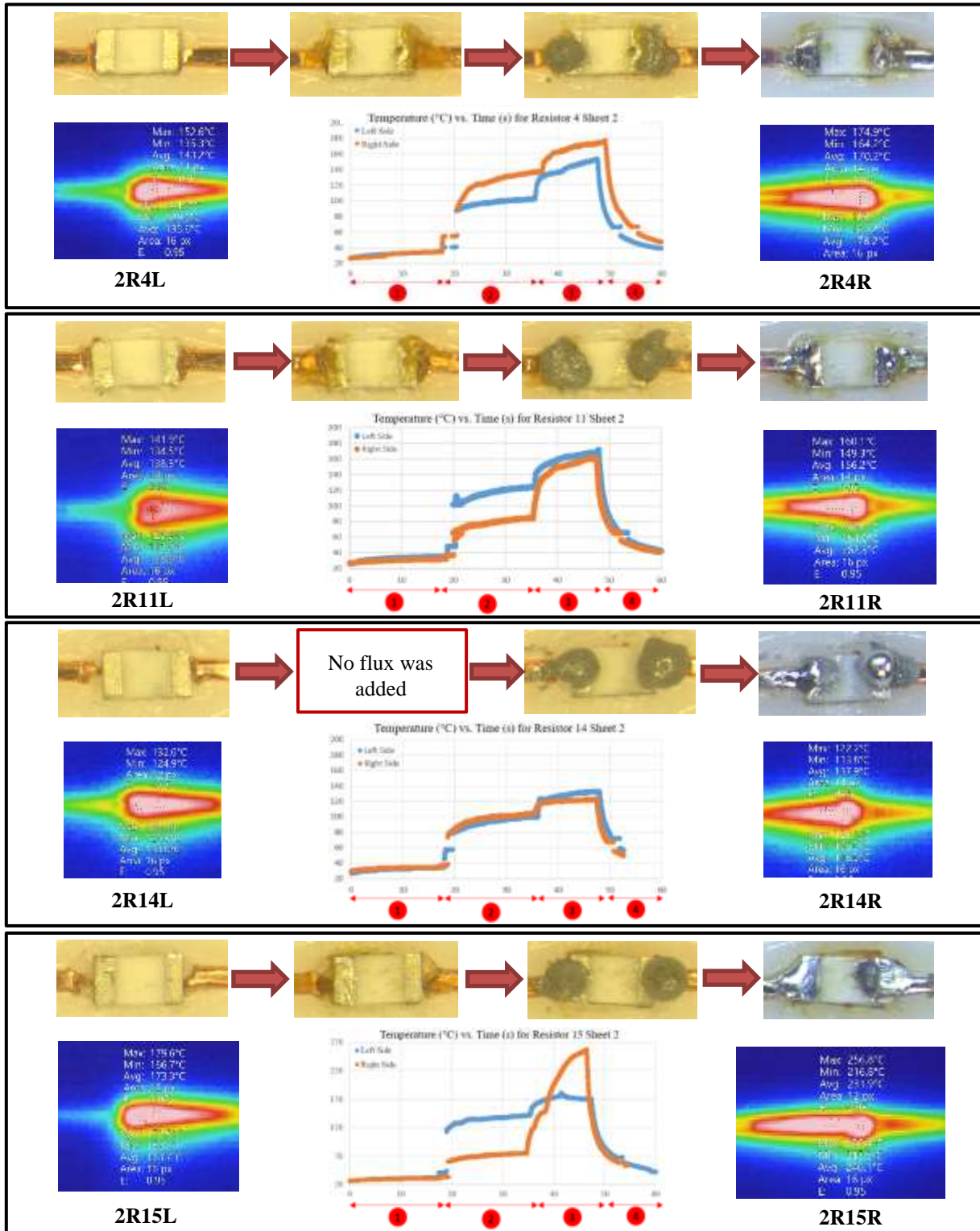


**Figure 63:** Time-temperature profiles for select resistors on sheet 2.

lived as the vast majority of time-temperature profiles for other resistors recorded peak

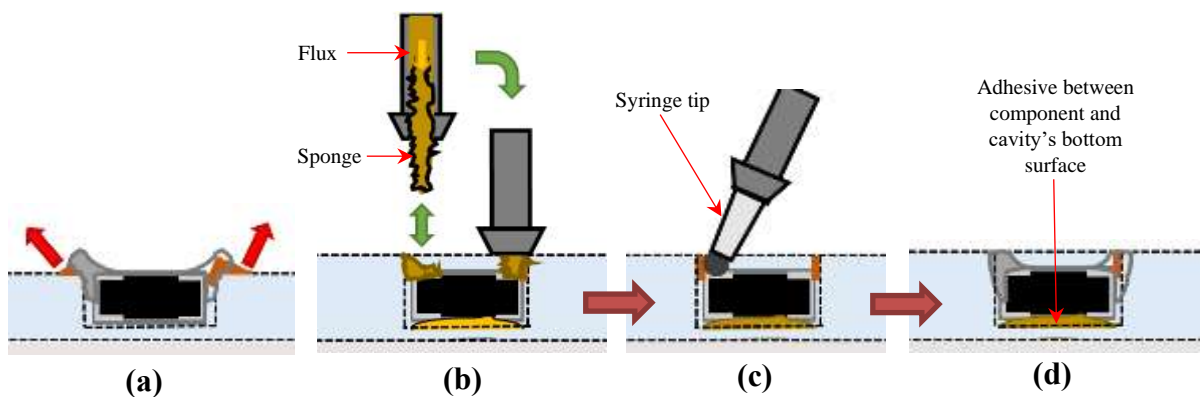
temperatures of right-side terminations to be less than left-side terminations. Thermal conductivity of materials typically lessen at higher temperatures, and as such, the already present heat at right-side terminations (although miniscule) will ultimately cause the joining surfaces to conduct heat from the reflowing paste at a slower rate to reach lower temperatures overall. Resistors 2R4 and 2R11 did well despite obvious temperature gradients, and was once more believed to be due to their preparation. The components sat snug within their cavities and remain fixated due to proper machining and severing of wire via end mill to leave small “slits” of space between wire and termination (some better than others), which allowed solder to flow in between during reflow. Although barely visible, the pressing of some components into a cavity created a slight taper of a wire’s edge to create convenient pockets for solder joint creation. Flux amounts brushed onto both sides of both components were relatively consistent for these two components, and were believed to be the ideal amount. The flux was also believed to have been placed in ideal fashion; as much of the flux volume as possible laced solely onto wire and termination surfaces while avoiding the polycarbonate substrate. Solder volumes were not as easy to maintain, but were relatively equal in amount to produce mostly identical solder joints on each side of these resistors. These resistors were ultimately hallmarked due to little or no need for cleaning. Figuratively speaking, resistors soldered at this caliber would be ready to go upon soldering and would eliminate adding a cleaning process/step to the Multi<sup>3D</sup>’s overall process plan.

Figure 63c and 63d show the time-temperature profiles for resistors 2R14 and 2R15 (respectively) to highlight improper preparation of a component before laser soldering and the extreme damage induced to a component if its interior alumina-ceramic surface is accidentally targeted (again due to CNC backlash). Both sides of 2R14 produced remarkably identical curves to represent equal heat delivery to both solder joint areas, believed to have been due ideal targeting of a properly positioned solder paste volume; the laser’s beam was accurately positioned with its center directly aligned to the center of a well-rounded solder volume, positioned with each half on a joining surface. Consequently, accuracy in targeting a well-placed solder volume also centers the laser’s beam diameter equally across both wire and termination to deliver an equal amount of

energy to each surface. Unfortunately, this component was found to have been accidentally skipped over during specimen preparation, and did not receive flux. Fortunately, the incident provided an opportunity to observe soldering without additional flux, and test the solder paste with only its own flux content to depend on. Both sides of this resistor reached meager temperatures 133°C (left side) and 122°C (right side) to exhibit poor solder joint characteristics indicative of inefficient localized heating, believed to be due to the absence of the additional flux as targeting and positioning conditions were ideal. This component also exemplifies the challenge in depositing equal and consistent amounts of solder paste, and the ramifications of even small variations in volume. Resistor 2R14R contained slightly more paste content than 2R14L and resulted in a rather large solder sphere (solder balling) at the same amount of energy, and signifies a highly sensitive threshold of acceptable solder paste amounts. Resistor 2R15 shows the result of improper targeting and positioning of the laser beam inwards towards the center of a resistor, past the termination's surface (in contrast to positioning it too far the opposite direction to target and burn the polycarbonate). The laser's beam marking can be seen on the ceramic surface as a badly charred circular area, which caused the right side's trial to reach a peak temperature of 257°C.

Overall, testing for this particular SMT package size proved successful at the right conditions and parameter settings, leaning heavily on the proper preparation of solder joint areas. The accuracy in machining/severing cavity edges and wire, consistency in the paste(s) amounts used and their deposition onto adjoining surfaces, and accuracy in targeting constituent materials were all considered to be most impactful to the overall production of unacceptable wire-to-component solder joints. All of these areas could be further improved with implementation of specially designed tools and/or methods, with the most apparent being a precision dispensing tool which can deposit consistent amounts of solder paste at desired locations (similar to material extrusion via nozzle or syringe), along with a separate dispensing tool equipped with a sponge or brush to lightly coat (or dab) solder joint areas with consistent flux amounts (Figure 64). These additional tools would essentially require additional stages to the process plan, but would ultimately improve success and consistency in wire-to-component joining, and remove variability

in further testing of various parameter settings for finely-tuned heat delivery. The backlash experienced with the Techno CNC that creates difficulty in properly positioning accuracy-dependent tools (laser head and machine spindle) within ten thousandths of an inch (0.0254 mm) could be improved by performing a backlash compensation process to alleviate the additional distance the heavily populated gantry travels due to its force of motion after stopping (inherent in lead screw usage). Although no side views of resulting solder joints were shown, some items (ends of wire and resistors) were slightly pulled up out of their channels/cavities during reflow, which left either component and/or wire slightly elevated above the substrate surface. Mostly, wire directly under solder volumes would be pulled out of the channel and onto the top surface of the termination (capillary tombstone effect) to form superior solder joints if a component remained properly fixated (Figure 64a), and may prove useful to submerge and fixate components further into the substrate in future experimentation such that wire remains within its channels and curvilinear solder joint can be formed (Figure 64d). Resizing of cavities during CAD design could potentially help in the fitment of components for fixation (smaller, tighter widths), or even use of a suitable adhesive within each cavity. Changes in the end mill's toolpath during CAM design



**Figure 64:** **a)** commonly occurring result seen during wire-to-component experimentation, **b)** concept of a flux dispensing/dabbing tool, **c)** concept of a precision solder paste dispensing tool, and **d)** suggested placement/orientation for future experimentation.

could also better size the cavity and sever wire to ensure adequate spacing between component and wire for better joint filling.

Ultimately, the redesign of the laser soldering system would provide the greatest success, to where either the laser's beam is split to target both ends of a component at once (mirrors, galvanometers, etc.) with double the power, or done so with addition of a second laser. Increasing the available power of the laser driver would of course be required for either solution, and will likely be required for terminating components of larger package sizes; the maximum 3.7 W power available from this laser driver was enough to reach the eutectic temperature of the PbSn 37/63 solder paste (without burning of course), but will undoubtedly struggle to reach higher eutectic temperature ranges like that of the hazard-free, silver-based solder pastes (SAC) which recommend temperature spikes of 249°C in peak duration 3, or that of the typically larger active components containing leads/legs for solder joint creation (non-passives, semiconductors, etc.). The reconfiguring of this laser soldering system's to dual-beam application would also alleviate temperature gradients between each sides of a resistors termination's, and substantially reduce the likelihood of tombstoning imbalance of a component during laser soldering. Nonetheless, the current laser soldering system proved a functional solution to the soldering of wire-to-component joints, which accomplished the goal of delivering enough heat energy to highly sensitive areas of a substrate without damaging/melting surrounding areas to lose the current layer's dimensioning for return to a 3D printer.

As the emissivity of polycarbonate ( $\epsilon = 0.90 - 0.97$ ) is relatively close to that of correction fluid's ( $\epsilon = 0.95$ ), the pseudo temperatures values reported at the polycarbonate surface around the solder joint area (default temporal values of general ROI that is the full image) helped to confirm average temperature differences between solder joint areas and the substrate areas around it; with bright red areas nearest the wire reporting a 20°C difference between correction fluid ROI and general ROI at temperature peak, 30°C difference between bright red and dark red areas (next hottest area), 30°C difference between dark red and yellow areas, and 40°C difference between yellow and blue values (room temperature), for an overall temperature difference of 140°C between a solder joint area and surrounding substrate areas roughly 3 mm away (Figure 65). Evidently, the 20°C difference between correction fluid ROI and the general ROI aligned with the

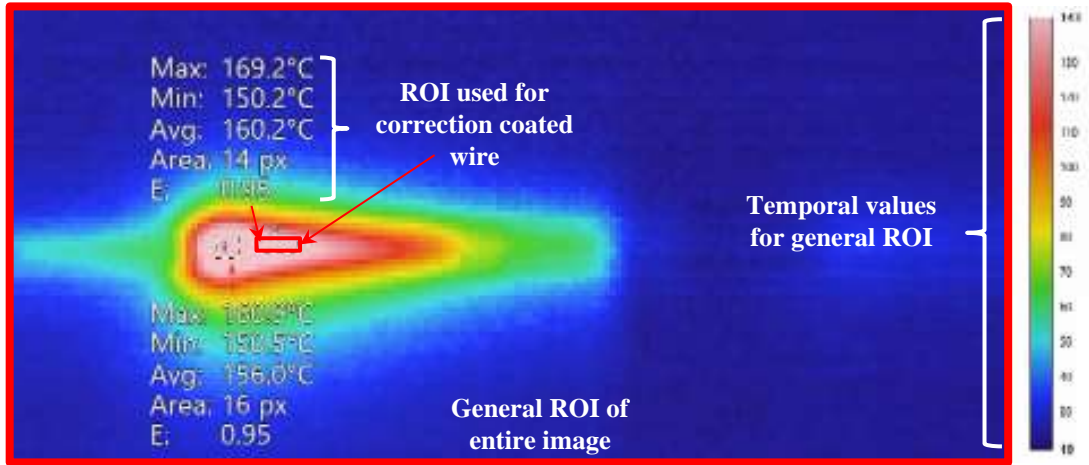


**Figure 65:** Pseudo temperatures values reported at the polycarbonate surface surrounding the solder joint area for 2R11R, with a scale of temporal values for the general ROI that is the full image.

presumed difference of 25°C for temperature differences between coated wire and solder paste areas seen in wire-to-wire joining. The ability of the solder joint areas to receive what was clearly enough heat energy to produce adequate solder joints between wire and components while limiting substrate damage was overall a success. Joining surfaces appeared to reach near-eutectic values with this laser soldering system at low powers and paste amounts, while limiting surrounding substrate areas to or near the polymer's glass-transition temperature (140°C) to avoid damage was particularly exciting.

## **Chapter 7**

### **Conclusions**

The purpose of this document is to provide an initial vantage point for the design, development, and implementation of a non-contact laser application system and method for soldering/terminating electrical interconnections between conductors and surface-mount technology (SMT) embedded within thermally sensitive thermoplastic substrate materials. This system and the techniques presented were designed and tested to accomplish a specific task within a multi-machine hybrid additive manufacturing system, which utilizes several reconfigurable manufacturing systems and auxiliary processes in a serial manner to embed conductors and electronics within FDM-manufactured parts through a stop-and-go process (during a build) to enable rapid prototyping of multi-functional, end-use parts with embedded sensing capabilities.

This system was successfully integrated and tested on a 3-axis CNC gantry and proved functionally compatible with other task-specific technologies which work together within the CNC routing station to deposit conductive materials on any X-Y layer of a 3D printed part during pauses in fabrication. The laser system and its methodology motivated the redesign and enhancement of the wire embedding tool and the general process plan in terms of capability and consistency, although, will eventually require additional fabrication steps in the overall process plan and the tooling for their execution as well (dispensing technologies for solder paste and flux) to enable a higher efficiency and consistency in soldering conductors with less human intervention. Ultimately, the laser application system's design and technique for heat delivery saves valuable design time that would have been required for implementation of a traditional contact-soldering process (tip-soldering, convection soldering, etc.) and appears promising as a technology for development in this application in terms of automation and rapid prototyping. Its compact size and nonexistent maintenance requirements invite further minimization of its overall size and weight for eventual integration to other end-use hybridized fabricators (desktop, multi-axis, and large-scale AM printers). The combination of constituent materials are believed to be compatible



with one another for sensing applications; the conductive materials (wire, components, solder paste) embedded and soldered within this polymer substrate material (Polycarbonate) may be proven to exhibit similar coefficients of thermal expansion (CTE) to reduce thermal expansion in areas for soldering and end-use, and may also exhibit low enough dielectric constants to avoid capacitance between circuit layers in a final part, in addition to low dissipation factors for minimal dielectric heating.

The experimentation in this work proved successful in non-destructive solder joint creation which saw remarkable success in wire-to-wire laser soldering to enable bridging of two perpendicular conductive pathways for electronic node creation, and moderate success in wire-to-component laser soldering which combined to enable embedded circuitry within white polycarbonate material (in theory). All experimentation was analyzed through the use of an infrared thermography (IR) camera and video feed from a HD camera, which was first evaluated with use of thermocouples in preliminary wire-to-wire soldering experiments, and was determined to be accurate only in reporting pseudo temperature values for copper wire coated with a highly emissive material (correction fluid). The correction fluid was not useful in predicting true temperature of a solder paste volume (highly variable emissivity, rapid changes in temperature, phase changes of solder) or of the highly reflective copper and tin surfaces in direct contact with a heated solder paste volume, as these surfaces could not be coated and remain clean for soldering (to avoid contamination of the solder joint). Both laser soldering scenarios produced relatively skewed pseudo time-temperature profiles which did not fully reproduce the recommended profile behavior provided by the Pb 37/Sn 63 solder paste's manufacturer due to the rapid manner of heat energy delivery via laser, although, were able to reproduce two of three key phases of the time-temperature profile which enabled the necessary preheating of metallic surfaces for joining, the evaporation of solvent from the solder volume, and the activation of the flux within the solder joint area for adequate removal/cleaning of oxides to enable proper wetting and wicking characteristics during reflow if near eutectic temperatures were reached. The difficulty of either solder joint area to surpass the paste's eutectic temperature to the recommended peak temperature

(235°C) in ramp duration 3 was attributed to the low power available from the laser driver, which can be easily be increased with customization or redesign. Another possible mediator in the reproduction of the time-temperature profile in duration 3 was believed to be the proper preparation of solder joint areas, namely, the proper deposition of solder paste and flux in consistent amounts (for both wire-wire and component-wire), and the proper creation of cavities for fixation of components during the component-wire soldering process.

The wire-to-wire laser soldering process was enacted to produce seemingly high quality solder joints within junction cavities at the right conditions and established an initial threshold of suitable parameter settings for repetitive processing of wire-to-wire solder joint areas. Power settings between 2 W, 3.3 W, 3.7 W and 3.3 W, 3.7 W, 3.7 W produced adequate solder joints, with those within time durations scaled to a 1/3rd and 1/4th of the manufacturer's full duration performing the highest quality solder joints and junction points. These better performing parameter sets seemed to deliver between 185 – 385 J of laser energy within 50 s and 70 s durations to produce a desirable balance between solder joint size and wetting length traveled to reveal formidable solder joint fillet sizes of high strength and aesthetic. These settings were confirmed in repeatability testing.

The wire-to-component soldering process proved the most challenging, as the size of the 1608 SMT package required exceedingly accurate targeting of substantially smaller solder joint areas which remain in close proximity to substrate material. A single pair of parameters settings were found to produce quality solder joints between a wire's end and a resistors termination, which provided an extremely narrow processing threshold for successful wire-component solder joint creation, and were only discovered due to the swapping of preheat duration 1 with ramp duration 3 times to allow longer preheating times to dispel solvent and activate flux and limit higher laser intensities in ramp duration 3 to a smaller window. The setting also required adjustment of duration 3 times during testing to meet success. The parameter settings of 0.3 W, 2 W, 3.3 W at 18 s, 18 s, and 12 s (respectively) were selected for repeatability testing that saw 12 resistors survive scraping and cleaning tests to reveal fundamentally sound and functional solder joints which produced

relatively accurate resistance values, although, were found to exhibit overwhelmingly unacceptable solder joint characteristics (obvious cold joints, excessive paste residue, damaged solder joint area, etc.) which were not considered passable for application. Five resistors which did remarkably well in terms of desired visuals, fully reflowed and wetted solder volumes on both ends (with minimal splatter), and zero damage were considered of exemplary quality. This was believed to be due proper preparation of solder joint areas with constituent materials along with high accuracy in targeting the solder volume which was properly oriented on both joining surfaces.

Overall, this particular combination of constituent materials paired with the 808 nm wavelength proved successful, as the low absorption of heat energy by the organic material (polycarbonate substrate) allowed for a high energy delivery mostly to the metallic solder paste and partially to copper wire with a low likelihood of substrate damage at the right parameter settings. The poor absorption of the 808 wavelength in copper forced a dependence on heat transfer mostly via conduction and radiation from a heated/and or reflowing solder paste volume. This experimentation was performed at room temperature, which is likely not indicative of success with the same parameter settings for parts transferred to the CNC station from a build chamber kept at 140°C, which will ultimately affect thermal conductivity behavior and require further testing and development of parameter settings during actual builds. As current solder joint failure inspection techniques for the evaluation and assessment of solder joint quality involves a limited number of mostly destructive failure analysis tests (cross-sectioning, SEM, EDX, dye and pry, etc.) which must be induced by time consuming failure detection methods (temperature cycling, thermal shock/power cycling, etc.) to determine a solder joint's official quality and reliability, the testing and evaluation methods performed in this experimentation involved simple resistance & continuity checks, visual inspection, and evaluation of mechanical strength. As such, these predominantly qualitative assessments are not representative of actual solder joint quality and will require the quantitative testing assessments provided by the IPC and EIA standards/guidelines for official evaluation in future work.

## References

- 52915:2016, S. (2016). Standard Specification for Additive Manufacturing File Format (AMF) Version 1.2. *ASTM International*.
- Attaran, M. (2017). The rise of 3-D printing: The advantages of additive manufacturing over traditional manufacturing. *Elsevier*, 677-688.
- Berman, B. (2012). 3-D printing: The new industrial revolution. *Business Horizons*, 55, 155-162.
- Bourell, D. (2017). Perspectives on additive manufacturing . *Annual review of Materials research*, 659-681.
- Brogårdh, T. (2007). Present and future robot control development-An industrial perspective. *Annual Reviews in Control*, 31(1), 69-79.
- David Espalin, J. (2012). *Development of a Multi-material, Multi-technology FDM System for Process Improvement Experimentation*. El Paso: ProQuest LLC.
- Denavit, J., & Hartenberg, R. (1955). A Kinematic Notation for Lower-Pair Mechanisms Based on Matrices. *Journal of Applied Mechanics*, 22, 215-221.
- Dijkshoorn Alexander, W. P. (2018). Embedded sensing: integrating sensors in 3-D printed structures. *Journal of Sensors and Sensor Systems*, 169-181.
- Doren, M. V., & Slocum, A. (1995). Design and Implementation of a Precision Material Handling Robot Control System. *International Journal of Machine Tools and Manufacturing*, 35(7), 1003-1014.
- Espalin, D., Ramirez, J., Medina, F., & Wicker, R. (2012). Multi-Material, Multi-Technology FDM System. *Solid Freeform Fabrication Conference*.
- F2792-12a, A. ((Withdrawn 2015)). Standard Terminology for Additive Manufacturing Technologies. *ASTM International*.
- Gibson, I., Rosen, D., & Stucker, B. (2010). *Additive Manufacturing Technologies Rapid Prototyping to Direct Digital Manufacturing*. New York: Springer.
- Hernandez, K. V. (2012). A Review of Additive Manufacturing. *ISRN Mechanical Engineering*.
- Innovation, W. K. (2021, August 11). *W.M. Keck Center for 3D Innovation*. Retrieved from The University of Texas at El Paso: <https://keck.utep.edu/>
- Lewis, F. (2004). *Robot Manipulator Control Theory and Practice*. New York: Marcel Dekker.
- MacDonald Eric, S. R. (2014). 3D Printing for the Rapid Prototyping of Structural Electronics. *IEEE Access*.
- Marasso, S. C. (2018). PLA conductive filament for 3D printed smart sensing application. *Rapid Prototyping Journal*, 739-743.
- Martinez, N. L. (2020). Development of an Automated Ultrasonic Wire Embedding Process for use with Material Extrusion Additive Manufacturing and Rapid Electronics Fabrication. *Proquest LLC*.
- Mavroidis, C., DeLaurentis, K., Won, J., & Alam, M. (2000). Fabrication of Non-Assembly Mechanisms and Robotic Systems Using Rapid Prototyping. *Journal of Mechanical Design*, 123(4), 516-524.
- Medina Francisco, M. E. (2009). Electronics integration in conformal substrates fabricated with additive layered manufacturing. *ResearchGate*.
- Mellor, S., Hao, L., & Zhang, D. (2014). Additive manufacturing: A framework for implementation. *Int. J. Production Economics*, 149, 194-201.
- Motoman. (2011, June). *DX100 Robot Controller*. (Yaskawa Motoman Robotics) Retrieved January 2014, from <http://www.motoman.com/datasheets/dx100%20controller.pdf>

- Motoman. (2012, January). *Yaskawa Motoman Robotics*. Retrieved January 2014, from [https://www.motoman.com/datasheets/mh50\\_mh50-35.pdf](https://www.motoman.com/datasheets/mh50_mh50-35.pdf)
- Ravi, J., Muruges, B., Srivatsa, S., Sastry, P., & Raman, P. (1988). Robotic Operating System for Material Handling Robot. *Robotics and Autonomous Systems*, 4(2), 157-168.
- Sayler, S., & Dillman, R. (2011). Experience-based optimization of universal manipulation strategies for industrial assembly tasks. *Robotics and Autonomous Systems*, 59(11), 882-898.
- Sayler, S., & Dillmann, R. (2011). Experience-based optimization of universal manipulation strategies for industrial assembly tasks. *Robotics and Autonomous Systems*, 59, 882-898.
- Spathopoulos, M., & de Ridder, M. (1999). Modelling and distributive control design of a flexible manufacturing system. *Computers in Industry*, 38(2), 155-130.
- Sun, Q., Rizvi, G., Bellehumeur, C., & Gu, P. (2008). Effect of processing conditions on the bonding quality of FDM polymer filaments. *Rapid Prototyping Journal*, 14(2), 72-80.
- Sung-Yueh Wu, C. Y. (2015). 3D-printed microelectronics for integrated circuitry and passive wireless sensors. *Microsystems & Nanoengineering*.
- T. Wohlers, T. G. (2020). History of additive manufacturing. *Wohlers Report*.
- T.J. Horn, O. H. (2012). Overview of current additive manufacturing technologies and selected applications. *Sci Progress*, 95-255.
- Tofail, S. (2018). Additive Manufacturing: scientific and technological challenges, market uptake, and opportunities. *Materials Today*, 22-37.
- Vock, S., & Bhurghardt Kloden, A. K. (2017). Powders for powder bed fusion: a review. *Progress in Additive Manufacturing*, 383-397.
- Vyavahare, S. (2019). Fused Deposition Modelling: A Review. *Rapid Prototypin Journal*, 176-201.
- Z. Zhu, V. D. (2013). A review of hybrid manufacturing processes - state of the art and future perspectives. *International Journal of Computer Integrated Manufacturing*, 596-615.

## **Vita**

Emerson Roland Armendariz was born on August 9, 1993 and is the son of Mrs. Guadalupe Baeza and Mr. Dwight Lynn Armendariz. Emerson received his high school diploma in May of 2011 from Montwood High School, and began his engineering career shortly thereafter. He obtained a Bachelor of Science Degree in Mechanical Engineering from the University of Texas at El Paso in May of 2017. As an undergraduate, Emerson was a member of the Society of Automotive Engineers where he served as a captain of the UTEP AERO Design Team. He frequently tutored undergraduate students throughout his time at UTEP, and worked as a Teacher's Assistant within the Mechanical Engineering Department during his graduate studies. He seeks to one day become a Professional Engineer (PE) and tackle the world's climate change issues by designing and developing green energy solutions, whether within a company of similar ideology or within his own engineering firm.

Permanent address: 11732 Jennifer Dr.

El Paso, TX, 79936

This thesis was typed by Emerson Roland Armendariz